To the Graduate Council:

I am submitting herewith a dissertation written by Ling Zhou, entitled " The Soft X-Ray Spectra of Sulfur Compounds." I have examined the final copy of this dissertation for form and content and recommend that it be accepted in partial fulfillment of the requirements for the degree of Doctor of Philosophy with a major in Physics.

Thomas A. Callcott, Major Professor

We have read this dissertation
and recommend its acceptance:

Gerald D. Mahan

Frederick A. Grimm

Leo L. Riedinger

Accspted for the Graduate Council:

Associate Vice Chancellor
and Dean of The Graduate School

The Soft X-Ray Spectra of Sulfur Compounds

A Dissertation

Presented for the

Doctor of Philosophy

Degree

The University of Tennessee, Knoxville

Ling Zhou

December 1995

Acknowledgments

In my graduate course study and dissertation research, countless people in the physics department, from other departments, or even first met, have encouraged me and given me a helping hand. In particular I am indebted to Professor Tom Callcott, my dissertation advisor, whose teaching, guidance and encouragement made this dissertation possible. His help and kindness encouraged me to overcome my difficult time. I also wish to thank Professor Dave Ederer from Tulane University for his discussion and help when I was in CAMD.

I wish to thank to all the past and present members working at synchrotron facilities, Ken Miyano and Q.Y. Dong at beam line U10A at BNL, J. Jia, J. A. Carlisle, L. Shirley at ALS at Lawrence Berkeley Laboratory, Eizi Morikawa, A. Asfaw at TNT beam line at CAMD at Baton Rouge. Due to their efforts, spectrometers at these synchrotron facilities worked well and I had opportunity to finish soft x-ray spectroscopy experiments.

I want to extend my thanks to D. H. Lowndes's group, solid state division in Oak Ridge National Laboratory for providing samples of ZnS and ZnS_xSe_{1-x} alloys used in my research.

I want to thanks to Professor G.D. Mahan, F.A. Grimm, and L. Riedinger, who were very kind to serve on my graduate committee.

I want also to thanks to Professor M. Breinig for her graduate courses teaching and many other helps to graduate students.

All the research in this dissertation was carried out in our old beam line U10A at the National Synchrotron Light Source at Brookhaven National Laboratory, the

Advanced Light Source at Lawrence Berkeley Laboratory, the Center of Advanced Microstructure and Devices at Louisiana State University. I wish to extend my acknowledgment for using synchrotron facilities.

All of the data analysis and most of writing were prepared on computers in the Mac Lab., the CS computer Lab. and nuclear physics group, I would like to extend my thanks to these owners for free use. Their kindness and assistance made the research move quickly.

Table of contents

List of Figures

List of Tables

Chapter I

Introduction

This dissertation deals with the soft x ray spectroscopy of solids. Soft X-rays, as we define them, have photon energies from 50 eV to 1000 eV. Our studies do not deal with core to core transitions, but will be restricted to spectra generated by transitions between a core level and the valence and conduction band states of solids. These spectra are different from atomic and molecular spectra and contain information about the electronic interactions that bond the atoms of a solid.

Three spectroscopes will be distinguished. **Soft X-ray Absorption** (SXA) spectroscopy measures spectra generated by transitions from a core level to empty conduction band states just above the Fermi level, and generally provides information about the density of the lowest energy excited states of the solid. These studies are also frequently referred to as X-ray Absorption Near Edge Spectroscopy (XANES) to contrast them with Extended X-ray Absorption Fine Structure (EXAFS) which measures electronic interference effects in absorption spectra that extend for several hundreds of eV above threshold to obtain information about near neighbor separations of atoms in crystals. **Soft X-ray Emission** (SXE) spectroscopy measures spectra generated by the radiative recombination from valence band states of the solid to an empty core level, and thus provides a measure of the electronic density of the filled valence states. The traditional excitation source for SXE spectra has been an energetic electron beam. **Soft X-ray Fluorescence** (SXF) spectra refer to SXE spectra excited by x-ray photons rather than electrons. For excitation well above an x-ray threshold, absorption and emission

processes are decoupled so that the spectra generated are usually the same as those produced by electrons. For excitation near threshold, the excitation and emission are coupled in different materials by a number of physical processes that modify the spectra and provide new types of information about the solid and its response to a core hole.

The goal of the research reported in this dissertation is to study the electronic states of various sulfur containing compounds using SXA, SXE and SXF spectroscopies.

A brief review of history. Since the discovery of x rays in the 1895, the development of solid state physics has been closely tied to developments of applications of x rays. They help each other progress. From the earliest days, the diffraction of hard x-rays was used to determine lattice structure. Experimental work on the soft x-ray spectroscopy of solids started in the nineteen forties [1.1-1.4]. The first conference on soft x-ray and electronic band structure was held in 1967 [1.1]. By the nineteen sixties, sophisticated methods of calculating the electronic state of solids, such as OPW (Orthogonalized-Plane-Wave) and KKR (Korringa-Kohn-Rostoker) calculations, had been devised. These calculations could be used to predict electronic density of states, appropriately weighted by transition probabilities, for comparison with spectra measured by various electron and photon spectroscopes. It is worth mentioning that G. D. Mahan's many body theory has been extremely important in the theoretical explanation of soft x-ray spectra. He predicted the threshold singularity at the Fermi level observed in simple metals [1.5]; and more recently, the d band behavior in transition metals was successfully explained based on his Green function theory of many particle system, which considers the exchange and correlation of many body theory.[1.6] The latter calculations are relevant to the discussion of transition metal sulfides in chapter VI.

From the beginning, SXE spectroscopy was severely limited by the very low radiative yields in the soft x-ray range, and by the complexities of experimental design. The spectra were always weak and sometimes unobservable in the presence of Bremsstrahlung generated by the exciting electron beam. Low radiative yields in the soft x-ray region also made e-beam excited photon sources marginal for SXA studies, and entirely inadequate for SXF studies. Since the nineteen seventies, the continuum spectrum of synchrotron radiation has provided a strong source for the soft x-ray region. The early synchrotron sources, consisting of bending magnet sources and relatively inefficient monochromators, were good for SXA studies, but were still much too weak for most SXF studies.

In the last decade, rapid advances on a number of fronts have made the soft x-ray spectroscopies versatile and generally applicable probes of the electronic structure of solids. These improvements include:

1) Insertion devices such as Undulators and Wigglers have increased the available fluxes of synchrotron sources by about two orders of magnitude, and the brightness of the sources by three orders of magnitude or more.

2) Improved x-ray optics and monochromator designs have provided beamline monochromators with improved throughput, resolution, and suppression of scattered light and higher orders.

3) Great improvements have been made in the sensitivity and measuring efficiency of emission spectrometers, primarily through the use of single photon counting area detectors for the measurement of spectra.[1.7, 1.8]

These developments in soft x-ray spectroscopy are but a small part of the enormous developments in many areas of sample preparation and characterization that

have revolutionized condensed matter physics and the material sciences. The ultimate understanding of most of the exotic new materials that can now be produced depends on knowledge of the electronic structure. In the following section, we summarize features of SX spectroscopies that make them especially powerful tools for understanding the electronic properties of complex materials.

The electronic states of covalently bonded, tetragonally coordinated, narrow band gap semiconductors such as Si, Ge and GaAs have been intensively studied for nearly 40 years, both for their value as testbeds for theory and because of their practical importance in the electronics industry. Si technology has revolutionized communication, computation and control technologies, and the other narrow bandgap semiconductors, Ge and GaAs and related alloys, have found specialized technological niches. In recent years, electro-optic and energy conversion technologies have increased interest in wide band gap II-VI semiconductor compounds such as CdS and ZnS. This dissertation is devoted to a study of electronic properties of these and other S bearing compounds using the techniques of soft x-ray spectroscopy.[1.9 -1.11]

The dissertation is arranged as follows: The principles of the soft x-ray spectroscopies are discussed in Chapter II, the experimental equipment and procedures are described in Chapter III. Experimental results for ZnS and CdS are described in Chapter IV, and of the ZnS_xSe_{1-x} alloy in chapter V. The chemical bonding of transition metal-sulfur compounds (TM-S) are discussed in Chapter VI.

Chapter II

Principle of SXES

There is a saying, "The sparrow may be small but it has all the vital organs, small but complete." Let us use ZnS as our sparrow to present the major features of SXES, and to lay the groundwork for the following chapters.

A. An Example

Fig 2.1 is a schematic diagram illustrating how crystalline ZnS is derived from the electronic levels of Zn and S atoms. The energy levels for the atomic orbitals of Zn and S are plotted on either side with the density of states of ZnS [2.1, 2.2], derived from band structure calculations, plotted on the same energy scale between them. ZnS crystallizes in the zincblende structure which has the tetragonal local symmetry characteristic of covalent sp^3 bonding. The valence bands of the compounds are formed from the 3d, 4s and 4p orbital of Zn and the 3s and 3p orbital of S, and the overall bonding is generally described as a combination of covalent and ionic bonding. The energy scales make plausible, and band calculations confirm, that the lower valence band (LVB) of the compound is derived primarily from the S 3s orbital, and may be understood qualitatively as a broadened atomic orbital. The upper valence band (UVB), on the other hand, is derived from strongly interacting p electrons of S and 3s and 3p electrons of Zn. It can be understood qualitatively in terms of covalent bonding of these electrons. The gap between the LVB and UVB provides a measure of the contribution of ionic bonding in these solids. The Zn 3d electrons produce a narrow d-band that lies in the gap between

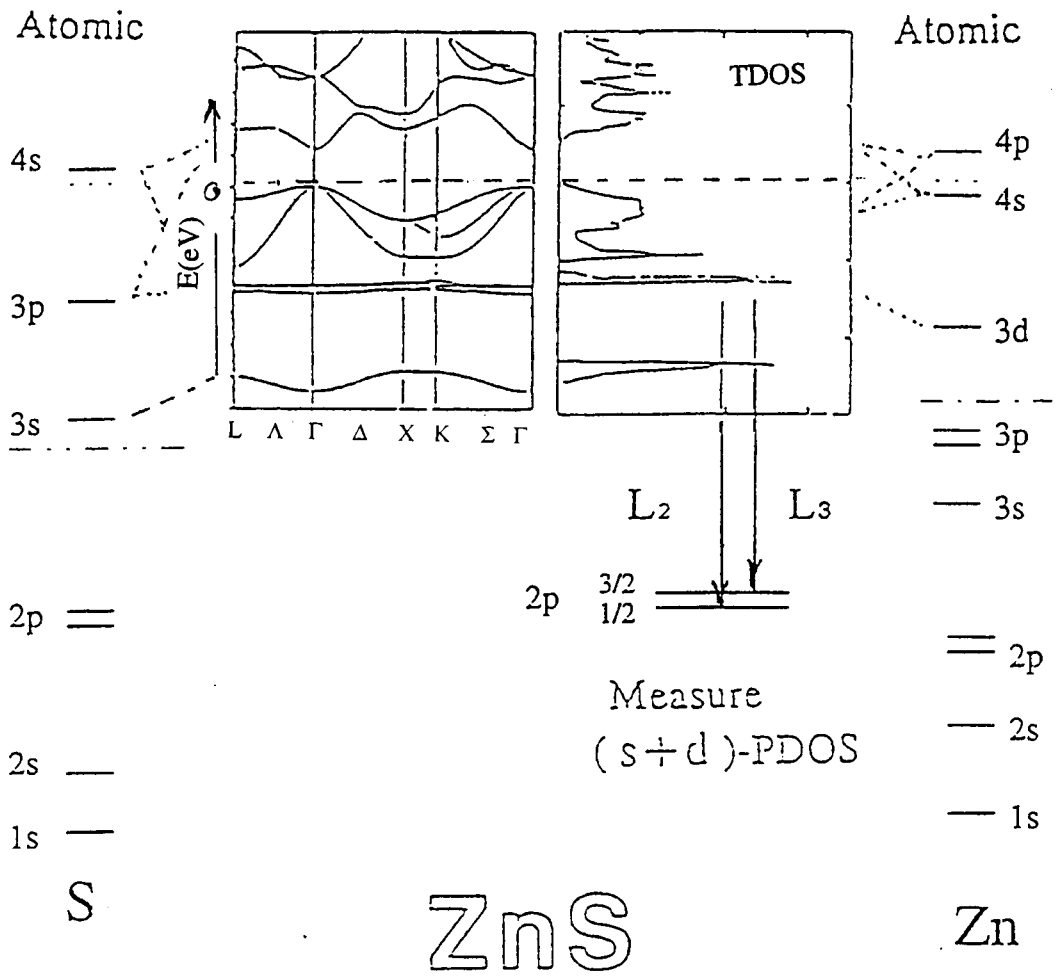

Fig 2.1 Energy states of Zn, S and crystalline ZnS.

the LVB and UVB, and plays a relatively minor role in the bonding of this compound. We will see in a subsequent chapter devoted to the TM-S compounds that d-bands are broader and contribute strongly to the bonding when they overlap the other valence levels in energy. The Fermi energy level is located at the position of the dashed line separating valence bands from conduction bands.

The calculated density of states (DOS) for ZnSe are illustrated in Fig 2.2 taken from the Linear Muffin-tin-orbital (LMTO) calculation of Ref.[2.3]. Because of the similarities in electronic band structures of ZnS (IIB-VI) and ZnSe (IIB-VI) [2.3-2.5.], the densities of states of ZnS and ZnSe should be approximately the same. We use these published DOSs of ZnSe to illustrate the similar distributions in ZnS in the absence of equally detailed published information on ZnS. The total density of states (TDOS) is shown at the top and the local partial densities of states (LPDOS) specified by element and angular momentum symmetry are shown at the bottom. Clearly evident in these plots are the Zn d states lying in the subband gap between LVB and UVB. The predominantly sulfur S nature of the LVB is illustrated as well as the mixed nature of the UVB and conduction bands.

A special power of soft x-ray spectroscopy is that it can provide information about the LPDOSs of complex compounds, because the observed spectra are produced by dipole transitions to atomic core levels of a particular element.

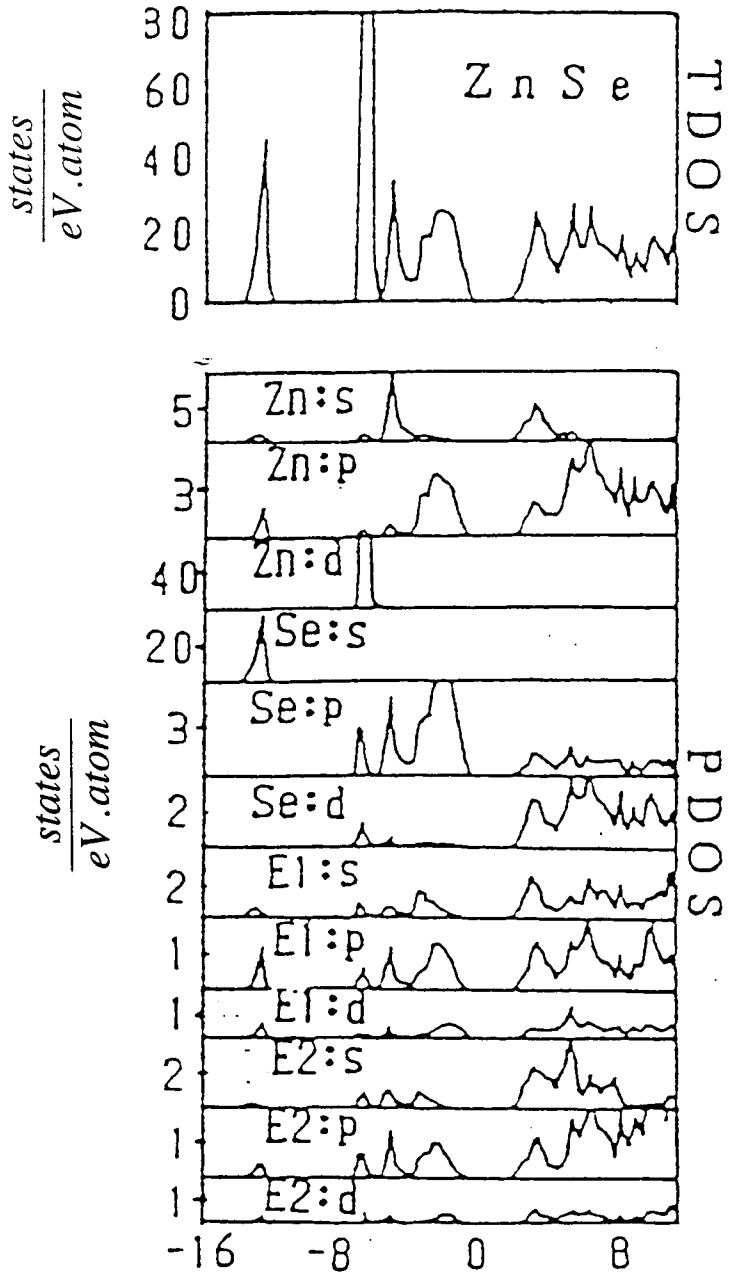

Fig 2.2 The Partial-Density of State (P-DOS) in ZnSe.

B. SXA, SXE, SXFS and Soft X-ray Transition Rate

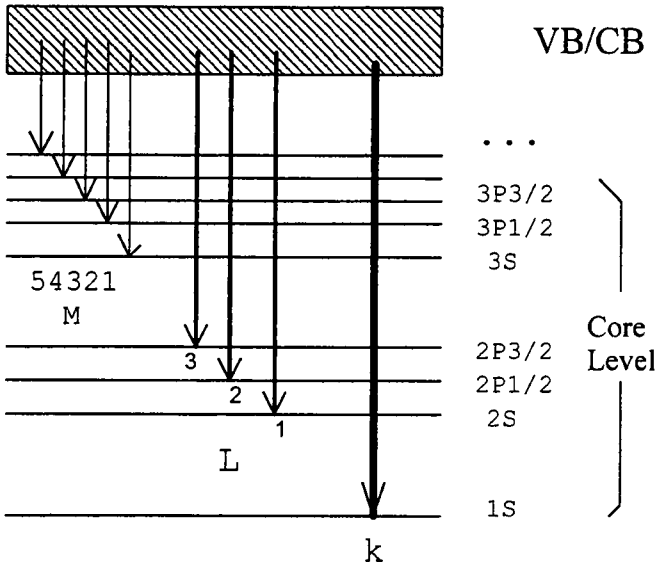

Fig 2.3 Notation for x-ray transitions.

Emitted x rays involving valence band states are classified as K, $L_{1,2,3}$, $M_{1,2,3,4,5}$, $N_{1,2,3,4,5}$,... according to the final states of the transitions as shown in Fig 2.3. K spectra are produced by transitions from electronic bands to the 1s core level with n = 1. L spectra are produced by transitions to states with n = 2; e.g. $L_{2,3}$ designates transitions to $2p_{1/2}$ and $2p_{3/2}$ core levels. M's stand for transitions to levels of n = 3; e.g. $M_{2,3}$ are transitions from bands to $3p_{1/2}$ and $3p_{3/2}$ core levels. N's stands for transition to levels of n = 4, and so on. VB/CB represents the filled valence and/or conduction bands in the figure.

X ray emission and absorption transitions in the soft x ray spectral range obey the dipole selection rules as follows:

$$\Delta n \geq 0 \, , \, \Delta l = \pm 1. \qquad (1)$$

Here n and l are the atomic principle and angular momentum quantum numbers of single electron orbital. This is based on the fact that photons have one unit of intrinsic spin.

The transition rate W_{fi} for a single x-ray emission is given by [2.6, 2.7]

$$W_{fi} = \left|M_{fi}\right|^2 = e^2\Omega^3 / hc^3 2\pi \left|\left\langle \phi_f \left| t \right| \phi_i \right\rangle\right|^2 \qquad (2)$$

assuming the decay of a core hole by a single X-ray emission channel. Here $\Omega = 2\pi C\nu$ is the radiation frequency, t the dipole operator, Φ_f and Φ_i are the final and initial state wave functions.

The intensity of an emitted x ray for a given element (Z) and given angular momentum orbital l, $I_{z,l}(E,\rho)$, is given by

$$I_{z,l}(E,\rho) \infty \Omega^3 \sum_{\Delta l=\pm 1} W_{fi} \cdot \rho_{z,l} \qquad (3)$$

where E is the energy of the emitted x ray, ρ the LPDOS consistent with the dipole selection rules. This assumes that the transition matrix elements are constant in transitions between selected core levels and valence states of a particular angular momentum symmetry. For the sulfur $L_{2,3}$ emission from ZnS, spectra can be produced by transitions to the sulfur $2p_{1/2}$ (L_2) and $2p_{3/2}$ (L_3) core states. The dipole selection rules require that transitions are from states of d ($\Delta l = +1$) and s ($\Delta l = -1$) symmetry in the valence bands. Therefore, the intensity of L_2 radiation would be given by two terms.

$$I_{Z,L}(E,\rho) \infty \Omega^3 [W_{i+1,i} \cdot \rho_{Z,\Delta L=1} + W_{i-1,i} \cdot \rho_{Z,\Delta L=-1}] \qquad (4)$$

The soft x ray spectroscopies are illustrated in Fig 2.4 as Soft X-ray Absorption (SXA) is the photon-in process in which incoming photons excite a transition from a core level to empty states in the conduction band. Soft X-ray Emission (SXE) is a photon-out

process in which photons are outgoing particles generated by the radiative decay of a previously excited core hole. Soft X-ray Fluorescence is a photon-in and photon-out process in which both incoming and outgoing particles are photons and absorption and emission processes are considered together For photon excitation far above threshold, and for e-beam excitation, the excitation and emission processes can be treated independently. For excitation near an absorption threshold, the absorption and emission process are often strongly coupled so that fluorescence is best described using an inelastic scattering formalism.

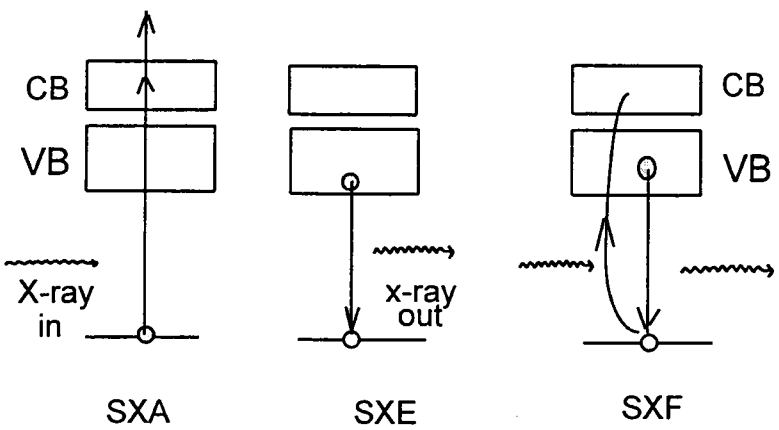

Fig 2.4 Excitation of solid by photon

In SXE, electrons in the filled valence band or conduction band make radiative transitions to fill previously excited core holes. For example, in ZnS, if the core levels are sulfur $2p_{1/2}$ and $2p_{3/2}$ atomic levels, S-$L_{2,3}$ transitions take place from valence bands to the core levels. Only s and d components appear in the emitted soft x-ray spectra. After

dividing by E^3, the spectra are a measure of the (s+d) LPDOS for S in ZnS. Thus soft x ray spectra are able to measure a chemical selected and angular momentum selected partial density of states.

Besides the x-ray decay channel, core excited atoms may decay by Auger processes. In fact, in the soft x-ray range below a few hundred eV, radiative processes are very inefficient, and most atoms decay by non-radiative processes. The resulting low radiative yields have many consequences for soft x-ray spectroscopies. Among these are:
(1) Conventional x-ray sources in the soft x-ray range are weak so that relatively little work was done in SXE spectroscopy before the development of synchrotron sources;
(2) Emission spectra are weak, placing very great demands on the development of high efficiency emission spectrometers;
(3) Some radiation yields are so low that the spectra are not observed (An example is the L_1 spectra of sulfur, where the 2s core hole is filled by a Koster - Kronig transition from the 2p core levels);
(4) In $L_{2,3}$ spectra, the intensity of the L_2 spectrum may be suppressed by non-radiative filling of the $2p_{1/2}$ from the $2p_{3/2}$ levels, with an accompanying VB to CB excitation. However, if the band gap exceeds the L_2-L_3 splitting, this electronic de-excitation process will be suppressed.

C. Resonant Fluorescence Near Threshold

A variety of phenomena have been observed when SXF spectra are excited near threshold, which may best be understood in terms of an inelastic scattering process in which the exciting photon excites an electronic transition and is re-emitted at a lower

energy.[2.8] Though all may be described with the inelastic scattering theory, they may be distinguished through the nature of the electronic transitions induced in the material.

Scattering theory is encompassed in a straightforward application of second order perturbation theory in which a summation is made over a set of intermediate states according to the expression:

$$\frac{d\sigma}{d\Omega} \propto \sum_f \left| \sum_m \frac{\langle f|p.A|m\rangle\langle m|p.A|i\rangle}{E_e - E_h - h\nu_{in} - i\Gamma_m/2} \right|^2 \bullet \delta(E_f + h\nu_{out} - E_i - h\nu_{in}) \tag{5}$$

where the $h\nu_{in}$ and $h\nu_{out}$ are energies of incident and scattered photons respectively, i is the initial(ground) state, j a final state of system, and m an intermediate state to be summed over. Γ_m is the width of intermediate state m of the system. In the case of inelastic process, the valence electrons are excited to the final state f that contains an electron in a conduction band state E_e and a hole in valence state E_h. Energy conservation requires the energies of incident and emitter photons be related to that the electron and hole by

$$h\nu_{in} - h\nu_{out} \cong E_e - E_h \tag{6}$$

Since two photons are involved, the selection rule is

$$\Delta L = 0, 2 \tag{7}$$

For excitation at and above threshold, depending on materials, excitations have been observed which are localized either in momentum or real space. In covalently bonded materials such as Si [2.9], graphite [2.10] and diamond [2.11], the electronic

transition is localized in momentum space(k-space), so that photoexcited electron and the valence hole remaining in the valence band are correlated in k-space.

In other materials, strong elastic and inelastic scattering transitions occur to states localized in real space. These states may be localized by the core-hole itself and can be understood as core excitons. In the K spectrum of hexagonal BN, for example, a strong exciton is derived from the π electrons directed perpendicular to the bonding plane. [2.12] In other materials such as CaO and CaF_2, excitons are from d-states at the conduction band edge.[2.13] Similar excitonic states have also been observed in oxides such as TiO_2.[2.14] Typically, a strong resonant elastic scattering peak is observed when core electrons are exited to the energy of this excitonic state. In addition, an inelastic peak is observed at lower energies associated with electronic excitation from valence band states. The final state of the inelastic scattering process is often a *valence* exciton in which the excited electrons bound to a valence hole.

In these materials with localized electronic excitations, the inelastic loss processes may still be visible at energies well below the excitation threshold. These inelastic process are very much weaker and correspond to Electronic Raman processes. At and above threshold, these losses evolve into electronic Resonant Raman processes.

In work reported in this dissertation, we have excited the S $L_{2,3}$ spectra near threshold in CdS, ZnS, MoS_2, WS_2, FeS, NiS and CaS. The effects of near edge excitation are less prominent than in several other system studied, but show a significant enhancement in spectra associated with the upper valence band. We have also measured the Zn $M_{2,3}$ spectra near threshold in ZnS and ZnSSe alloy and find a strong inelastic scattering process associated with the Zn d-states.

D. Comparison with Other Spectroscopies

There are numerous methods of measuring properties of the electronic band structure of solids. Most of these, other than SXE and SXF spectroscopies, measure electron spectra excited by either photons or electrons. Ultraviolet photoemission spectroscopy (UPS), Photon Emission Spectroscopy (PES), and Angle Resolved Photoemission Spectroscopy (ARPES) measure the electronic spectra of photon-excited electrons from filled valence states. UPS and PES spectroscopies provide transition rate weighted measures of Total Density of States (TDOS) of the material. ARPES, which measures both the angular and energy distributions of photoemitted electrons, is a particularly powerful technique because, in favorable cases with single crystals, clean surfaces, an conducting samples, it can map energy bands in momentum space. These valence state spectroscopies provide information similar to that of SXE and SXF spectroscopies, but without either the chemical or angular momentum selectivity.

Auger Emission Spectroscopy (AES) measures the excited electrons produced in the non-radiative de-excitation of a core excited atom. The interpretation of Auger spectra is difficult because both "up and "down" electrons originate in the valence states of the solid, so that the spectra involves a convolution of the TDOS with itself. In practice, it is used principally as an analytical tool to measure concentrations of elements in complex solids. Auger spectra are nearly always excited by energetic e-beams.

Electron Spectroscopy for Chemical Analysis (ESCA) and usually X-ray Photoemission Spectroscopy (XPS) measure electrons photoexcited from core levels, and derive information about bonding of selected elements in complex solids from small shifts in the core level binding energies induced by changes in the charge and chemical state of selected atomic species.

Electron Energy Loss Spectroscopy (EELS), in the transmission (TEELS) or reflection (REELS) geometry, measure the energy losses of incident electrons associated with transitions to the empty conduction band states above the Fermi level of a solid. The technique can provide information about the empty-state TDOS comparable to that provided by SXA spectroscopy, but without either the chemical or angular momentum selectivity.

All of the electron spectroscopies probe the near-surface region of sample, because of the short attenuation lengths for low energy electrons in solids. This makes them particularly valuable for the study of surfaces, but limits their value for studies of bulk states, particularly where easily cleaned single crystal samples are not available. These techniques (except for EELS) also cannot generally probe the lower energy excited states of solids due to the surface coulomb barrier which prevents the escape of excited electrons. Finally, electron spectroscopies are difficult for insulating samples, where sample charging can distort the electronic spectra in an unpredictable way.

In comparison with these spectroscopies, soft x-rays have attenuation lengths in the range of 100 to 1000 Angstroms, so that SXE, SXA and SXF spectroscopies are essentially bulk probes that are relatively insensitive to surface contamination, and are capable of measuring buried impurities, buries layers or other structures. In addition, the techniques are chemically and momentum selective, so that they provide Local, Partial Density of State (LPDOS) information that gives detailed information for comparison with theory, and for the analysis of local bonding information. The chemical selectivity is particularly useful in the analysis of complex solids.

SXE spectroscopy has several major drawbacks, including weak spectra and various broadening mechanisms that limit detail in the spectra. The weak spectra are a

consequence of low radiative yield, and is dealt with primarily through the design of improved soft x-ray spectrometers. Some of the broadening mechanisms, such as core-hole lifetimes and valence-hole lifetimes are also inherent in the technique and cannot eliminated.

The use of photon excitation in SXF spectroscopy rather than e-beam excitation improves SXE spectroscopy in several ways. It eliminates the Bremstrahlung and thus improves detectability of weak spectra. It reduces multiple excitation that can increase spectral broadening in some materials. It permits selective excitation of particular core-levels that can reduce overlap in measured spectra. And perhaps most importantly, it provides new physics associated with inelastic scattering processes observed with near threshold excitation.

Generally, photoemission and SX spectroscopies have different and generally complementary strengths and both are important probes of electronic properties of solids. Table 2.1 provides a comparison of some of the spectroscopies described here.

According to the table, we see that SXF spectroscopy has several advantages, especially the capability of measuring LPDOSs, which makes it a very powerful tool for band structure measurements. The combination of advanced synchrotron light sources and modern SX spectrometers largely overcome the principal disadvantage of low yields and makes possible a new generation of band structure results.

E. Some aspects of theoretical models

This section gives a brief discussion of electronic band structure models and strong correlation approaches used in this dissertation [2.15-2.26]

Table 2.1 comparison of SXES with other methods. All values in units of eV.

Method	incident particle	particles to be detected	Advantages	Disadvantages
SXFS	X (20-1K)	X (20-1k)	clean spectra	Low yield
			low background	High cost
			PDOS(dipole)	
			Good resolution (Fine structure)	
			Bulk sensitive	
			no sample charging	
SXES	e(<35k)	X		Bremsstrahlung high background
				Multi-Excitation
				heating
				low yield
Electron Spectroscopy (UPS, PES XPS)	X (e)	e (to tens k)	High yield	surface sensitive
			Occupied TDOS	broadening
			low cost	charging
			surface sensitive	heating
UPS	X	e (10-50)	as Elec. Spec.	as Elec. Spec.
ARPES	X	e	E vs k	as Elec. Spec.
			other as PES	
EELS	e	e	as Elec. Spec. empty state TDOS	as Elec. Spec.

Our theoretical weapons in understanding electronic properties of these sulfur compounds are standard band structure model calculations such as the older methods usually described as Augmented Plane-Wave method (APW) [2.21-2.22], Linearized Muffin Tin Orbital LMTO [2.23], Tight Binding Approximation (TBA) [2.24], and more recent methods using the Local Density Approach (LDA) [2.25], Green's function based on KKR method [2.26], and so on. They are very good for most of semiconductors, insulators and alloy. But both band structure models and multiple scattering absorption theory are valid only within the weak correlation limits.[2.15] Recent experimental results of 3d, 4d, and 4f materials indicate strong d-d, p-d, d-f interactions can generate spectra with atomic-like behaviors in solids. To explain these results, a strong correlation limit approach- the Crystal Field Multiplet model (CFM) based on the charge transfer hypothesis is introduced.[2.1, 2.15-17] This model as well as Mott-Hubbard model works well for transition metal sulfides and oxides, especially for transition metal elements between Mn and Ni.[2.16-2.18] A real material may be between the weak and strong coupling limits.

The CFM theory deals with charge transfer states in solids by a simple combination of atomic multiplet theory and crystal field theory. According to this theory, a electron moves from a occupied state to a empty state with a charge transfer, the created hole state is strongly coupled with the new particle state into atomic multiplet states by L-S or J-J modes; then coupled states are transformed into the crystal group symmetry and re-grouped. These new features are classified as bonding and non-bonding sets. For transition metal sulfur compounds in Fig 2.5, two non-boning d bands are labeled with T_{2g} symmetry in valence bands, two bonding/antibonding d bands with e_g symmetry

located below/above near band gap. Since non-bonding bands are weakly interacting, the two T_{2g} bands are sharper and have lower energies.

Calculations derived from band structure calculations, scattering theory, crystal field multiplet approximation and Mott-Hubbard models are used as for a comparison to experimental spectra in present study.

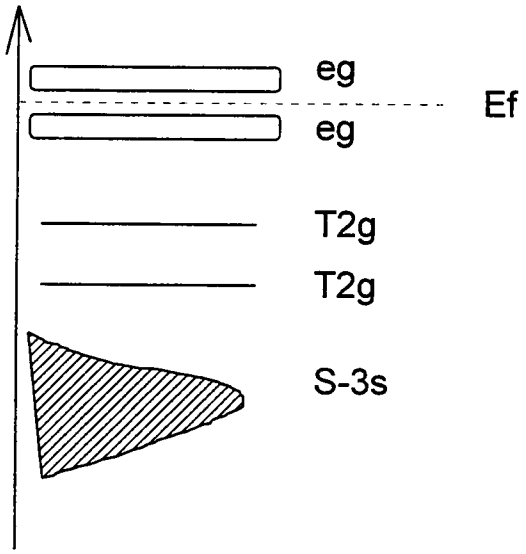

Fig 2.5 The d bands in TMS from CFM model.

Chapter III

Experimental Equipment and Procedures

A. Experimental Arrangement of SXES

The experiments described in this dissertation were performed, before 1994, at a soft x-ray beamline at National Synchrotron Light Source (NSLS) at the Brookhaven National Laboratory (BNL), and since summer, 1994 at beamlines at Advanced Light Source (ALS) at Lawrence Berkeley Laboratory (LBL), and at the Center for the Advanced Microstructure and Devices (CAMD) synchrotron light source at Louisiana State University (LSU).

The beamlines at NSLS and CAMD are very similar. For each of them, exciting photons are provided by a bending magnet source and a high throughout, variable-line-space (VLS) monochromator. The principle difference in the NSLS and CAMD setups is that the NSLS beamline used the e-beam of the synchrotron light source as the input slit for the monochromator, while the CAMD beamline adds a prefocusing mirror and input slit to improve stability and resolution of the exciting light. A schematic diagram of the NSLS beamline is show in the Fig 3.1. In this design, light from the synchrotron source is refocused at unit magnification by a large toroidal mirror with 2° angle of incidence. A plane, fixed, VLS grating disperses the light onto a focal plane with a fixed focal length. The spectrum is scanned by a plane mirror which scans through the spectrum along the exit axis of the monochromator. The principle design characteristics of the monochromators at NLSL and CAMD are summarized in Table 3.1 and have been

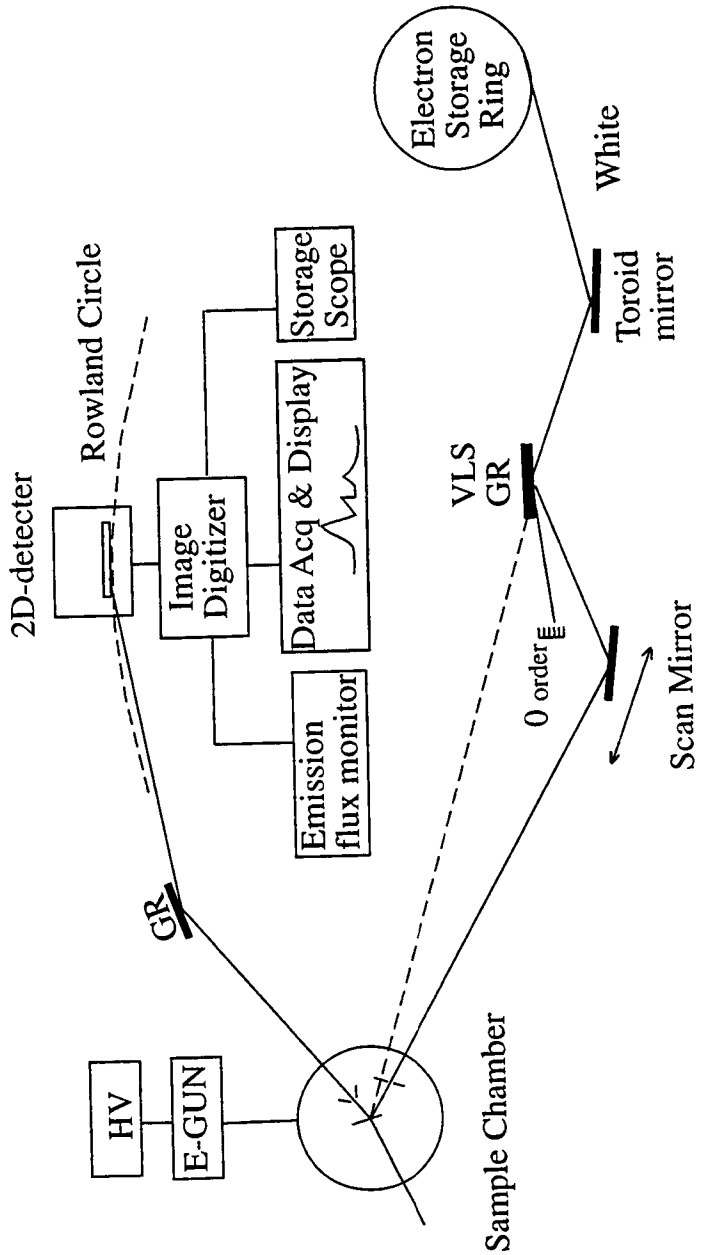

Fig 3.1 Experiment arrangement for SXF spectroscopy at NSLS, BNL.

Table 3.1. Design parameters for two grating monochromators in NSLS and CAMD. All dimensions in cm.

	NSLS	CAMD
Premirror	no	Gold-Colted-glidcop-toroid, 320 cm focal length(1:1), 2° incident
Entrance slit	no	Yes
Dimension: S_1 to S_0	640	1068
Focus Mirror(M1):		
Material	nickel coated, bent cylinder toroid on silica blank	nickel coated, bent cylinder toroid
Blank size	7.5 x 30	
Illuminated area	5 x 20	
Acceptance angle	16 mrad x 2 mrad	16 mrad
Grazing angle of incidence	2°	2°
Radii of curvature	Rm=9.170, Rs=11.2	
Grating(G):		
Material	gold coated ULE blank	gold coated plane
Ruling size	4 x 10	4 x 10
Nominal line density 1/d0	1000 l/mm	1000 l/mm
Grazing angle of incidence	4°	3°
Blaze angle	2°	2°
Plane scan mirror(M2):		
Material	nickel coated silica	nickel coated fused quartz
Blank size	5 x 12.5	same
Grazing diffraction angle scanned	$2° \leq \theta \leq 9°$	same
Grazing angle of incidence, Δ	$6° \leq \Delta \leq 12°$	same
Flux at 100Å(Photon/(S/0.2Å))	$3 \times 10_{12}$	
Gratings	300, 600,1200 l/mm	300, 600, 1200 l/mm
Photon energy(eV)	50-300	100-800

described in other publications.[3.1, 3.2] The notation of Table 3.1 is keyed to elements identified in Fig 3.2.

The monochromator delivers light to an UHV sample chamber onto a sample that can be rotated about an axis perpendicular to the excitation and emission axes, so that the

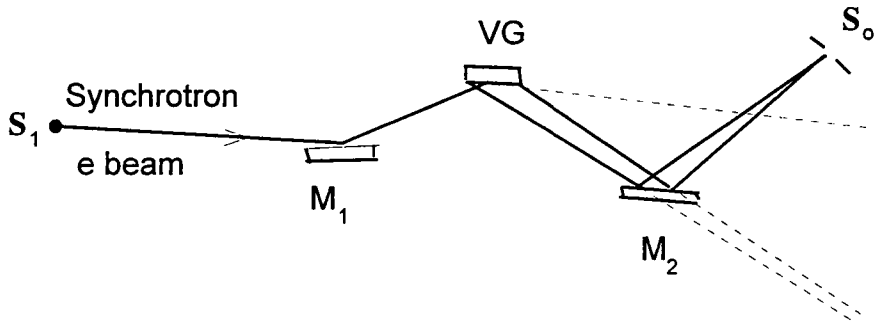

Fig 3.2 The optical setup for a spectrometer with the source at S_1. These notation are used in Table 3.1.

excitation and emission angles can be varied. In the NSLS and CAMD facilities, emitted light was analyzed by the same grazing incidence spectrometer. All reflections and dispersions in both the beamline monochromator and the emission spectrometer are in the vertical plane with the exciting and emission axes separated by 30°. Since synchrotron light is polarized in the horizontal direction, this geometry assures that the electric field vector remains in the plane of sample, traditionally called the s-polarization direction.

An electron gun is also mounted in the sample chamber, which can be used for exciting SXE spectra. This gun provides exciting energies in the range of 1-3 KeV, and

currents of ≤ 0.3 mA. Most of the e-gun excited spectra in this dissertation were excited with 3 KeV electrons at beam currents below 0.1 mA.

The emission spectrometer is a Rowland Circle design which has several features that greatly increase its measuring efficiency as compared with conventional designs. It is fitted with four interchangeable toroidal gratings, which optimize the spectrometer for different energy ranges. The input slit of the monochromator is located within a few mm of the sample surface, so that the large gratings can be filled directly through the input slit. And a photon counting area detector is used which images an extended segment of the dispersed spectrum. The spectrometer design parameters are summarized in the Table 3.2 and have been described in other publications.[3.3] For the sulfur spectra, which are the principle subject of this dissertation, 100 μm spectrometer slits and the 600 l/mm grating provided an energy resolution of 0.3 eV at 150 eV energy of the sulfur spectrum. With the 1200 l/mm grating the resolution is 0.15eV.

The ALS beamline differs significantly from those at NLSL and CAMD. The source of light is an undulator which provides light with about 50X the intensity of the bending magnet sources. The extra intensity and a high resolution spherical grating monochromator makes it practical to excite spectra at high resolution. The beam energy pass is 0.4eV at ALS, compared with 2eV at NSLS at 163ev photon energy. The ALS beamline is equipped with a somewhat improved emission spectrometer, but is similar to that used at the NSLS. The major difference is that the optical plane of the spectrometer is in the horizontal plane and the sample rotation axis is vertical, so that spectra are excited with p rather than s polarized light. The ALS beamline is shown schematically in Fig 3.3. Its properties have been described elsewhere in detail.[3.4]

Table 3.2 Soft X-ray spectrometer design parameters.

Type	Grazing incidence, 5m Rowland circle
Features	2mm sample to input slit distance four interchangeable gratings area detector
Incidence angle	4°
Scanning angle	78°- 86°
Range	20-1000 eV (600 -12 Å)
Resolution	0.125-1.0 Å
Gratings	4 cm x 10cm; Au on SiO_2
Radii	5m x 0.5m
Line densities	300, 600, 1200, 2400 /mm
Blaze	2°
Detectors	MCP with resistive sheet anode

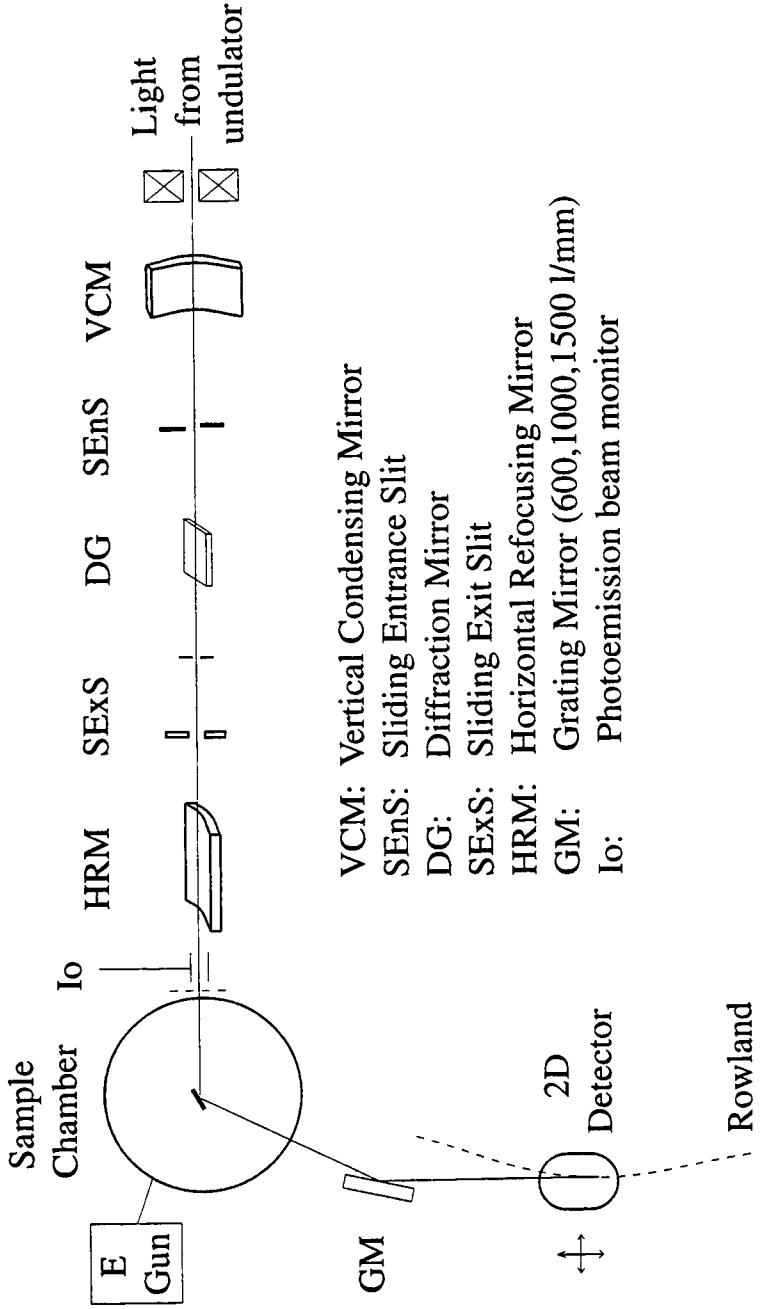

Fig 3.3 The simplified light path at ALS, LBL.

The photon counting area detector of each spectrometer is located tangent to the Rowland circle.[3.5] X-ray photons are incident on a 40mm diameter microchannel plate(MCP) over coated with MgF_2 to improve the quantum efficiency and resolution. A stack of 5 MCPs provides about 10^7 amplification of initial photoelectrons. The charge pulse from the MCPs falls on a resistive sheet detector and flows to its four corners. The X-Y position of particle on the detector is read out according to the scheme X=(2+3-1-4)/(1+2+3+4) and Y=(1+2-3-4)/(1+2+3+4), where corners are counted clockwise from the upper left. The detector provides a resolution of about 25μm. This detector is extremely effective for very low light signals because it has good quantum efficiency and is a true photon counting device. It is limited to a total count rate over the whole detector of about 10^5 cts/sec, so that it is not suitable for use with intense spectra.

B. Data Acquisition.

The photon counting area detector has been described briefly in the preceding section. Here we describe the electronics and software used to prepare the data for analysis. The Fig 3.4 shows the major steps in this process.

The MCP/resistive sheet detector and readout electronics are commercially available electronics from Quantar Technology. The charge pulses from corners of the detector are summed as noted above to produce analog pulses giving the X and Y positions. These pulses are then processed as a gated analog signal for real time readout to a storage oscilloscope, and as a digitized Xi, Yi signal for output to fast FIFO buffer memory in a CAMAC crate. A Macintosh (NSLS, CAMD) or PC (ALS) computer controls the data acquisition electronics and all detector scans via a IEEE 488 interface to the CAMAC crate, and a DMA channel to the buffer memory. Within the computer, raw

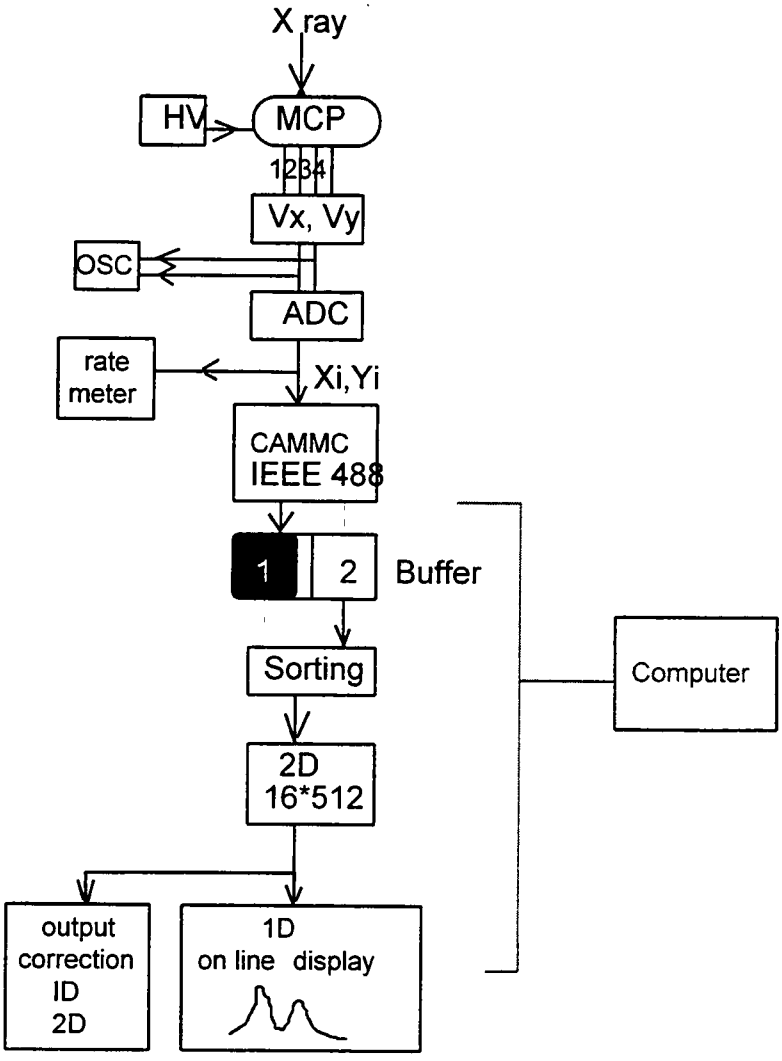

Fig 3.4 The data acquisition in the NSLS, BNL.

data is accumulated in 512 (or 256) by 16 array. The 512 slices are in the X or dispersion direction and the 16 slices in the Y or transverse direction. This array is the raw data which is retained intact, and used for all further data manipulation and analysis.

Further analysis of the data is illustrated in Fig 3.5. The spectrum incident on the detector has curvature due to optical aberrations in the spectrometer as shown in the top illustration. By shifting the 16 slices slightly, this curvature is removed. For real time monitoring, the 16 slices, or a selected subset, are then summed to produce a 1D spectrum. For more precise analysis, each bin is multiplied by a transition factor which compensates for non-uniformities in the detector response. The transmission factor file is determined in a separate experiment. The 16 slices are then summed to produce 1D spectrum used for further analysis.

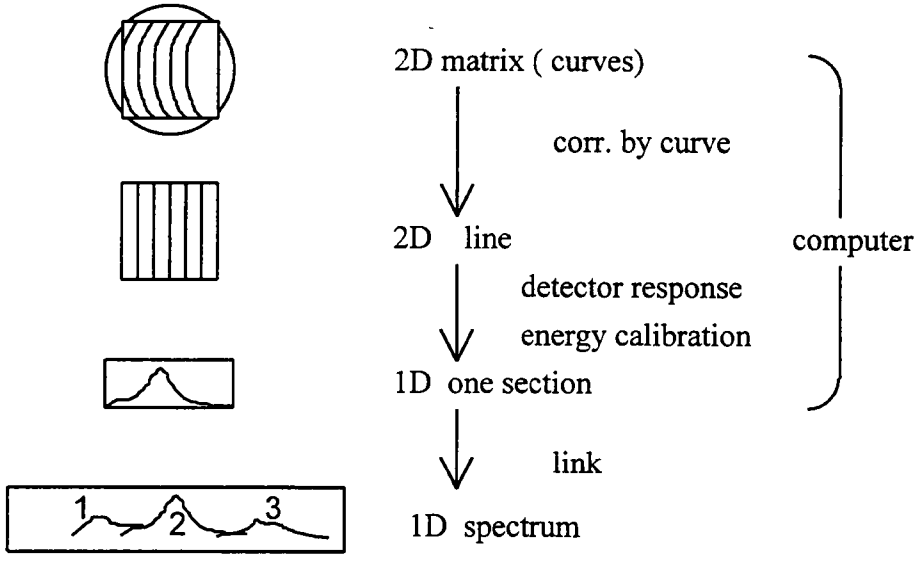

Fig 3.5 Corrections of spectra.

If the spectrum covers a wider energy range than can be acquired in a single 2D frame, the detector is moved along the Rowland circle and several overlapping 1D frames are acquired. These overlapping 1D spectral segments are then joined smoothly. If this operation can be carried out successfully, it is taken as evidence that the background subtraction and transmission corrections are satisfactory. Usually the very ends of the spectral segments have uncontrolled aberrations and are discarded from the data.

Calibration of spectrometer in the energy range of present experiments are based on the Fermi edge of emission spectra of metal Al (72.5eV), and on the exciton peaks in BN(188eV).

C. Sample preparation.

The CdS sample is a bulk crystal with the Wurtzite structure grown by molecular beam epitaxy (MBE). The cubic ZnS thin film samples with (001) and (111) orientations and thickness of 5200 Å and 2100 Å respectively and the ZnS_xSe_{1-x} sample were grown at ORNL as epitaxial films on GaAs (001) substrates by pulse-laser ablation of semiconductor alloys.[3.6] CdS samples were freshly cleaved just prior to inserting into the sample chamber. All other samples were etched in dilute H_2SO_4/H_2O immediately before loading to remove oxide layers and contaminants.

The powder samples, MoS_2 (99%, Hexagonal), WS_2 (99.8%, Hexagonal), α-SnS (99.5%, Orthorhombic), NiS(99.995%, Hexagonal) and FeS(99.9%, Hexagonal) were pressed into pills by applying a pressure of a few tons. These samples have a smooth, shining surface. Commercial single crystal GaS (99.999%, Hexagonal) was used directly due to its the natural shiny surface. C and O contamination were found in the FeS samples. CaS and MgS are powder samples.

Samples were loaded in the experimental vacuum chamber, which was typically operated in the range of (5-9) x 10^{-9} Torr for e-beam excitation experiments, and in the range of (1-5) x 10^{-9} Torr for experiments using synchrotron beam.

Chapter IV

CdS and ZnS

As the first step, CdS and ZnS were studied due to the availability of good theoretical studies. The sulfur $L_{2,3}$ soft x-ray emission spectra of wurtzite CdS and cubic ZnS and the zinc $M_{2,3}$ spectra of ZnS were measured using both e-beam and photon excitation, and analyzed to determine the S and Zn (s+d)-Local Partial Density of States in these materials. Broad features of the $L_{2,3}$ spectra, derived from the sulfur s-orbital, are typical of materials with mixed ionic-covalent character. Narrow peaks associated with overlap of the Zn-3d and Cd-4d orbital onto the S site are used to precisely locate these bands with respect to other band structure features. Band gaps and valence hole life time broadening were determined. These data are also used to determine spin orbit splitting and to separate overlapping S L_2 and L_3 spectra. Using photon energies near threshold, structural features in the sulfur $L_{2,3}$ spectra show **only small** changes in intensity with photon energy. **For Zn $M_{2,3}$ spectra, however, excitation near threshold produces very striking spectral features that indicate strong contributions from inelastic scattering processes.**

A. Semiconductor CdS and ZnS

The II-VI sulfur compounds CdS and ZnS and related semiconductor alloys have important applications in modern science and technology. For example, light emitting diodes utilizing ZnSxSe1-x provide intense light ranging from blue to violet which may be tuned by varying the direct band gap by controlling the S concentration [4.1, 4.2]. The

electronic properties of CdS have attracted attention by its application in solar cells [4.3, 4.4]. The design of such electronic devices is based on a detailed knowledge of electronic band structure. In addition, the zincblende structure of ZnS and wurtzite structure of CdS are relatively simple and well characterized so that these materials are good candidates for theoretical model development in solid state physics. Some theoretical calculations of ZnS [4.5-4.15] and CdS [4.16-4.21] have been reported. Some experiment results on density of states, mostly determined from photoemission measurement, have been reported for CdS [4.22- 4.29] and ZnS [4.22, 4.25, 4.26, 4.29].

The electronic properties of IIB-VI compounds with IIB elements Zn, Cd, and Hg and VI elements S, Se, and Te are still not completely understood. It is now established experimentally that the d-bands, derived from the IIB elements, lie in the sub-band gap between the lower valence band derived from the s-orbital of the group VI elements and the upper valence band derived from the p-states of the group VI elements and the s states of the IIB elements. The locations of these bands within the gap disagree with the best available calculations, however.

The problem may be traced to the difficulty of treating de-localized s-p electrons and localized d electrons in the same calculation. Older calculations, using OPW and KKR methods, are well adapted for treating s-p bands, but usually ignored the d bands altogether, treating them as part of a frozen core. More current calculations use psudopotential plane wave and linearized augmented plane wave methods and the local density approximation (LDA). These calculations, in common with most LDA calculations, underestimate the measured band gaps between valence band and empty conduction band states. They also locate the d bands higher in the sub-band gap than is observed in photoemission. The latest GW calculation on CdS has improved band gap

essentially. But the d location is still about 15-20% higher than experimental results.[4.21] Some authors argue that this discrepancy between theory and experiment results from the fact that the photoemission process leaves a hole in the d bands which increases the apparent binding of the d-electrons. In any case, band gaps, sub-band gaps, band widths and the precise locations of 3d (ZnS) and 4d(CdS) bands are important parameters for comparing experiment with theory, and no current calculations give good agreement with all of these parameters.

Some experimental data providing electronic density of states information is available for ZnS and CdS. Data are available from UV photoemission spectroscopy (PES) [4.25, 4.26], angle-resolved photoemission spectroscopy (ARPES) [4.4, 4.24] and x-ray photo-emission spectroscopy (XPS) [4.8, 4.25, 4.30]. In photoemission, the 3d (Zn) and 4d (Cd) electron spectra are very intense and dominate the weak s emission. This fact, in combination with problems of sample charging, limits resolution for both the d band and s-p band spectra and makes it difficult to precisely determine band widths and separations. A few soft x-ray absorption and emission results [4.22, 4.23, 4.28] have been reported for ZnS and CdS. Good quality K and L spectra were reported for CdS, but an accurate interpretation of the spectra was not given. Soft X-ray Emission Spectroscopy (SXES), when combined with synchrotron radiation excitation, has many advantages for band structure measurement and provides a powerful tool for the study of the electronic density of state.

Recent publications [4.31-4.34] show that the energy position of valence band SXE spectra may shift and the relative magnitude of spectral features may change when spectra are excited by photons with energies near threshold. In Si and Graphite, changes in spectral shape are observed which are attributed to k-conservation between the

photoelectron generated in the excitation process and the valence hole remaining after the coupled emission process.[4.33, 4.34] In BN, photon excitation of a core electron into a core exciton state, rather than the conduction band, results in both energy shifts and changes in spectral shape [4.31]. In this chapter, we report S $L_{2,3}$ SXE spectra excited near threshold for both CdS and ZnS, but find much smaller effects than have been seen with some other materials. It was possible, however, to use excitation between the L_2, and L_3 thresholds to obtain a clean L_3 spectra of S in both CdS and ZnS.

In the remainder of this chapter a brief description of experimental procedures is given in part B, results with some explanations are reported in part C, and are discussed and compared with other work in part D.

B. Experimental Procedures

The SXES equipment at NSLS's is shown in Fig 3.1 of above chapter III.[4.35-4.37] The spectrometer input slit was about 100 μm. Two gratings with groove densities of 600 l/mm and 1200 l/mm were used. With this slit width, the energy resolution of the spectrometer is about 0.3 eV for the 600 l/mm grating and 0.15 eV for 1200 l/mm grating at the 150 eV energy of the sulfur spectrum.

Most of the SXE spectra reported here were measured on beam line U10A of the National Synchrotron Light Source at Brookhaven National Laboratory (NSLS). Some of these spectra have been remeasured at the CAMD with the essentially the same results. Near threshold spectra have also been measured at the Advanced Light Source (ALS) with substantial improvement in resolution of the exciting x-rays. These beamlines have been described in chapter III and in publications [4.38, 4.39]. The sample $ZnS_{0.5}Se_{0.5}$ was provided by ORNL [4.40].

Both e-beam bombardment and photon excitation were used in our experiments. Electrons with energies of 1 to 3 KeV and beam currents of $\leq$ 0.05 mA were used. Photon excitation was accomplished with photon energies of 140-180 eV and an energy resolution of 0.4 eV at ALS and about 2eV at NSLS.

During measurements with e-beam excitation, pressures were $\leq 5 \times 10^{-9}$ Torr and with photon excitation, $\leq 1 \times 10^{-9}$ Torr. The excitation region with e-beam excitation was a spot of $\leq$ 0.2 mm diameter, and with photon excitation a rectangle with dimensions of approximately 0.2 mm x 1.0 mm. Visible luminescence from the samples greatly simplified proper alignment of the electron or photon excitation beam.

Several different experiments were performed. Using 3 KeV e-beam excitation, the S $L_{2,3}$ and the Zn $M_{2,3}$ spectra of CdS, ZnS, $ZnS_{.51}Se_{.49}$ and ZnSe were measured. Measurements were also performed on CdS and ZnS with 1.5 KeV excitation to check for the effects of self absorption on the emission spectra. No significant differences in the spectra were observed. The sulfur spectra were also measured with 174 eV photon excitation, an energy well above the sulfur $L_{2,3}$ threshold in order to compare spectra excited by electrons and photons. Finally, for ZnS and CdS, spectra were excited for a range of energies near threshold in order to look for modifications of the spectra with near threshold excitation. The fact that spectra did not change with e-beam excitation energy between 1 and 3 KeV is taken as evidence that the spectra are characteristic of the bulk.

For the threshold studies, spectra are normalized to the incident flux taken to be equal to the beam current (I_b) times the exposure time (Δt). We also obtain some relatively crude data on the absorption near threshold by plotting the total fluorescent yield determined as

$$Y(E) = \text{Spectral area} / (I_b \times \Delta t).$$

as a function of photon energy E. I_b was taken from direct beam value at NSLS and CAMD, and from Io, the current monitor in the incident light path of ALS as shown in Fig 3.2. These measurements determined the absorption threshold with sufficient accuracy to permit us to determine the band gap near threshold.

C. Results

We first present data obtained for the sulfur $L_{2,3}$ spectra. Fig 4.1 depicts these spectra for ZnS (001) and CdS (wurtzite) with 3 KeV e-beam excitation at NSLS. The spectra of CdS and ZnS are very similar, but with some difference in detail. Three spectral features are present which can be identified with large scale valence band features. The largest peaks at the lowest energy position, which peak at 148.7 eV for ZnS, 148.6 eV for CdS, are derived from the sulfur s-orbital. Measurements on a variety of sulfur compounds reported in subsequent chapters also show a strong peak at nearly the same energy position. A relatively weak shoulder or peak located at the top of the spectra at about 156 eV for ZnS and 157 eV for CdS is located at the position of the primarily p-orbital at the top to the valence band. Its presence in the spectra is evidence of the covalent bonding which contributes to the stabilization of the tetrahedral coordinated wurtzite and zincblende structures.

The most interesting feature is the narrow peak located at 151.4 eV in CdS and at 152.1 eV in ZnS. We believe that these peaks are derived from the Zn 3d and Cd 4d orbital that overlap onto the sulfur site. Theoretical calculations agree that in these compounds, the d-states form a narrow band lying in valence band sub-band gap associated with the ionic potential of these II-VI compounds [4.8]. The location of this d-band lying in the gap between the two valence bands has also been confirmed from

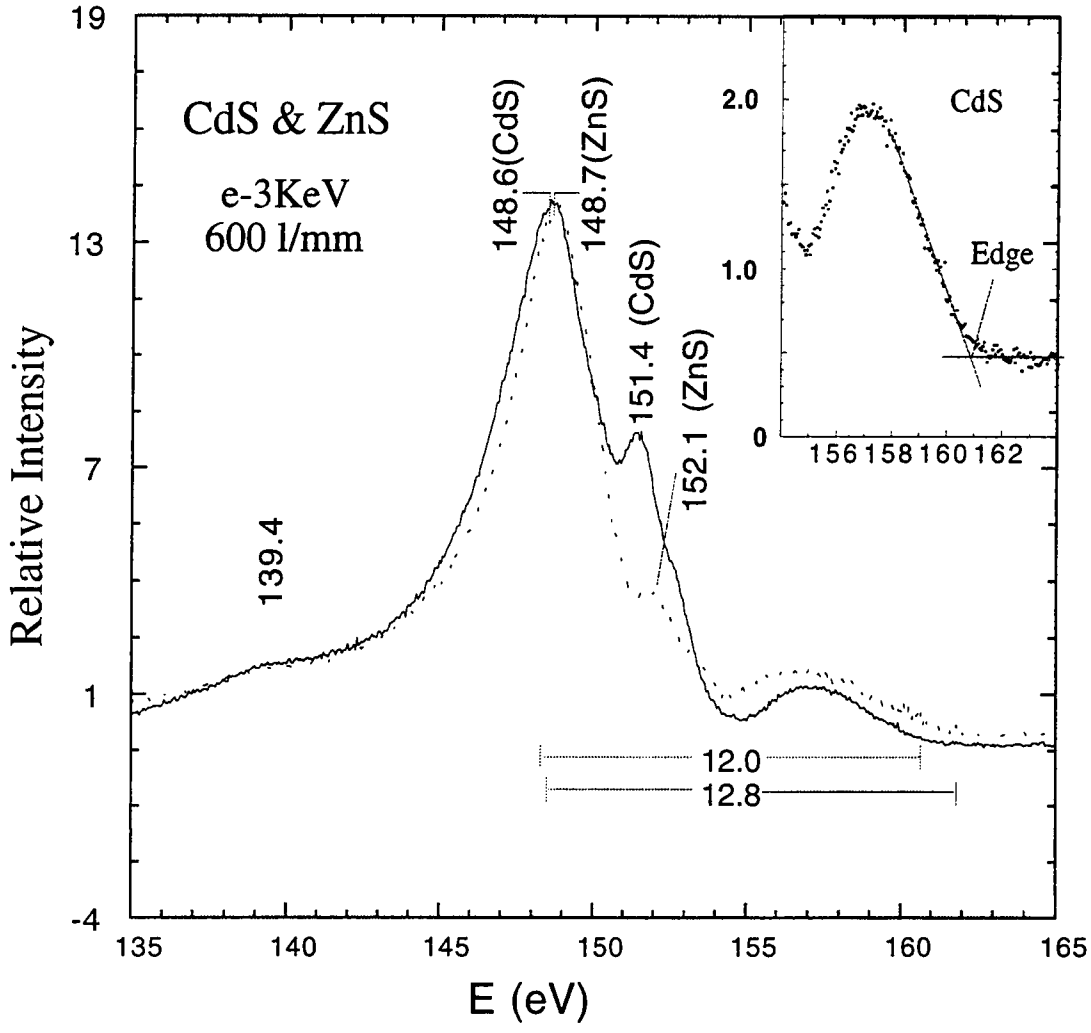

Fig 4.1 The $L_{2,3}$ soft x ray spectra of CdS and ZnS with 3 KeV e-beam excitation at NSLS. The solid line is for CdS. The dashed line is ZnS. The insert shows spectra at valence band maximum.

photoemission measurements for ZnS, CdS and HgS [4.29]. Data from this study is included in Table 4.1 which is described further below.

A low energy satellite is observed about 9 eV below the sulfur s-band. It probably results from a "shakeup" process in which a valence band to conduction band electronic transition reduces the energy of the radiated photon

The upper edge of valence band (VBM) is determined as shown in the insert of Fig 4. 1 from the crossing point of the extrapolated spectral edge and the base line. This value of the VBM is properly associated with the L_2 edge which lies above the L_3 edge by the value of the spin-orbit splitting of the sulfur 2p core levels. A correction for this splitting must be made before comparisons with theoretical densities of states are made.

Figs 4.2a and 4.2b exhibit sulfur $L_{2,3}$ spectra from CdS and ZnS excited by electrons at NSLS (solid line) and photons at ALS (dashed line). The most notable feature is that the photon excited spectra are greatly sharpened with respect to the e-beam spectra. In the photon excited spectra, the doubling of the sulfur s-bands and Cd(Zn) d-bands due to the spin-orbit split core levels are clearly resolved. Both the 1:2 intensity ratio of spin-orbit split d bands and their separation of about 1.1 eV are consistent with the spin-orbit splitting of sulfur 2p core level. The observed spectra can be interpreted in a straightforward manner as the superposition of an L_3 spectrum and an L_2 spectrum of half the intensity displaced to higher energy by 1.15 eV. Another surprising thing in the ZnS spectra is that the photon excited spectra are much more asymmetric than the e-beam spectra for the valence s bands. All these spectra are lined up with sharp d bands. The energy positions of various features of these CdS and ZnS sulfur L spectra taken from Figs 4.1 and 4.2 are summarized in Table 4. 1.

Table 4.1 Energy positions of major features in the $L_{2,3}$ SXE spectra of ZnS and CdS.

All in units of eV.

ZnS	$L_{2,3}$(EB)	Ref.[4.29](EB)	Ref.[4.23]	L2,3(NSLS,photon)	L3(ALS)
LVB peak	148.7	148.4		148.8	148.5
d1	152.1	152.0		152.2	152.2,(151)*
d2	153.2	153.1		153.3	
UVB peaks	156.5	157.8		156.3, 158	155.8, 157.7
VBM	161.5	161.5		160.6	160.6
CBM				164.25(abs.)	
CdS					
LVB peak	148.6	148.4	148.1	148.4	148.5
d1	151.4	151.0	151.1	151.3	150.5, 151.6
d2	152.6	152.2	152.2	152.5	
UVB peaks	157	156.7	156.4		156.7, 158.8
VBM	161.5	162		160.3	160.5
CBM				162.95(abs)	

Key to abbreviation in Tables: abs - from absorption data; EB-e-beam excitation; Photon - photon excitation; L3(ALS) - measured with photon energy low than L2 threshold at ALS; LVB - lower valence band; UVB - upper valence band; VBM - valence band maximum; CBM - conduction band minimum. * Estimated from ZnS spectra.

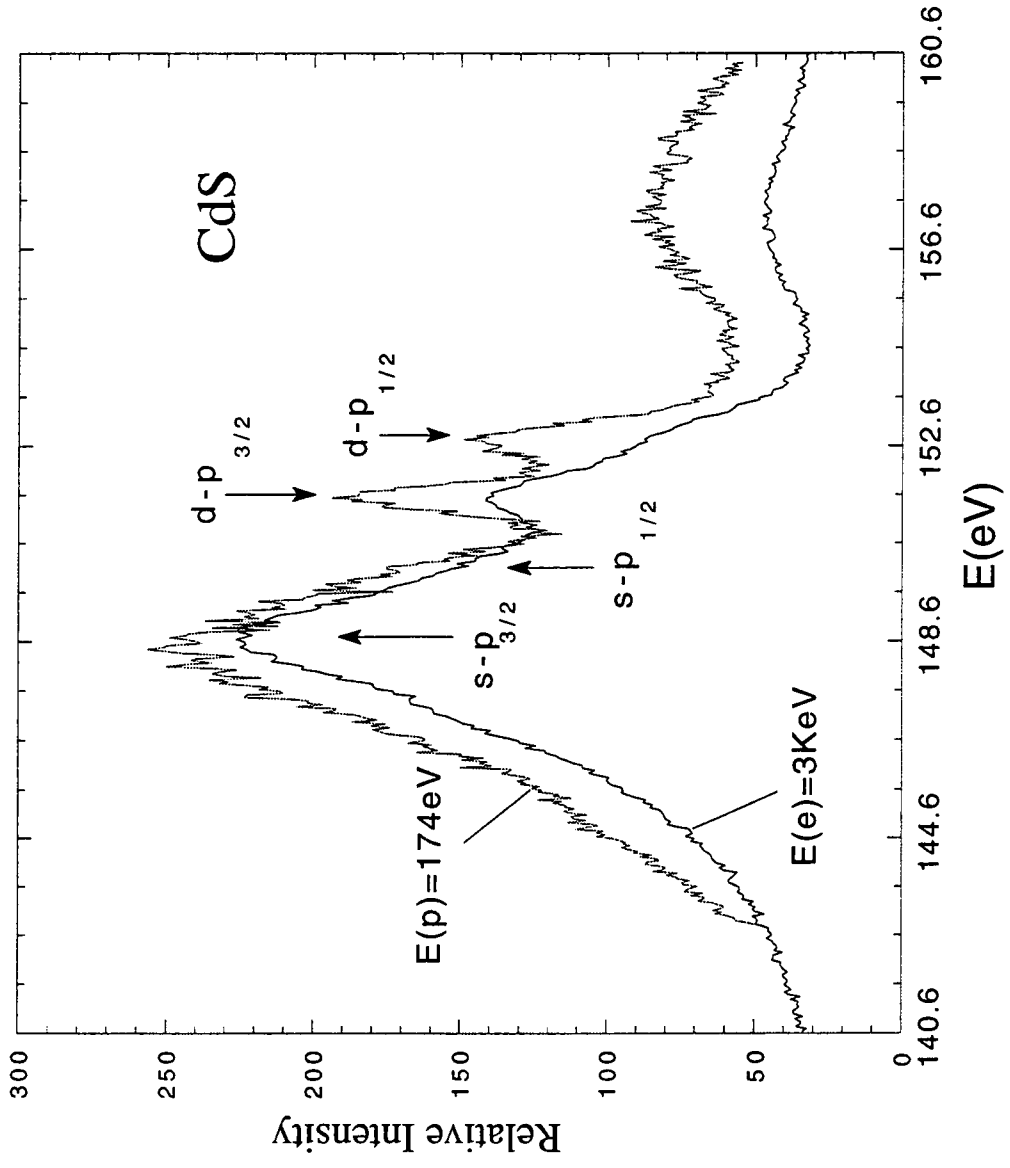

(a). CdS .

Fig 4.2 Comparison of $L_{2,3}$ spectra for 3 KeV e-beam and 174 eV photon excitation.

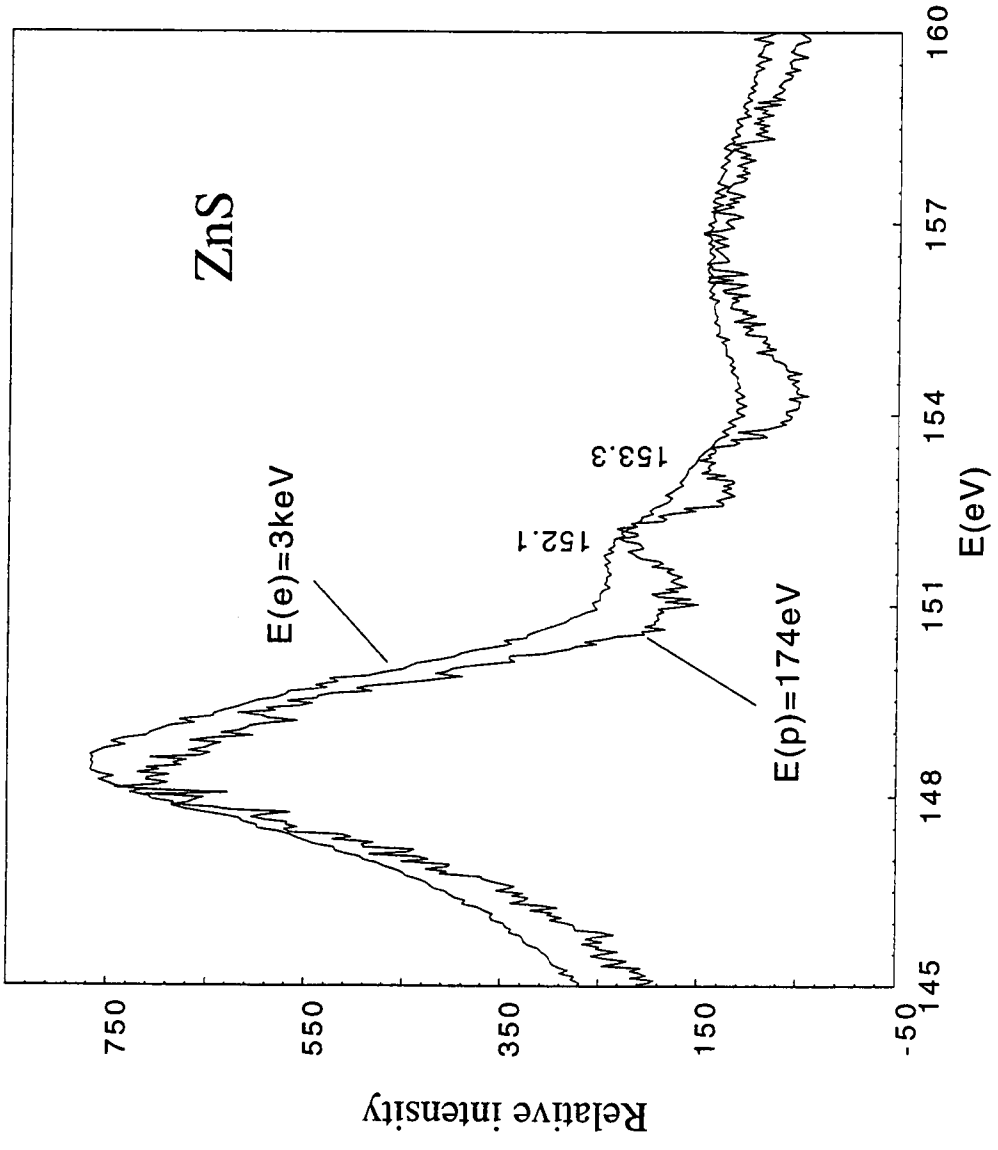

(b). ZnS.

Fig 4.2 (continued)

The L_3 spectra can be obtained from a deconvolution of $L_{2,3}$ spectra using an L_2/L_3 intensity ratio of 1/2 and a spin-orbit splitting of 1.15 eV. It is more accurate, however, to use the improved intensity and resolution of the ALS beamline to tune between the L2 and L_3 thresholds in order to excite the L_3 spectrum alone. Spectra obtained in this way are shown for CdS in Fig 4.3 and ZnS in Fig 4.4. Other near threshold excitation spectra are presented in later paragraphs. These spectra are divided by E^3, a factor which in the optical transition matrix elements, to make them more directly comparable with calculated densities of states.

The L_3 spectra show several important features that are obscured in the $L_{2,3}$ spectra. Both the upper and lower edges of the valence band(UVB) and its broad structural features are resolved. The detection of the L_2 spectrum from the upper edge of the lower valence band(LVB) derived from the Cd and Zn d-states, and allows a more precise determination of the density of states and width of these bands. The remarkable improvement in resolution observed with photon excitation as compared with electron excitation is discussed further in section IV D.

In Fig 4.5a, we display zinc $M_{2,3}$ electron excited spectra for ZnS and $ZnS_{0.51}Se_{0.49}$ taken with e-beam excitation at NSLS. The spectra are normalized to the peak at 74.1 eV. This strong band peaking at 74.1 eV, which decreases in relative magnitude with decreasing S concentration, is the second order sulfur $L_{2,3}$ spectrum. The wider features at 78.5eV and 81.2 eV, which have a separation of 2.7 eV and the intensity ratio of 2:1, are double d bands from zinc 3p core level spin-orbit splitting. The peaks

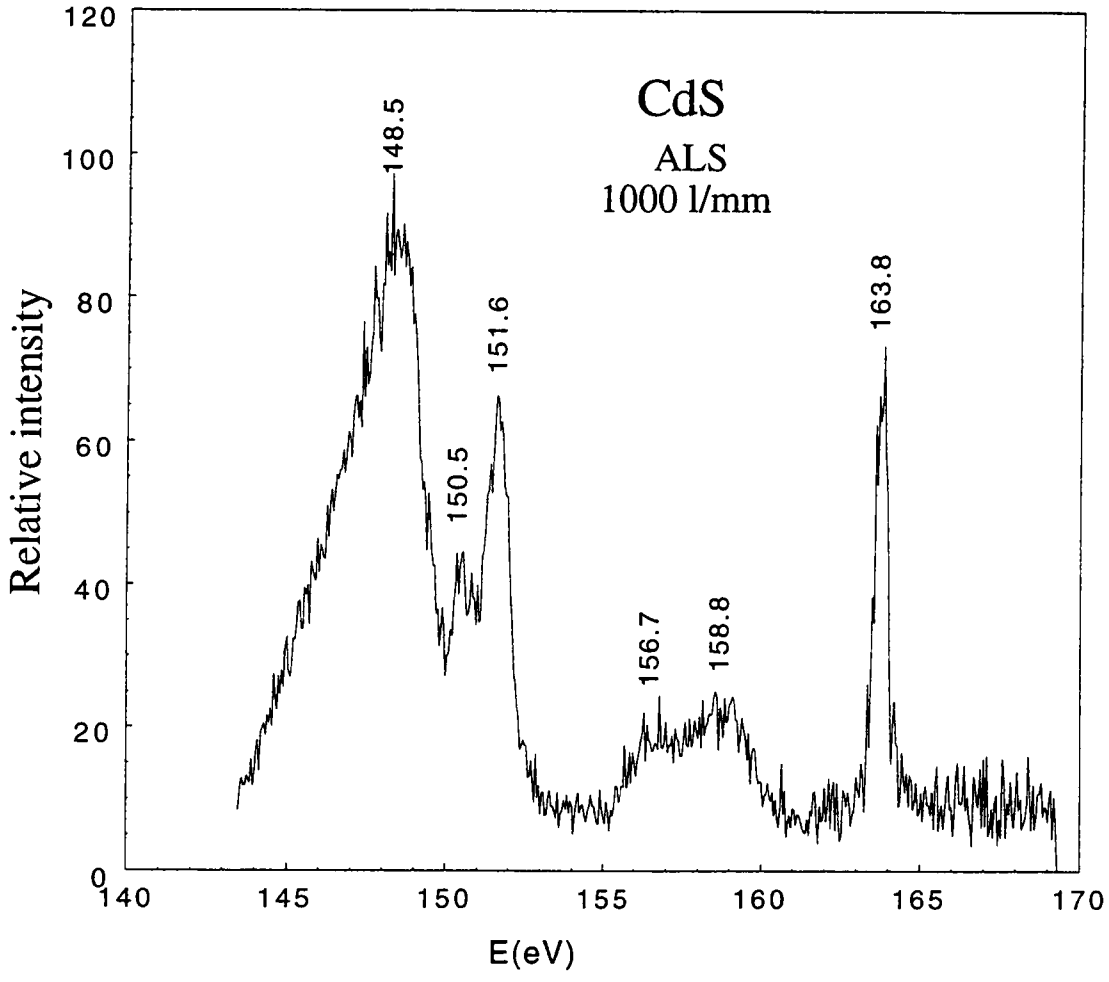

Fig 4.3 The S L_3 spectrum of CdS taken at ALS.

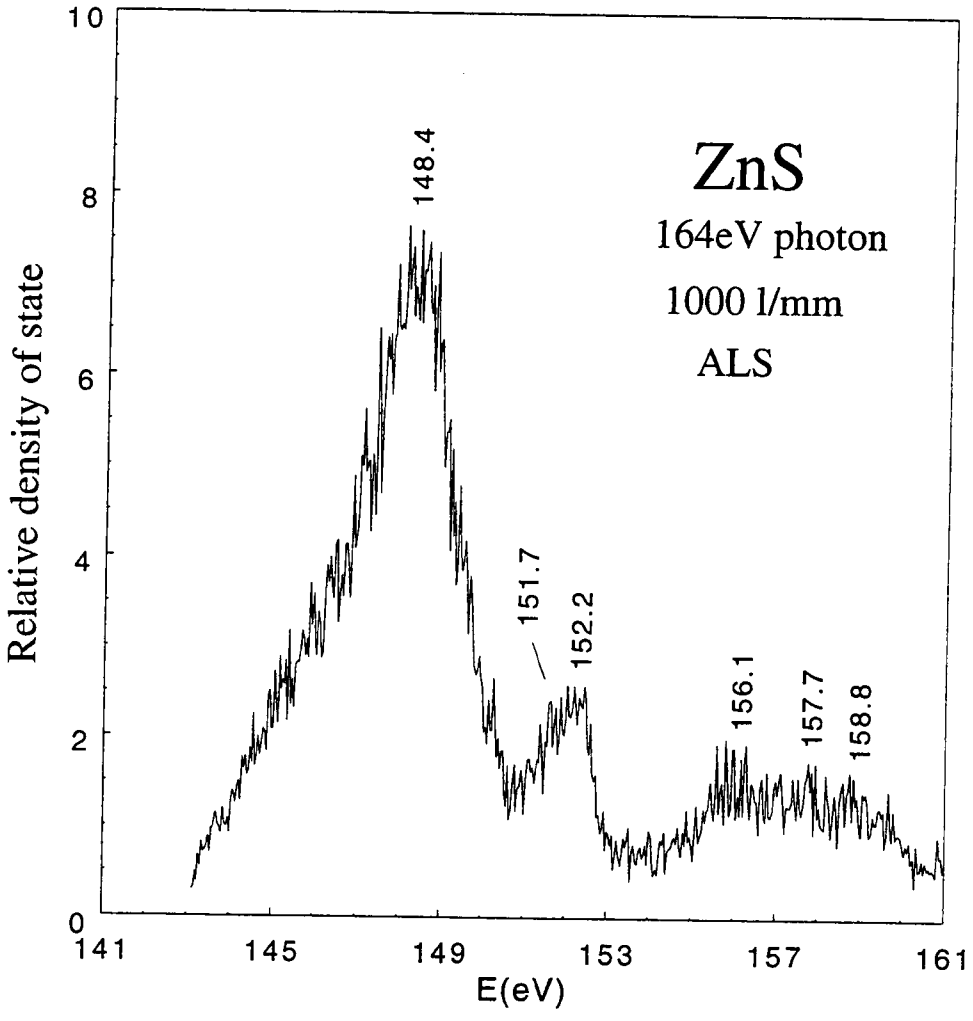

Fig 4.4 S L_3 spectrum of ZnS taken at ALS.

correspond to transitions from the d bands to the $3p_{3/2}$ (M_3 spectrum) and $3p_{1/2}$ (M_2 spectrum) core levels respectively. The structure extending to about 90 eV is derived from the upper valence band. The peak at 93 eV is probably a third order carbon K spectrum associated with carbon contamination of the sample.

In Fig 4.5b, two methods have been used to obtain measures of the zinc $M_{2,3}$ spectra. In one, the first order sulfur spectrum $L_{2,3}$ of ZnS is halved in energy, normalized to the peak at 74.1 eV, and subtracted from the ZnS spectrum in Fig 4.5a. In the other, the ZnS spectrum in Fig 4.5a was subtracted from the $ZnS_{.51}Se_{.49}$ spectrum. In both cases, the broad M_2 and M_3 spectra are resolved. Compared with d bands visible as overlap spectra in the sulfur $L_{2,3}$ spectra, these bands are much broader. The main contribution to this extra broadening is the $M_{2,3}$ core-level lifetime broadening of about 2.0 eV [4.41]. From these spectra we estimate the d-band separation from the VBM to be 8.8 eV. Values derived from the sulfur $L_{2,3}$ spectra are 8.3 eV with photon excited spectra and 8.2 eV from e beam excitation after subtraction of the spin-orbit splitting. In Table 4.2, band structure parameters derived from the zinc M-spectra are presented.

Table 4.2 Energy positions of spectral feature in Zinc $M_{2,3}$ spectra of ZnS. All in units of eV.

	$M_{2,3}$ (alloy, EB)	$M_{2,3}$(127eV, ZnS)
d1	78.5	78.5
d2	81.2	81.3
peaks at UVB	86.6, 88.9	
VBM	89.9	

Key to abbreviation in Table: alloy, EB- data from $ZnS_{0.51}Se_{0.49}$ with e-beam excitation. 127eV, ZnS- data from photon excitation with energy of 127 eV.

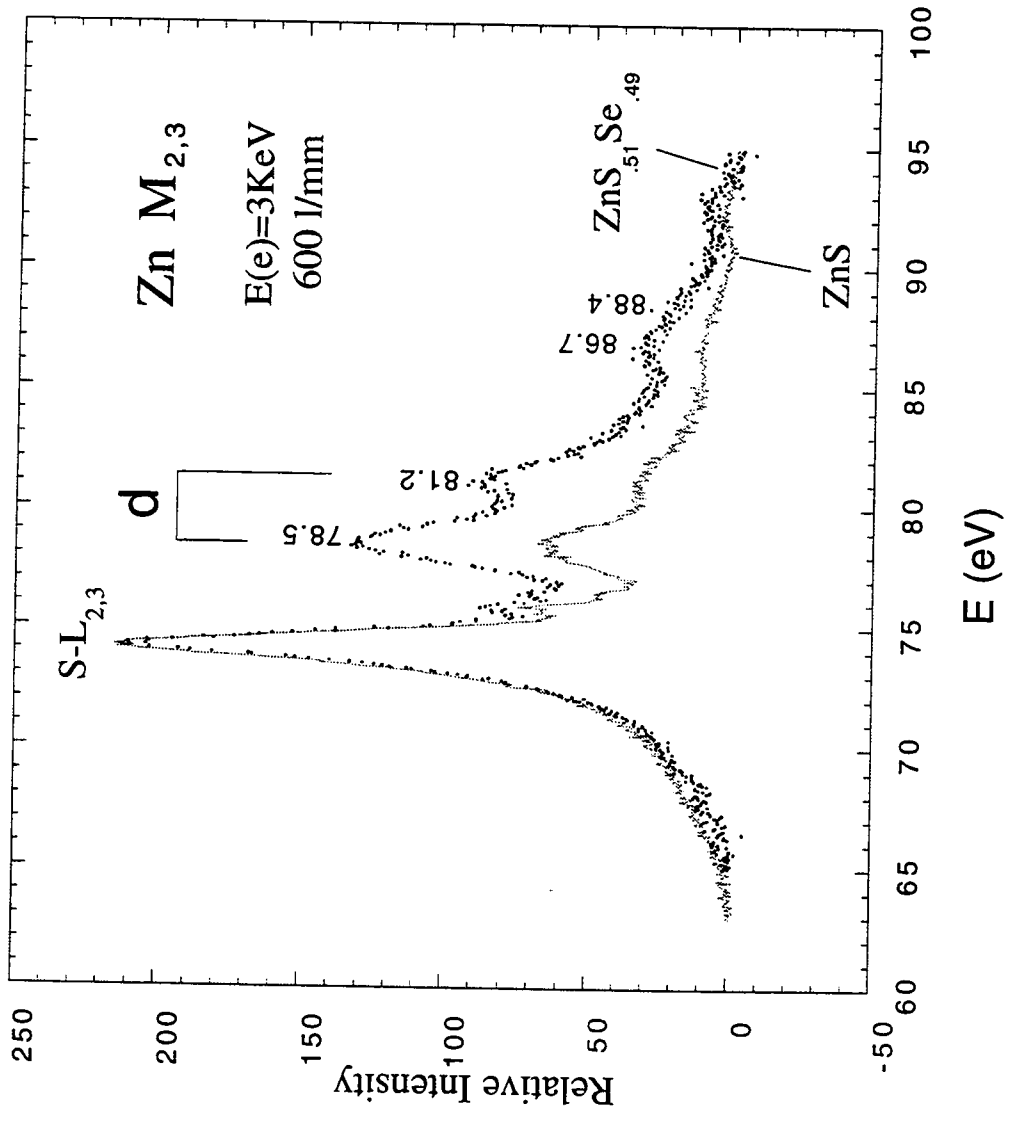

(a) The original zinc spectra.

Fig 4.5 Zn $M_{2,3}$ spectra of ZnS and $ZnS_{0.51}Se_{0.49}$ from 3 KeV e-beam excitation at NSLS.

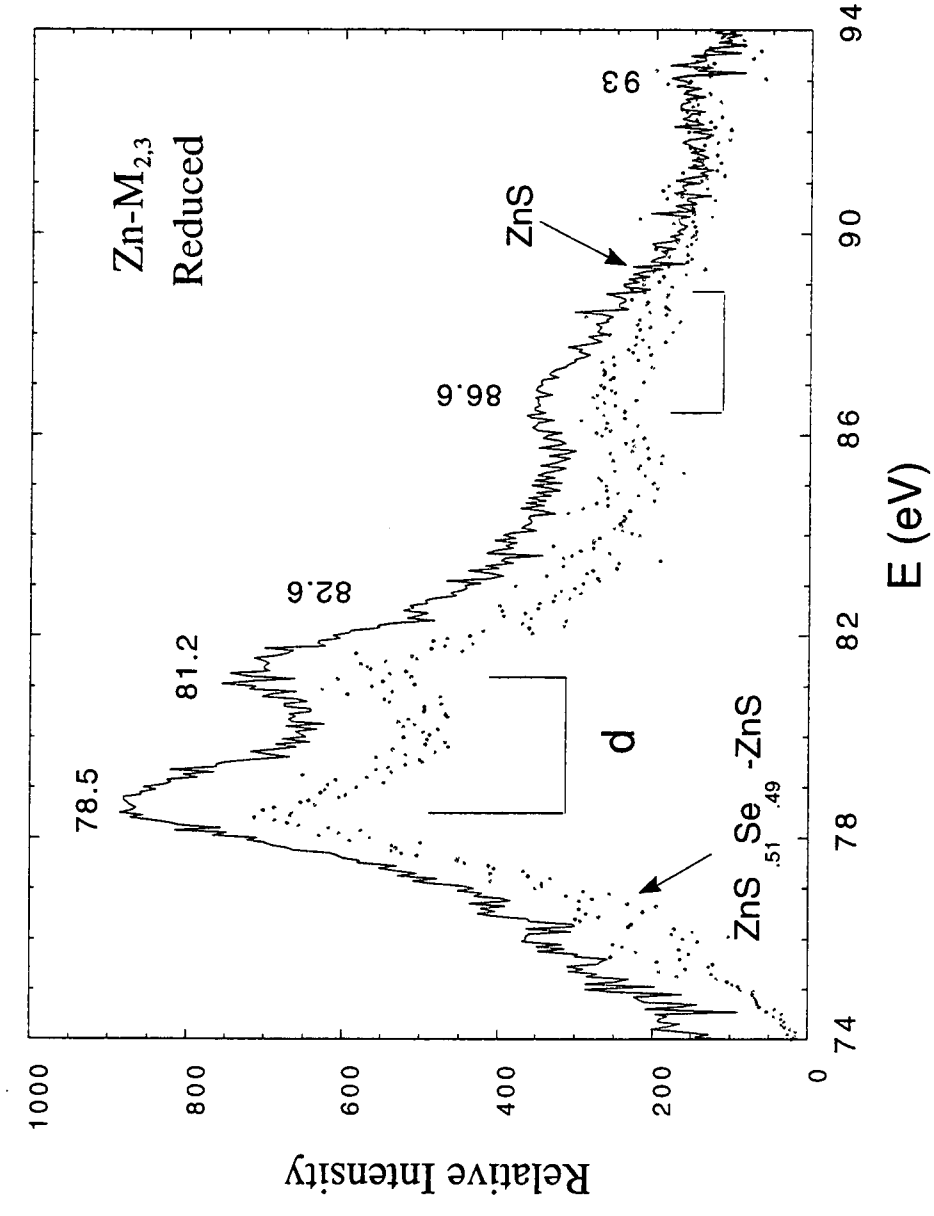

(b) The reduced $M_{2,3}$ zinc spectra of ZnS from (a)

Fig 4.5 (continued)

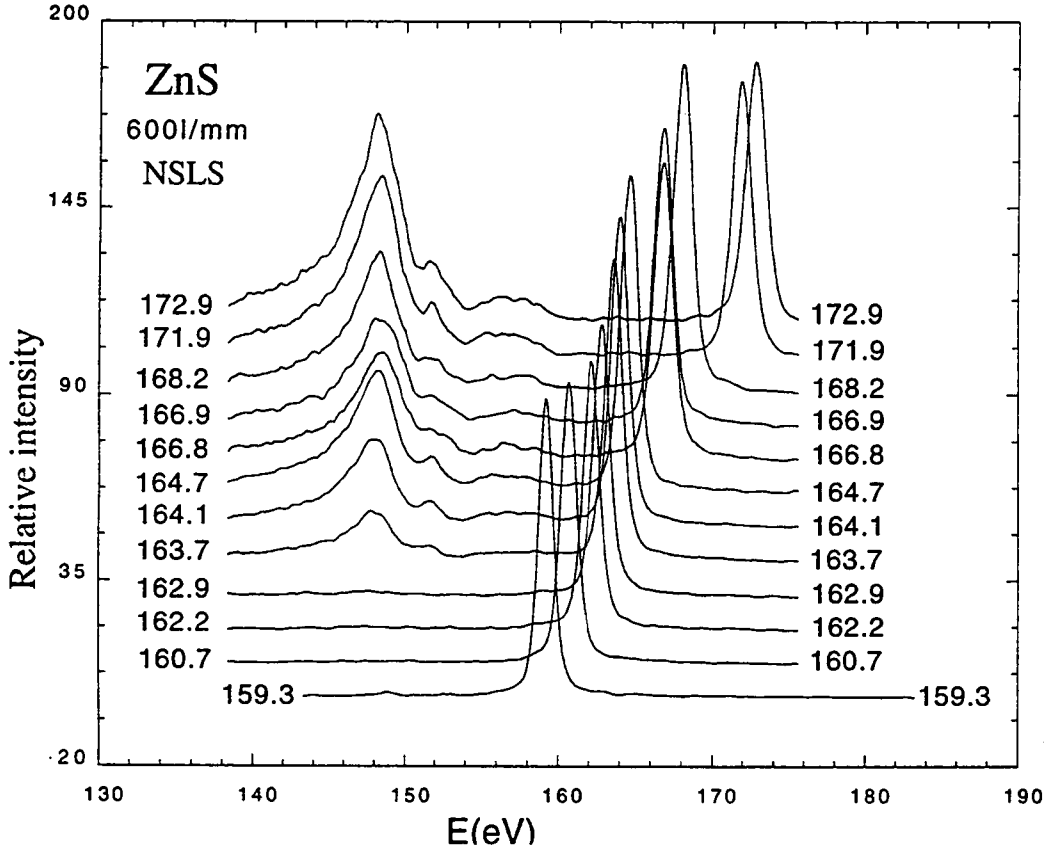

(a). A general view.

Fig 4.6 The S $L_{2,3}$ spectra of ZnS with photon excitation near threshold using 600 l/mm grating spectrometer at NSLS.

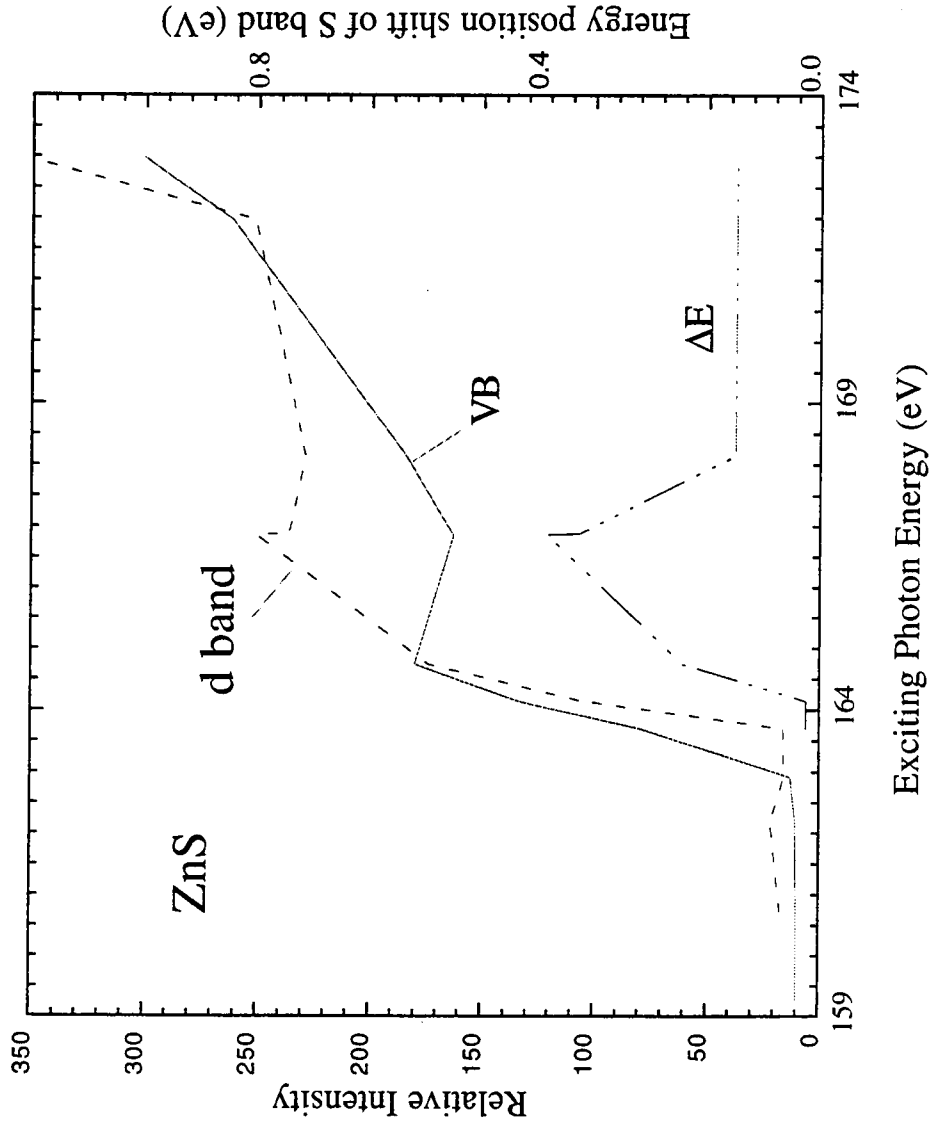

(b). The absorption of ZnS derived from 4.6a. The solid line is derived from the whole valence band. The dashed line derived from the d bands only. The dot-dashed line is for energy shift of s band of ZnS near threshold.

Fig 4. 6 (continued)

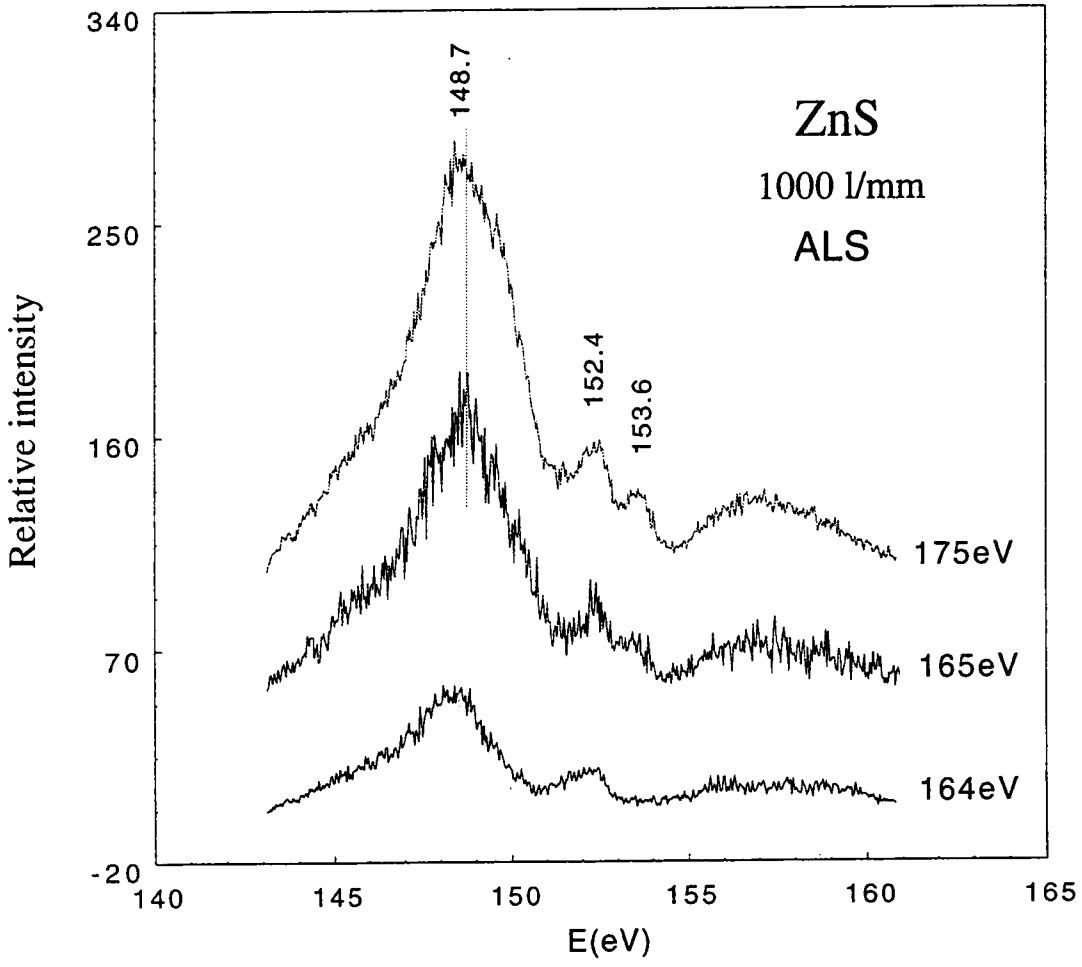

(c). The $L_{2,3}$ spectra of ZnS from photon excitation at ALS.

Fig 4. 6 (continued)

The emission spectra of ZnS and CdS were measured near threshold with photon excitation at NSLS and re-measured at ALS to gain better resolution. Fig 4.6 presents the results for ZnS and Fig 4. 7 for CdS.

Fig 4.6a, taken with an excitation band width of approximately 2 eV at NSLS, shows general features in photon excitation. These spectra are normalized to the integrated excitation flux determined by multiplying beam current by excitation time. Two separated groups of spectra are seen clearly. The narrow high energy peaks are produced by reflection of the incident beam. The lower energy spectra, which remain approximate fixed in energy are the fluorescence spectra. In Fig 4.6b, the energy shift of the peak of the s band near threshold is shown as well as excitations for whole valence band and d band in CdS derived from Fig 4.6a. The curve marked with VB is a plot of the integrated intensity of the emission spectrum as a function of the excitation energy and thus provides a relatively low resolution plot of absorption at the L edge derived from emission spectra. Fig 4.7b is an absorption curve of CdS measured at ALS by electronically integrating the total fluorescence yield between 145eV and 160eV as the incident energy is scanned, and thus is a higher resolution version of absorption curve presented for ZnS. These absorption curves determine the core-level to conduction band spacing, and when combined with emission spectra, are also useful for the determination of band gaps. In Fig 4.6c and 4.7c, threshold spectra of ZnS and CdS obtained with higher resolution at ALS are presented.

It is also possible to obtain a measure of the position of the absorption threshold by monitoring the sample current produced by photoemission as a function of excitation energy. The photoemission current increases at threshold due to the opening of new Auger de-excitation channels. Thresholds derived from such measurements are in good

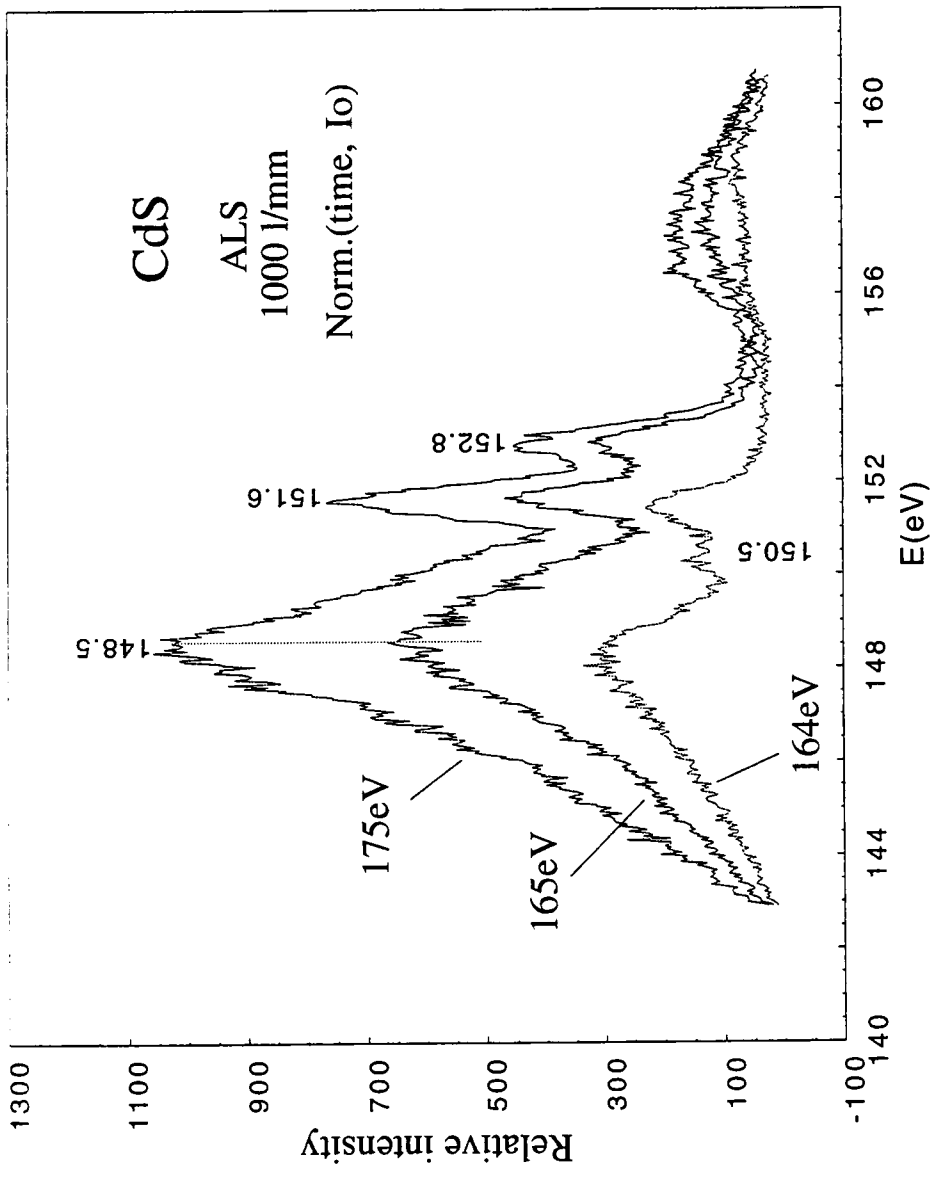

(a). Emission spectra of CdS at ALS.

Fig 4.7 The S $L_{2,3}$ spectra of CdS with photon excitation near threshold at ALS.

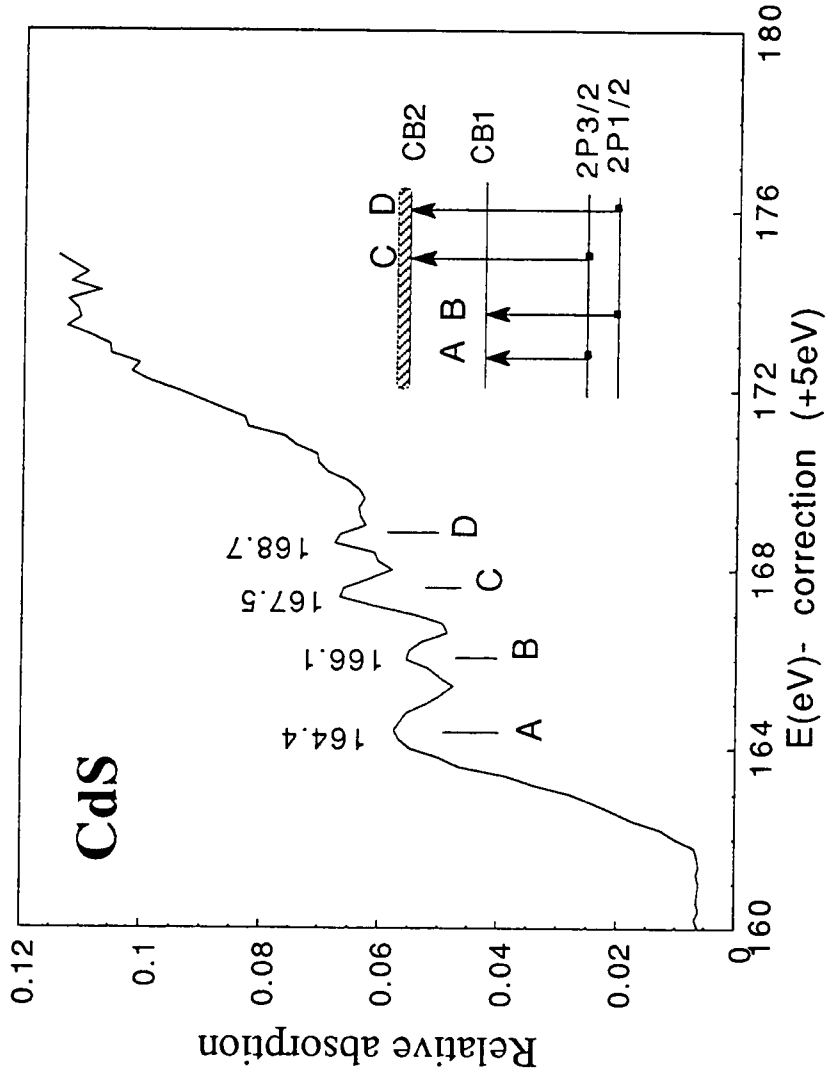

(b) The absorption of CdS taken at ALS.

Fig 4.7 (continued)

agreement with those derived from the x-ray yields. Two papers reported absorption experiments at the $L_{2,3}$ for cubic ZnS [4.22] and CdS [4.22, 4.23]. The onset of absorption and lowest absorption peak that we observe at about 164 eV are consistent with these published results.

Two principal qualitative modifications are observed for near-threshold excitation of spectra. Separated thresholds are visible for the L_3 and L_2 spectra. The higher energy L_2 spectrum is only observed with excitation above about 165 eV for ZnS and CdS. The second qualitative feature is that for excitation within about 2 eV of its threshold, there is an enhancement of the L_2 spectrum relative to the L_3 spectrum about its statistical ratio. This is believed to be evidence that the local core levels $2p_{1/2}$ and $2p_{3/2}$ open at different excitation energy and contribute to the threshold effect very near threshold.

A measure of the energy band gap is provided by the energy difference between the top edge of the valence band from emission spectrum and the bottom of the conduction band from the absorption spectrum. The emission spectrum is not affected by the energy resolution of incident photons. At the valence band maximum, the principal broadening processes are the core-hole broadening and instrumental resolution. The best estimate of VBM is from the L_3 spectrum excited by photon at threshold. The width of the absorption edge, as measured by the 10% to 90% points on the edge, is consistent with the assumption that the absorption edge broadening is dominated by the 2 eV width of the exciting radiation. Hence the energy of the conduction band edge is taken at the inflection point of the absorption spectrum. Fig 4.8 shows the derived band gaps of ZnS and CdS. In order to eliminate the influence of spin splitting on the band gap determinations, spectra excited with photons between the L_3 and L_2 edges were used to

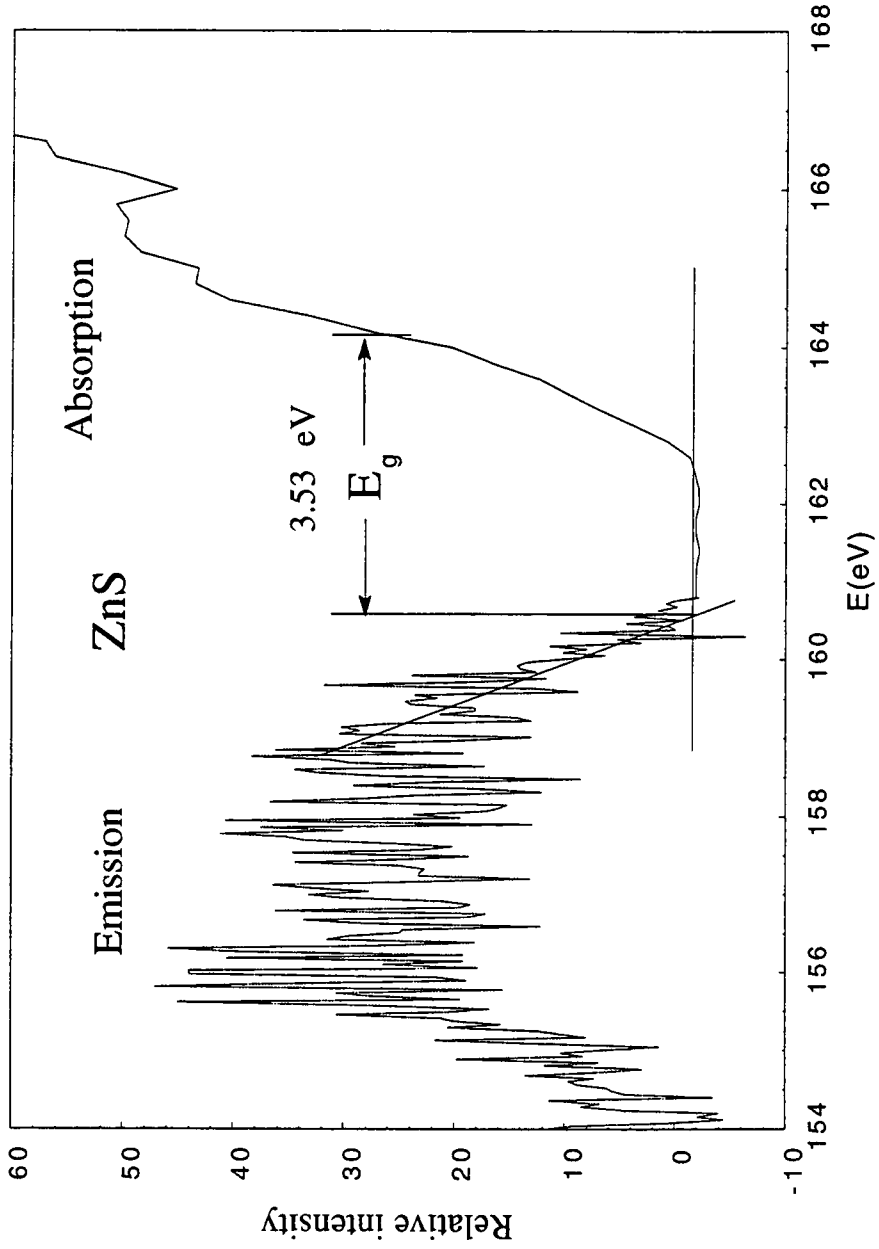

(a) ZnS.

Fig 4.8 The conduction and valence band edge and band gap taken at ALS.

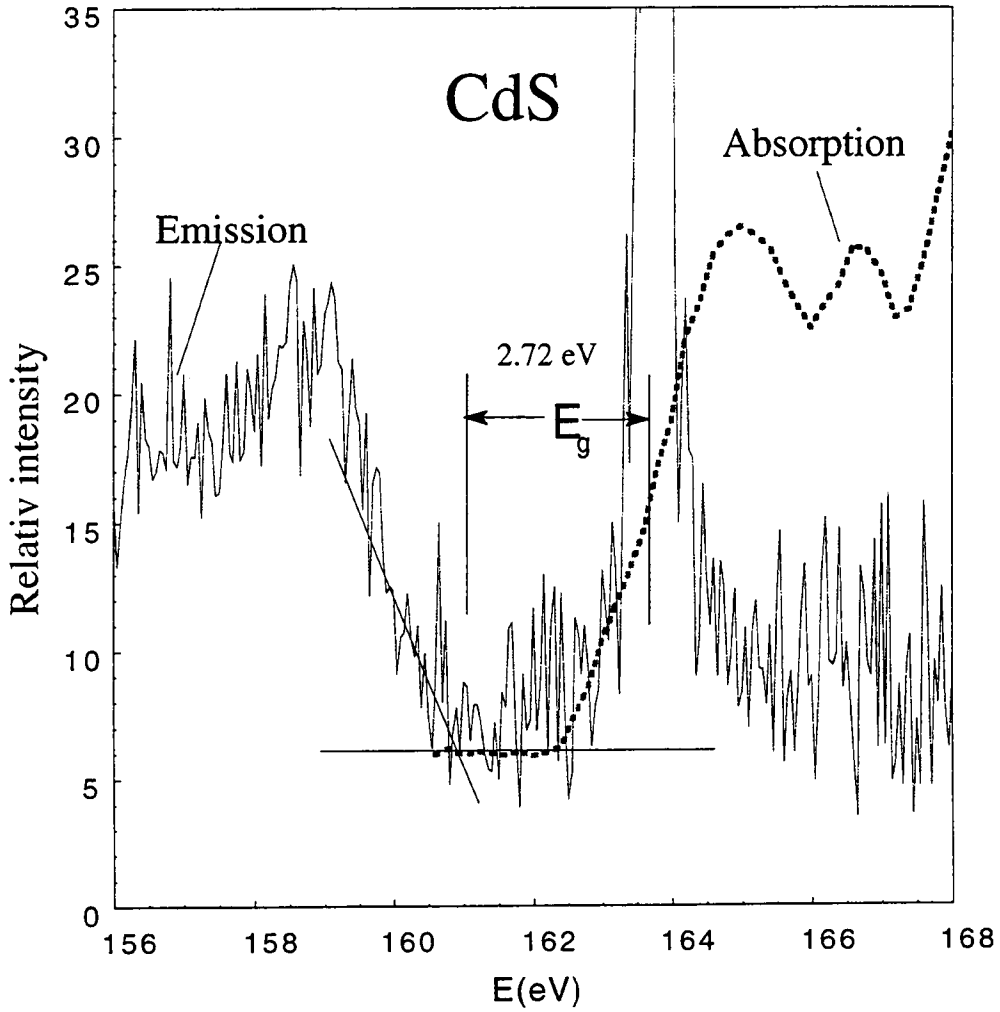

(b) CdS.

Fig 4.8 (continued)

determine the band gaps. This value is consistent with values of the VBM derived from other spectra and listed in Table 4.1. The band gaps are determined in this way to be **2.72** eV for CdS and **3.53** eV for ZnS at ALS, and **2.62**eV for CdS and **3.61**eV for ZnS at NSLS.

D. Discussion

Our results are consistent with previous measurements providing density of states information for CdS and ZnS. Comparison may be made with the e-beam excited sulfur K and $L_{2,3}$ spectra of CdS. [4.22, 4.23] The measured L spectrum is in good agreement with our results (see Table 4.1), except for minor differences in the absolute energies assigned to spectral features, which result from different spectrometer calibrations. The L and K spectra can be compared by aligning the spectra at the valence band maximum as shown in Fig 4.9. The major peak in the K-spectrum, which provides a measure of the p-PDOS, overlaps the weak upper valence band identified in our data, but no structure is present at the position of the lower valence band. A similar comparison can also be made with XPS data for both ZnS and CdS.[4.25] These spectra are dominated by the Zn 3d and Cd 4d spectra, but also clearly resolve the upper valence band. L and K SXE spectra and the XPS spectrum of CdS are compared in Fig 4.9.

In Table 4.3, the locations of spectral features observed with various spectroscopies are compared. Energies are referenced to the valence band maximum, which is difficult to ascertain exactly, so that the accuracy of listed values is limited to about 0.1 eV. Differences in spectral features, such as the determination of the spin-orbit splitting of the sulfur p levels, may be determined with much greater accuracy.

The results from all measurements are consistent with the general picture that the

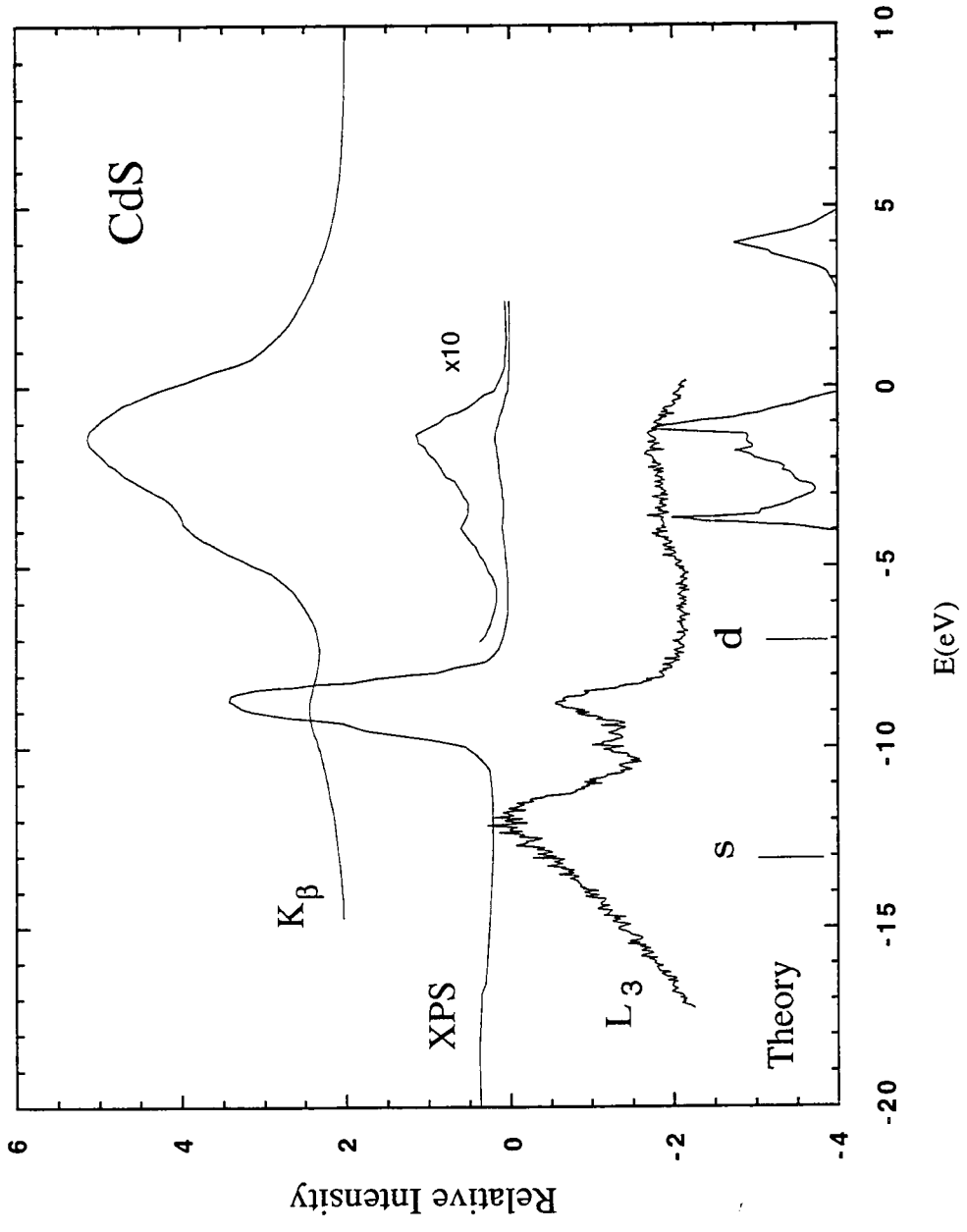

Fig 4.9 The comparison of results from various spectroscopes and theoretical calculation for CdS.

Table 4.3 Comparison of energy positions of major spectral features in various spectroscopes.

CdS	$L_{2,3}$(ours)	XPS	UPS	Theory	
VBM-UVB1	-2.13	-3.0[4.8,4.25]		-1.3[4.19]	
VBM-UVB2	-4.16	-5.3[4.8,4.25]		-3.5[4.19]	-3.29[4.16,4.17]
VBM-d1	-8.05				
VBM-d2	-9.2 -10.38	-9.64(15)	-10.0(4),-9.2(2) [4.16,4.17]	-6.73[4.19]	-8.1[4.21]
ΔE(d1-d2)	1.15	1.14(10)[4.27]		1.15[4.19]	
VBM-LVB1	-12.36	-12.5[4.16]		-12.5[4.19]	-11.69[4.16,4.17]
LVB1-d	3.72			5.4[4.19]	4.8[4.16,4.17]
E gap	2.72	2.56(8)	2.55[4.16,4.17]	2.00[4.19]	2.45[4.21]
ZnS					
VBM-UVB1	-1.83,-2.90	-2.4[4.8,4.25]		-1.9[4.11]	-1.96[4.15],-2.3 [4.8]
VBM-UVB2	-4.67	-4.7[4.8,4.25]		-4.6[4.11]	-4.6[4.15],-4.8 [4.8]
VBM-d1	-7.27				
VBM-d2	-8.37	-9.03(15)[4.8,25]		-6.63[4.11]	-6.84[4.15],-7.4 [4.8]
ΔE(d1-d2)	1.18	1.04(10)[4.27]			
VBM-LVB1	-12.32	-12.4[4.8,4.25]		-12.5[4.11]	-12.85[4.15],12.4[4.8]
LVB1-d	4.50	3.3[4.8,4.25]		5.9[4.11]	6.0[4.15]
E gap	3.53	3.6,3.8[4.8,4.25]		1.84[4.11]	2.74[4.15]

Key to abbreviation: All definitions are energy difference between two band points, e.g. VBM-UVB1 is the energy difference between upper valence band 1 and maximum of valence band; LVB1-d - average energy difference from d bands to s band (LVB1); Others are in Table 1.

lower valence band is s-like and derived almost entirely from the sulfur 3s orbital. The upper valence band is derived primarily from the Cd(Zn) s-states and the sulfur p-states with the small admixture of sulfur s-states that is characteristic of materials with partially covalent bonding. The Zn(Cd) d-states, which dominate the XPS spectra and the Zn $M_{2,3}$ spectra of Fig 4.5, appear in the sulfur K-spectra as weak crossover transitions. To facilitate comparisons with theory, experimental energy separations of spectral features derived from the various spectroscopes are compared in Table 4.3. These include measures of the spin-orbit splitting of the sulfur L core levels, the energy separations between the valence band maximum and peaks identified in the upper and lower valence bands and the Zn(Cd) d-bands, and energy separations between d-band and valence band features. These energy separations were taken from the L_3 spectrum of Fig 4.3 and Fig 4.4 except that energy differences with the valence band maximum were reduced by 1.15 eV to correct for the convolution of L_2 and L_3 spectra.

In Table 4.3, the energy separations are also compared with theoretical calculations. The agreement is generally satisfactory, with the exception that calculations systematically place the d-bands too close to the upper valence band, and the measured valence to conduction band gap is larger with all experimental spectroscopies than indicated by LDA calculations. The best agreement is found with the GW [4.21], MOPW calculations which include effects of exchange and correlation [4.10]. The widths of the d-bands and their positions with respect to the UVB are in good agreement with the photoemission data. The d bands in L_3 spectra are about 2eV wide and clearly show two components in Fig 4.4, Fig 4.6 and 4.7. Calculated one-electron d band is only about 1eV wide and does not show the doublet character. This doublet is also observed in the photonemission data and was allocated by Ley et. al to the combined effect of spin -orbit

interaction and crystal field interactions. The photoemission results indicates a splitting of about 0.8eV for CdS compared with our value 1.1eV. We observed an unresolved splitting of 0.5eV in ZnS.

The best theoretical result for CdS, so far, is the quasiparticle band structure GW calculation in which d electrons are treated as valence electrons and the d-p interactions are considered.[4.21]

An important feature of the spectra are the narrow overlap peaks from the Cd and Zn d-bands. The magnitude of these peaks in the sulfur L-spectra provide a measure of the overlap of the d-states onto the sulfur 2p cores. An experimental measure of the relative overlap is provided by the relative magnitude of these peaks normalized to the sulfur 3s peak at 148 eV. Normalization to the sulfur 3s peak compensates for most of the experimental factors affecting this comparison. The experimental value of this ratio is I(Zn-3d)/I(Cd-4d) = 0.39.

The decay of a core hole in a single x-ray emission channel [4.41] is by

$$W_{fi} = \left|M_{fi}\right|^2 = e^2\Omega^3 / hc^3 2\pi \left\langle \phi_f \left| t \right| \phi_i \right\rangle^2$$

where $\Omega=2\pi c\nu$ is the radiation frequency; t, the dipole operator; ϕ_f and ϕ_i, the final and initial state wave functions. Assuming that the dipole matrix elements are approximately equal for these two very similar systems, we obtained a calculated estimate of this ratio by calculating the two-center overlap integral between the Cd(Zn)-4d(3d) orbital and the sulfur 2p states calculated using atomic orbital [4.42] and the Cd(Zn)-S spacing of the two materials [4.43]. This calculation yields a ratio of 0.74 or nearly twice the experimental value. The large difference between the experimental value and the theoretical result suggests that a more thorough theoretical treatment would be of interest.

In Figures 4.2a and 4.2b, it is obvious that the d band overlap peaks and other spectrure fetures in photon excited spectra are sharper than those excited by an energetic e-beam. This sharpening of the spectra is most prominent for the d-band overlap peaks, but is also present for the sulfur 3s peak. This sharpening **is not** typical of the L-spectra we have observed in other light elements and light element compounds, where no difference is usually seen between e-beam excited spectra and spectra excited by photons at energies well above threshold. Such broadening is observed, however, in the L spectra of transition metals such as Fe and Cu, and is attributed to excitation of spectator holes in the d-bands of these metals and their compounds.[4.44] We believe that spectator holes in the Cd and Zn d-bands may be responsible for the excess broadening observed in the electron excited spectra.

The weak low energy satellite centered at 139 eV is interpreted as an inelastic "shakeup" de-excitation process in which the energy of the emitted x-ray is reduced by the energy required to excite a one electron from the valence to conduction bands. These weak inelastic peaks have been observed in many systems and have been carefully studied by Schnatterly et al for Si.[4.45]

An important source of broadening in emission spectra is the lifetime broadening of the valence hole that remains after radiative recombination. Near the valence band maximum(VBM) in materials with a band gap, only electron-phonon scattering affects the valence-hole lifetime so that core-hole broadening is the factor limiting spectral resolution. For energies more than about two gap widths below the VBM, electron-electron scattering provides the major broadening mechanism for the observed spectra. It is possible to obtain an estimate of this e-e scattering lifetime by measuring the width of features in the emission spectra. We have obtained an estimate of this broadening by

fitting a Gaussian function to the upper edge of the S 3s peak in Fig 4.9. A fit to the lower edge of the peak is not useful due to the presence of the inelastically scattered photons described in the previous paragraph. The instrument broadening in this range is small (0.15 eV). The FWHM widths attributable to lifetime broadening are about 2.0 and 2.2 eV respectively for CdS and ZnS. This translates to lifetimes of about 3 x10-16 sec for the valence holes deep in the band.

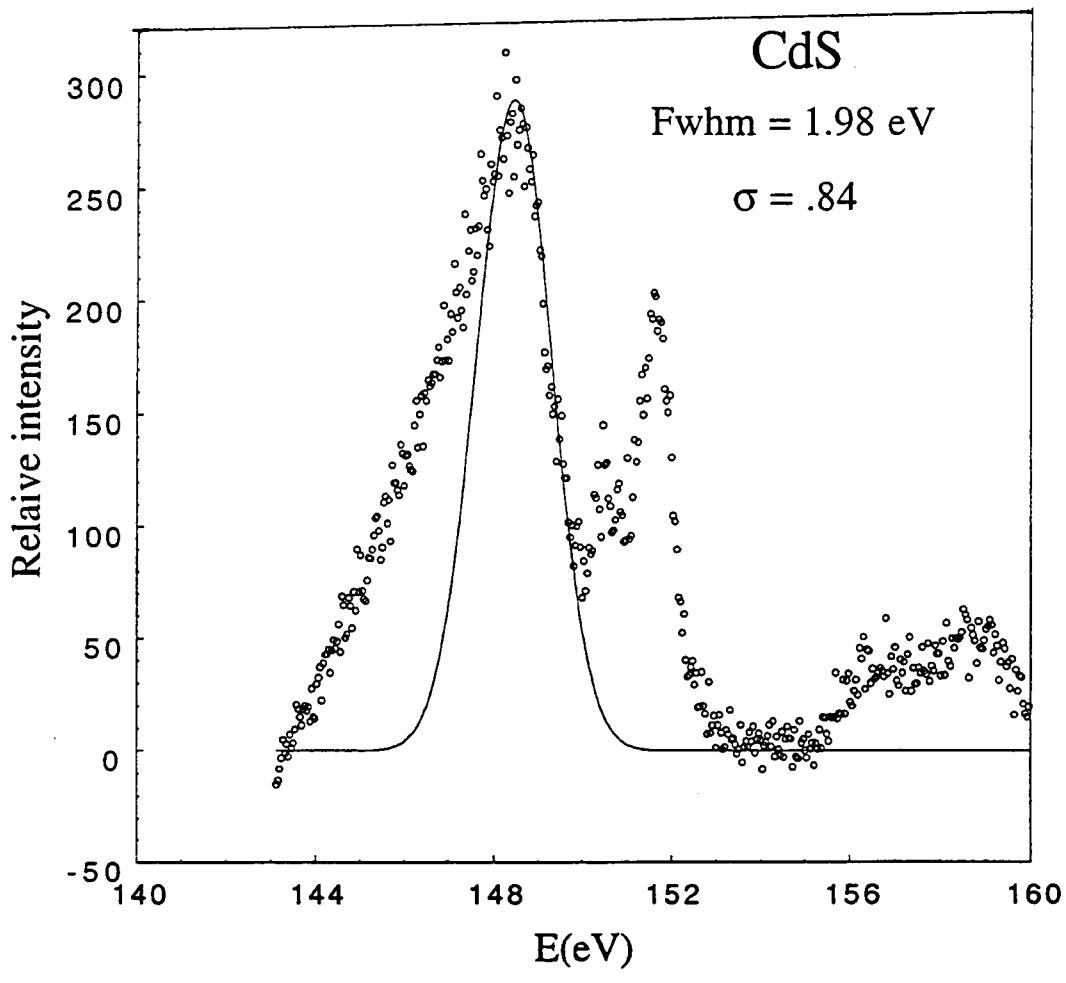

Fig 4.10 Gaussian fit to right side of L_3 s-band of CdS to determine hole lifetime.

E. Inelastic Scattering near threshold in the Zn $M_{2,3}$ Spectrum of ZnSSe

In this section, we present Zn $M_{2,3}$ spectra of ZnS and ZnSSe spectra excited near threshold which show strong inelastic scattering effects, and which can be explained using a simple model and an inelastic scattering theory based on second order perturbation theory.

For the sulphur $L_{2,3}$ spectra which were the principal focus of the previous sections of this chapter, the use of photon excitation near threshold had value for sharpening the observed spectra and for separating the L_2 and L_3 spectra, but there is little evidence of the contribution of the one step inelastic scattering processes that have been oberved near threshold in many other materials. Consequently our analysis was devoted primarily to a discussion of the traditional density of states information that can be obtained from SXE spectroscopy.

The case is very different for the near threshold excitation of the Zn $M_{2,3}$ spectra of ZnS and ZnSSe, which show dramatic inelastic scattering effects, whose principal features can be understood with the simple inelastic scattering theory presented in Chapter II. The data presented in this chapter are for the most part taken with the ZnSSe sample, for which the most complete data set is available, but essentially the same features are observed for Zn spectra of ZnS.

In Figure 4.11, photon exicted $M_{2,3}$ spectrum of ZnS is plotted along with the e-beam exited spectrum presented previously in Figure 4.5. The spectra excited with 132 eV and 148 eV photons are excited well above threshold, have the properties of ordinary SXE spectra, and are dominated by the strongly broadened transitions from the Zn 3d levels in the valence bands to the spin-orbit split Zn 3p core levels. The spectrum excited

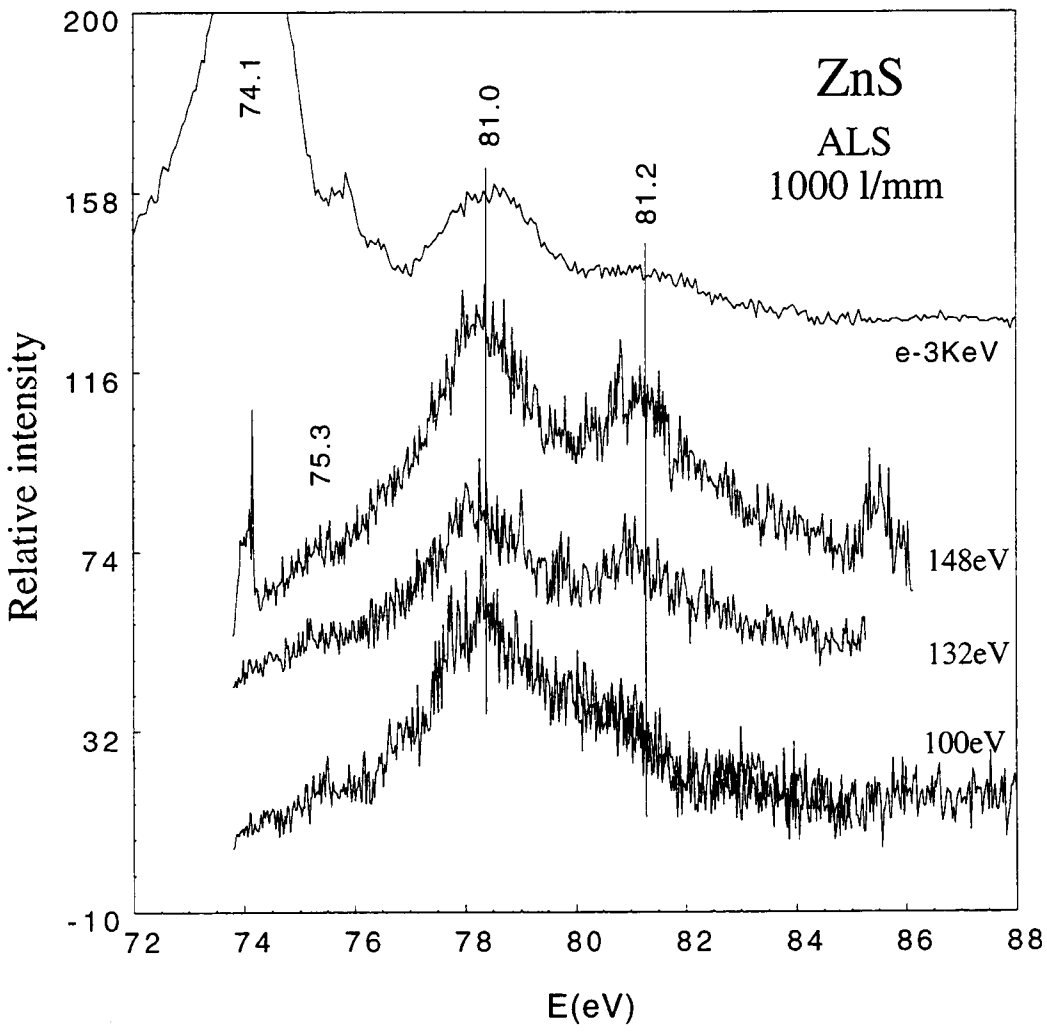

Fig 4.11 Zn-$M_{2,3}$ spectra of ZnS by photon excitation at ALS.

with 100 eV photons shows some variation of the intensity ratio of the M_2 and M_3 peak heights that are sometimes characteristic of inelastic scattering effects.

These effects are much more dramatically illustrated, however, by the Zn M spectra of ZnSSe presented in Figure 4.12. In this figure, the elastic and inelastic peaks for excitation are shown on the same energy scale, for near threshold excitation between 89 and 98 eV and for several energies well above threshold. The spectra excited well above threshold are similar to those presented above for ZnS and have the properties of normal fluorescence spectra, in which the excitation and de-excitation processes are decoupled.

The fluorescence spectra exicted at photon energies between 89 and about 96 eV, however. show dramatic evidence of the one-step inelastic scattering process. As the photon energy is increased within this range, a strong inelastic scattering peak about 2 eV wide moves through the normal fluorescence spectrum. Several features of this peak are noteworthy. First, within experimental resolutions and accuracy, it exactly tracks the elastic peak at about 12.4 eV lower energy, as is evident from Table 4.4, which lists the positions of the peaks taken from the experimental spectra. Second, the peak is much narrower than the normal fluorescence spectrum; its overall width of 2 eV is comparable to that observed for the d-band overlap peak in the sulfur L_3 spectrum. And third, its relative intensity as it moves through the normal fluorescence spectrum is approximately proportional to the intensity of the ordinary fluorescence spectrum, reaching maxima at energies of about 78 and 81 eV, the peaks of the normal fluorescence spectra.

These features can be understood using the using the second order perturabation theory for scattering presented in Chapter II and the energy level model of Figure 4.13.

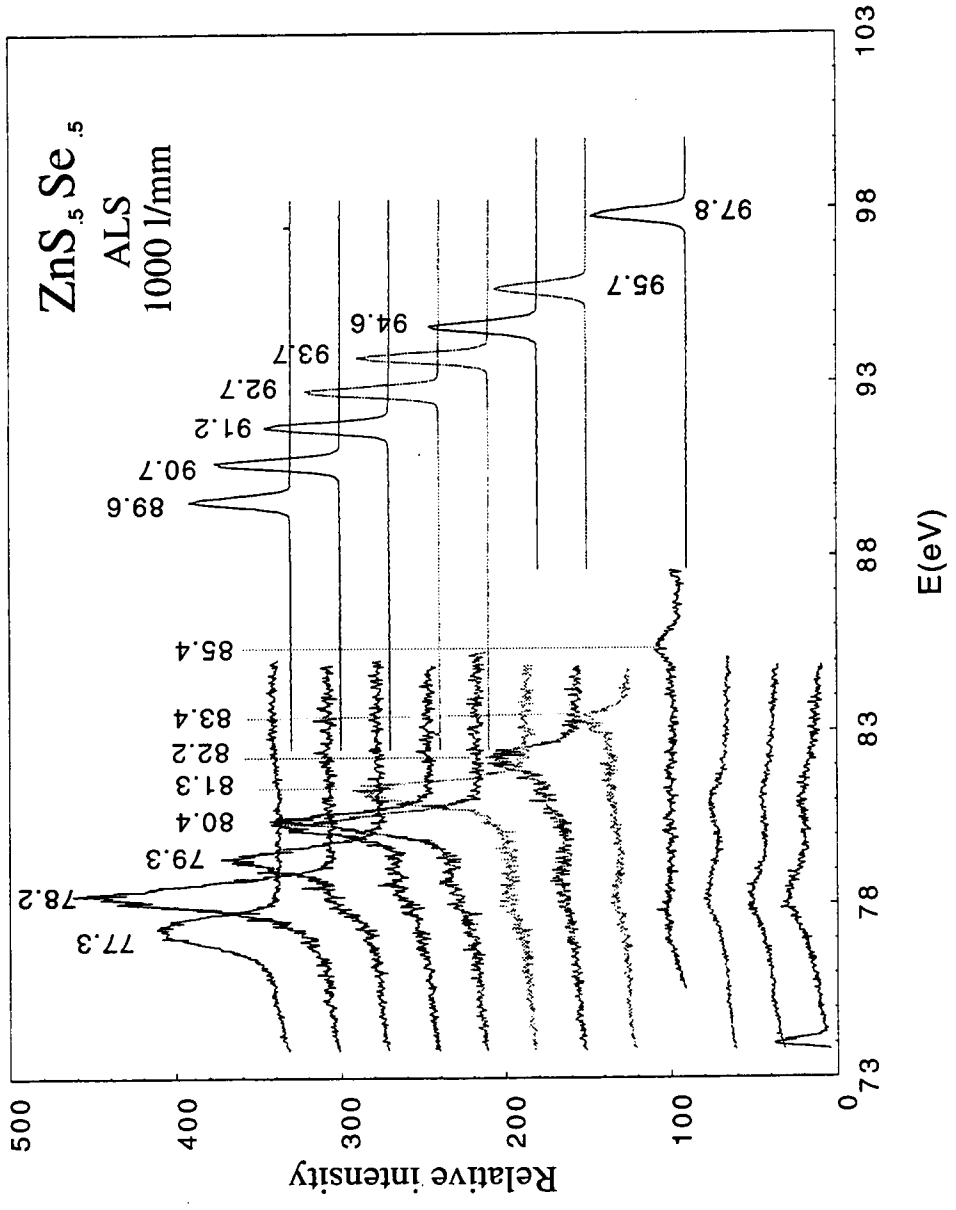

Fig 4.12 The Raman Resonance Scattering in Zn $M_{2,3}$ spectra of $ZnS_{.5}Se_{.5}$

Table 4.4 The energy lose of photon in $ZnS_{0.5}Se_{0.5}$ All in units of eV.

Reflected peak(eV)	ΔE(center-center)	ΔE(center-right side)
89.6	12.325	11.866
90.7	12.413	12.022
91.7	12.396	12.006
92.7	12.364	12.032
93.7	12.473	12.084
94.6	12.425	12.008
95.7	12.363	11.981
97.8	12.405	11.966
Ave.	12.39	12.00

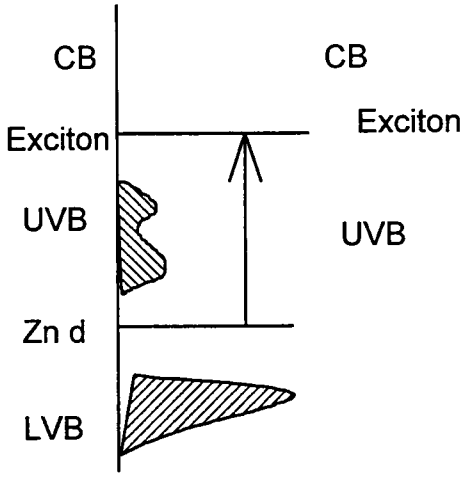

Fig 4.13 A proposed simple model

The process producing the spectra is analagous to a Resonant Raman process in which the scattering occurs through a real intermediate state. The electronic excitation producing the energy loss of about 12.4 eV must be from the Zn d-bands located between the upper and lower valence bands and a narrow exciton state located near the conduction band edge. We note that theory requires that the energy difference is between the electron and hole states in the final state of the second order process, so that the narrow exciton state is not a core exciton, but a valence exciton in which a hole in the d-band binds an electron in a localized orbital. Because the energy difference is associated with the final state of the scattering process, the width of the observed spectra is not limited by the core-hole lifetime which broadens the normal fluorescence spectrum. The influence of the core-hole lifetime in the intermediate state does, however, influence the observed spectra by causing the inelastic peak to be modulated according to the intensity of the broad normal fluorescence spectrum. In essence, the energy uncertainly associated with the limited core-hole lifetime, allows the resonant inelastic scattering to occur over an energy range consistent with the uncertainty principle.

Several additional features of this example of inelastic scattering deserve comment. The proposed explanation requires that their be a localized exciton state associated with the hole in the d-band. The results present in the previous chapter indicate that exciton effects are not observed in the sulfur L spectrum. This is consistent with results obtained in other ionic systems, in which localized excitons are found to be associated with the anion, but not the cation species. As examples, strong exciton effects are observed in the boron K-spectrum, but not the nitrogen K-spectrum of BN, and are observed in the metal, but not the oxygen K-spectra of many oxides. The physical origin of this difference seems to be that the electron density in real space is greater near the

cation species so that holes in inner shells are effectively screened and do not strongly bond local states near the cation in ionic solids.

In addition to informing us about the physics of coherent processes contributing to fluorescence from solids near threshold, these inelstic scattering processes provide a new means of studying the lowest energy electronic excitations in solids, and especially of the effects of screening on the processes that occur when an additional charge, in the form of a core or valence hole is introduced into the system. In subsequent chapters, inelastic scattering effects similar to those described here for ZnSSe will be presented for other sulfur compounds.

Chapter V

Zn(SSe) Alloys

A. Introduction

In this chapter, we describe measurements of the S $L_{2,3}$ spectra of a series of ZnS_xSe_{1-x} alloys, where x = 1.0, 0.51. 0.31, 0.19, and 0.09. These spectra were excited both with an energetic e-beam, and with photon energies well above threshold. Some information is also obtained about the Se $M_{2,3}$ spectrum which overlaps the S spectrum, but it has not been possible to obtain a reliable separation of this spectrum from the much more intense sulfur spectrum. In addition, we have measured the Se $M_{4,5}$ spectrum generated by transitions to the $3d_{3/2}$ and $3d_{5/2}$ core levels which provide a measure of the (p+f)-like LPDOS at the Se site. This spectrum is also extremely weak so that useful data was obtained only for the most Se rich alloy. None of the spectra reported in this chapter were obtained at the ALS after the low energy grating was installed in the beamline there. Consequently, insufficient intensity was available to acquire low noise spectra with the best available instrumentation. Consequently, these results may best be used to suggest directions for future, more definitive, studies.

In a previous paper on the AlGaAs alloys, we were able to obtain useful information on changes in the position of band edges and to make comparisons with the predictions of theory.[5.1,5.2] In the present alloy systems, such changes would be expected to occur primarily in the upper valence band, which is poorly resolved in these spectra, so that much less definitive information is obtained in the present studies. Even

so, we will first summarize briefly some of the previous work on these alloys that give context for these studies.

The Zn(S,Se) semiconducting alloy are used extensively in optoelectronic applications including visible light converting devices, compact-disk players and writable optical disk-storage systems.[5.3-5.6] The band gap for ZnSe is 2.62 eV, and 3.62 eV for ZnS at 300 K°. The band gap for the alloy, and thus electronic properties relevant to the optoelectronic applications, may be varied between these values by varying the value of x.

Previous experimental studies of the Zn(S,Se) alloy system have focused on the electronic band structure information for the states near the band gap edges[5.6-5.13]. These include excitonic luminescence, Raman scattering of exciton peak and its broadening [5.6-5.9], edge emission and absorption[5.10], optical properties[5.12] and its order/disorder properties [5.11].

Most discussion of AB_xC_{1-x} alloy has been within the general framework of Virtual Crystal Approximation (VCA).[5.14-5.15] This model treats the complex B_xC_{1-x} as a virtual atom with an average potential of "$(x)V_B + (1-x)V_C$ " on a lattice site, where V_B and V_C are the potentials of atom B and C respectively. In this model, physical properties, such as mass and bond-length are linear function of x, as illustrated by solid line labeled with VCA in Fig 5.1, and electronic properties, such as band positions, band widths, band edges, and band gaps are smooth quadratic functions of x. But recent EXAFS experiments [5.16] have observed that two nearest-neighbor distances coexist in some alloys, one to the AB bond and the other to the AC bond. Based on these results, a new model with a bimodal bonds has developed for the zincblende system. The

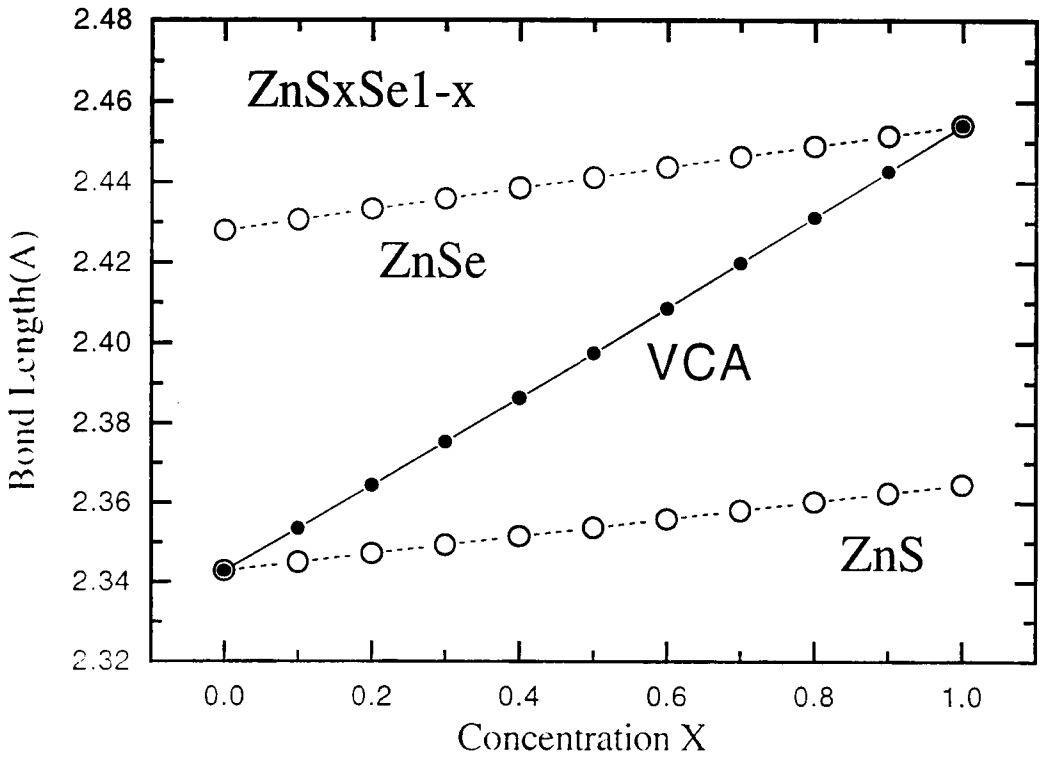

Fig 5.1 Theoretical prediction of bond lengths in ZnS_xSe_{1-x} calculated from [5.16].

coexistence of two bond lengths in Zn(S,Se) was predicted. Fig 5.1 was calculated by using published formula and parameters. The two dashed lines are for ZnS and ZnSe respectively, a solid line for VCA model. Also, the reflectivity spectra of ZnS_xSe_{1-x} have observed distinct ZnS-like and ZnSe-like features in the conduction bands near edge resulted from different potential of Vs(r) and Vse(r) [5.12]. Previous SXE studies of (Al, Ga)As alloy have also shown results suggesting a bimodal distribution of bond lengths.[5. 1, 5.2]

Some additional insights can be obtained from recently published electronic structure calculation for the Zn(S,Se) alloys using the tetragonal cluster system $A_nB_{4-n}C_4$ (n = 0, 1, 2, 3, 4) [5.18] on a mixed basis with all electrons. The unit cell of the cluster is double-sized as compared to original ones and contains both the AB and AC in a proper ratio. Therefore the cluster has the Bravias lattice structure of the end-point compounds AB or AC. For n = 0, the double unit cell of the cluster Zn_4S_4 is reduced to standard two ZnS in unit cells. For n = 4 and 2, they are reduced to normal ZnSe and $ZnS_{0.5}Se_{0.5}$ respectively. The results for ZnS, ZnSe, and Zn_2SSe are shown in Fig 5. 2.

B. Experimental results and Discussion

The soft x-ray spectroscopy experiments were performed at NSLS, ALS and CAMD during the past two years. The preparation of ZnS_xSe_{1-x} samples with x = 1.0, 0.51, 0.31, 0.18 and .09 was described in chapter III. The 600 l/mm, 300 l/mm and 1000 l/mm gratings were used in NSLS, CAMD and ALS respectively.

(1). The sulfur $L_{2,3}$ spectra of alloy ZnS_xSe_{1-x}.

Fig 5.3a depicts the e-beam excited, sulfur $L_{2,3}$ spectra for alloy ZnS_xSe_{1-x} with

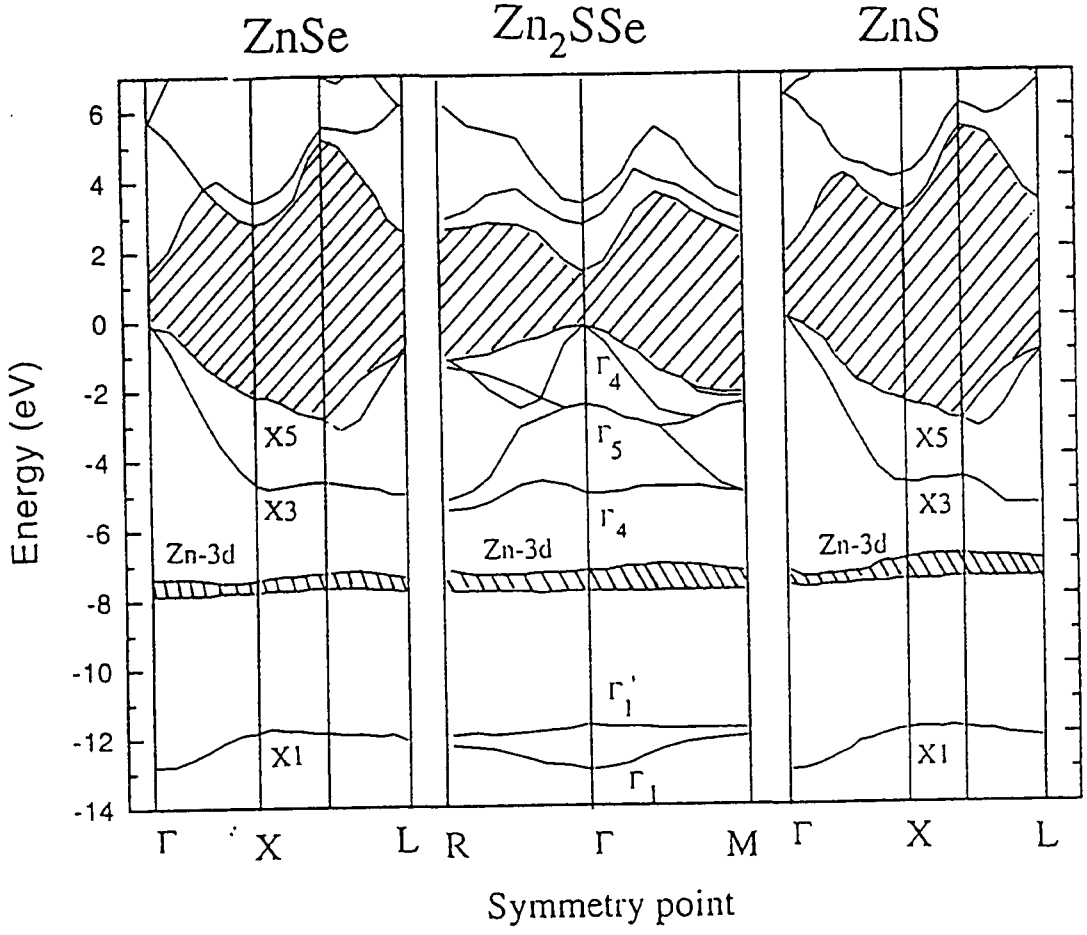

Fig 5.2 Band structures for ZnS, ZnSe and Zn_2SSe calculated from $Zn_4S_xSe_{4-x}$ cluster model [5.17].

sulfur concentrations of x = 0.09, 0.18, 0.31 and 0.51. Backgrounds have been subtracted from these spectra and they have been normalized to incident flux and sulfur concentration. In order to see them clearly, the scale factors labeled on the right side were used. They are very similar in shape. The major features of these spectra have been identified in previous chapters. The major peak centered near 149eV is the s-band derived mainly from sulfur 3s orbitals; the spin orbit splitting of this peak is marginally better resolved in the photon excited spectra. The asymmetry in this peak is the result of an unresolved spin-orbital split L_2 peak located 1.1 eV above L_3 peak. Weak features near 152 eV and 153eV are derived from Zn 3d orbitals which overlap onto the S site; these are better resolved in the photon excited than in the e-beam excited spectra. The broad structure centered near 157eV is a weak s-like component of the mostly p-like upper valence band. In the e-beam spectra, there is a shift of the entire spectrum to higher energies by nearly 0.4 eV as the sulfur concentration is reduced to x = 0.18. These spectra have been remeasured on three occasions, and this energy shift has been reproduced on each occasion, so that the shift appears to be a real effect. The FWHM band width of s band in ZnS_xSe_{1-x} was also observed to increase significantly at lower sulfur concentration. In Fig 5.3b, the width of the major peak of the x = 0.8 spectrum is clearly increased on both sides. On the lower edge of the main peak, the increase in width is associated with the development of shoulder at about 145 eV and the enhancement of the shoulder at 140 eV. These shoulders are almost certainly attributable to the presence of the Se $M_{2,3}$ spectrum underlying the S spectrum, both because the increase with increasing Se content and because the Se 3p core levels at 166.5 and 160.7 eV bracket the S core levels at 163.6 and 162.5 eV binding energies and thus should produce spectra bracketing the sulfur $L_{2,3}$ spectra. A more quantitative

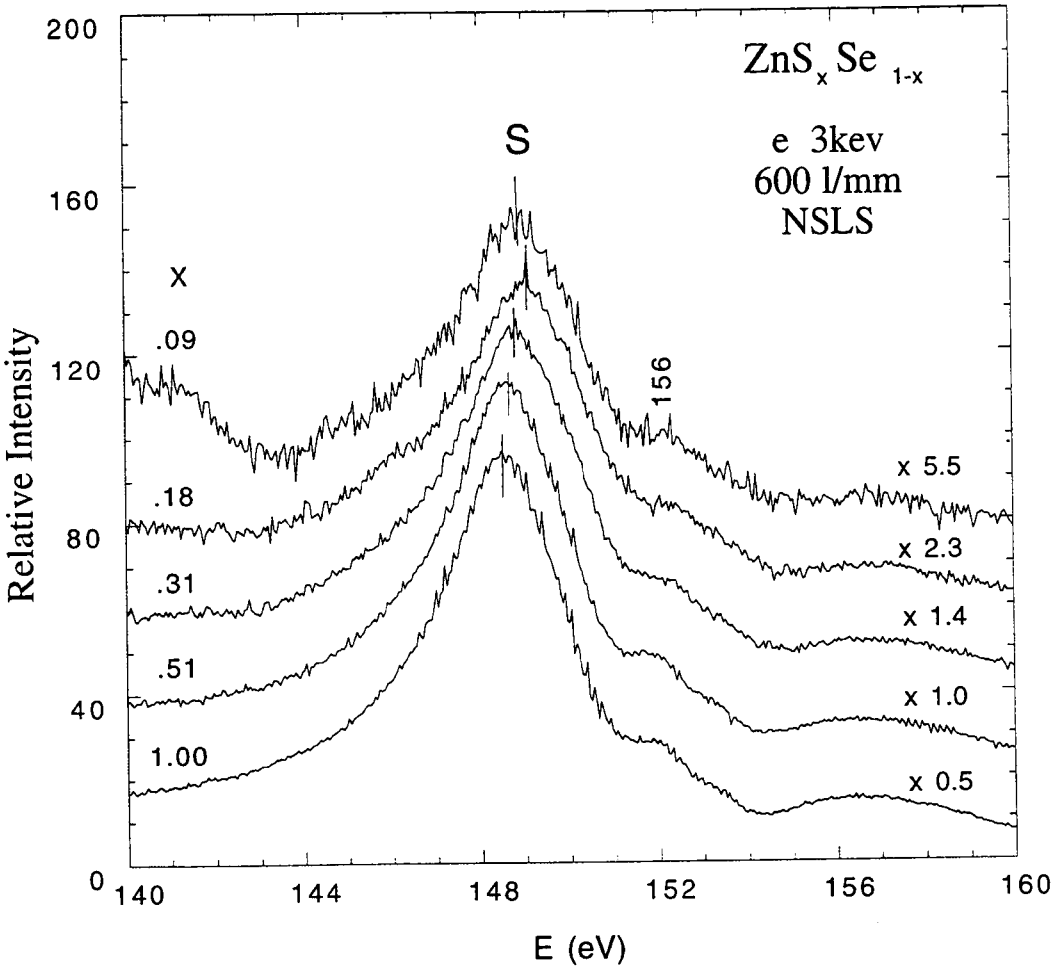

(a). The original S-$L_{2,3}$ spectra.

Fig 5.3 S-$L_{2,3}$ spectra for ZnS_xSe_{1-x} alloy from e-beam excitation at NSLS.

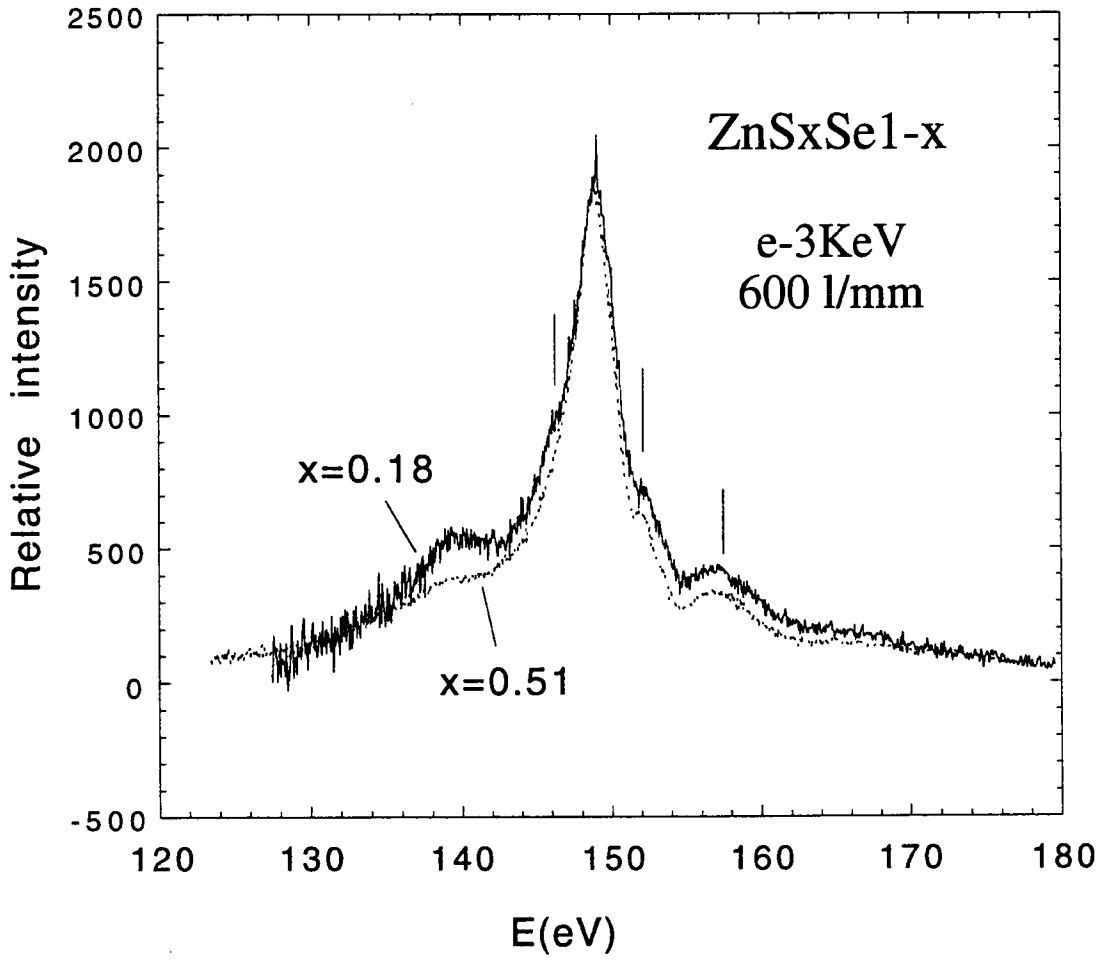

(b) Comparison of spectra with x = 0.51 and x = .18 after lined up.

Fig 5.3 (continued)

measure of the relative intensity of S and Se spectra is provided in a later paragraph.

Utilizing photon excitation well above threshold and three of the ZnSSe samples and a higher resolution spectrometer at the ALS, the sulfur $L_{2,3}$ spectra in Fig 5.4a and 5.4b were obtained. They show a feature about 1 eV above the s peak, which seems to grow in relative intensity with decreasing sulfur concentration. This feature is located in the position expected for the major peak of the L_2 spectrum. The apparent enhancement of this peak may be in part an artifact generated by the strong noise present in the spectrum, but also results from the general enhancement in this region of the spectrum generated by the presence of the underlying Se $M_{2,3}$ spectrum.

(2). The e-beam excited Zn $M_{2,3}$ spectra is shown in Fig 5.5. These spectra were normalized to incident flux, and printed with the multiplication factors on the right margin to provide curves of similar amplitude. The structure peaking near 74 eV and extending to approximately 77 eV is the second order of the S $L_{2,3}$ spectrum. The spectrum peaking at 78.6 eV and 81.2 eV and extending to approximately 90 eV is the Zn M spectrum. The Zinc $M_{2,3}$ spectrum was discussed in previous chapter. It results from transitions to 3p core levels at Zn site the peak separation is consistent with the spin orbital splitting 2.8eV between the $3p_{1/2}$ and $3p_{1/2}$ orbitals in Zn and the intensity ratio is about 2:1. The peak at 92.2 eV in spectra with x = 0.09 is from carbon contamination. The weak peaks at 86.6 eV and 88.6 eV may be transitions from (s+p)-like state of the upper valence band. Compared with sulfur s bands, the zinc $M_{2,3}$ bands are much wider. Its FWHM is estimated as ~5 eV from $ZnS_{0.51}Se_{0.49}$ spectra , which is much larger than the core level lifetime broadening of 2.0 eV cited elsewhere plus the energy resolution of this system (~ 0.2 eV).

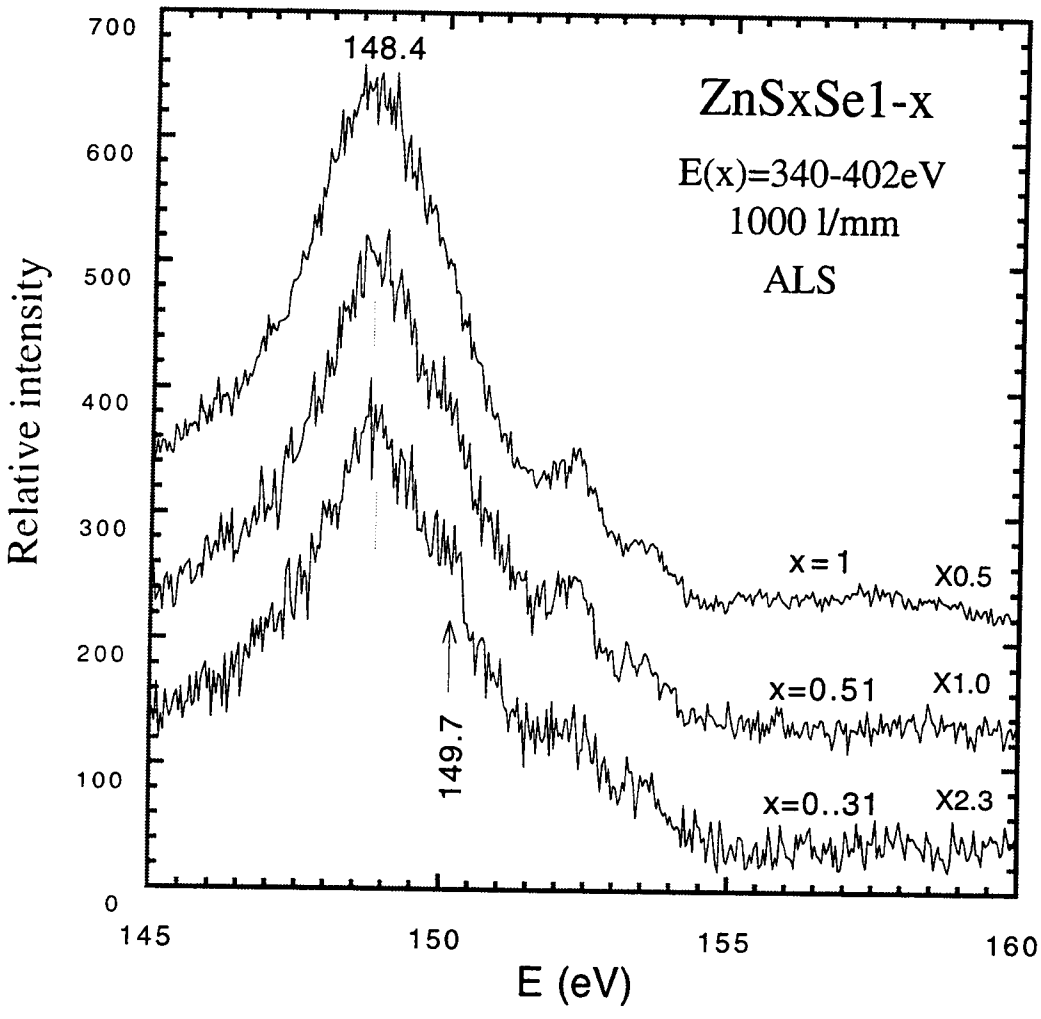

(a) With photon energies above 340 eV.

Fig 5.4 S-$L_{2,3}$ spectra of ZnS_xSe_{1-x} from photon excitation at ALS.

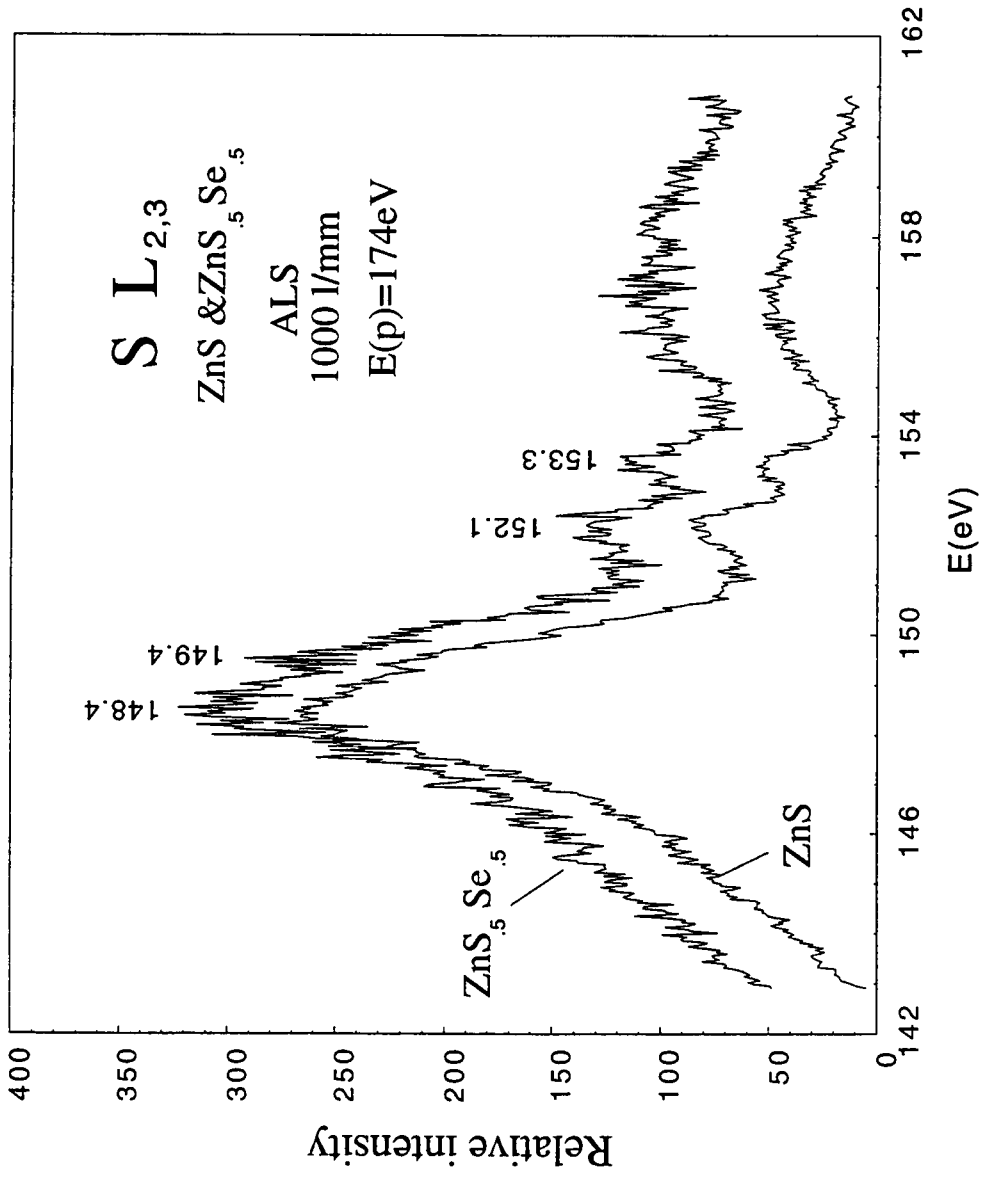

(b) For x =1.0 and 0.51 with 174eV photon excitation.

Fig 5.4 (continued)

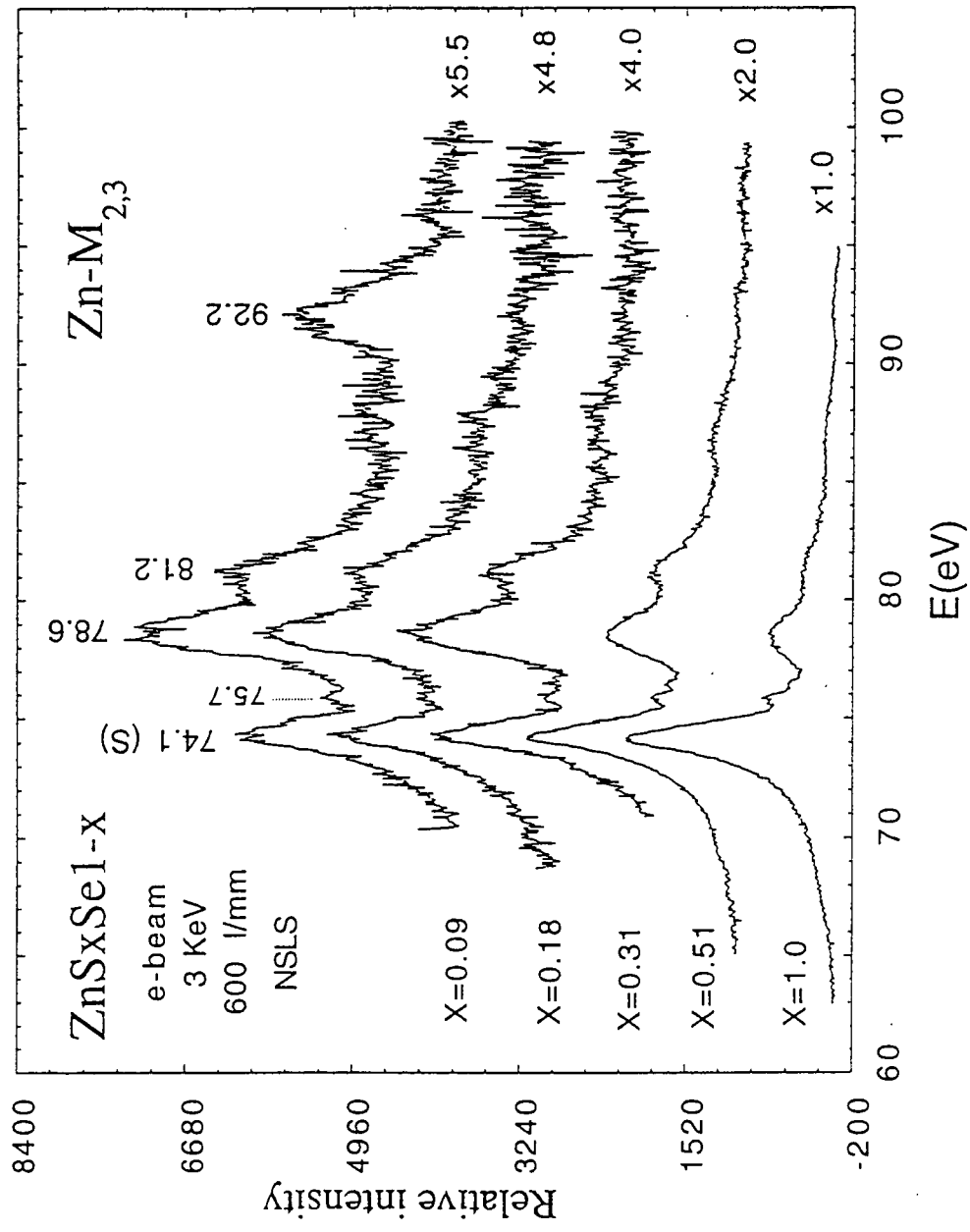

Fig 5.5 The Zn-$M_{2,3}$ spectra of ZnS_xSe_{1-x} from e-beam excitation.

Figure 5.6 shows the ratio of the peak height of S spectrum at 74.1 eV to that of Zn spectrum at 78.6 eV. The relative intensity ratio of $L_{2,3}/M_{2,3}$ in Fig 5.6 were derived from the second order $L_{2,3}$ x ray and first order $M_{2,3}$ x rays at above five sulfur concentrations in Fig 5.5. This ratio is very nearly proportional to the sulfur concentration except at the lowest value of x, where the measured ratio flatten, due primarily to contributions from the Se-M spectrum. The peaks at 74.1 eV and 78 eV are used to measure sulfur and zinc components of the alloy respectively. The relative intensity ratio of S-$L_{2,3}$/Zn-$M_{2,3}$ is a smooth function of composition x with small curvature in Fig 5.6. The non zero value at $x \rightarrow 0$ is due to the contribution of weak Se-$M_{2,3}$ of ZnSe, which overlaps with S-$L_{2,3}$ spectra in this energy range. The relative ratio of the two values at x = 1.0 (pure ZnS) and x = 0.0 (pure ZnSe) gives a measure of relative intensity of Se $M_{2,3}$ and S $L_{2,3}$, about 8%.

(3). The Se $M_{4,5}$ spectrum of $ZnS_{0.09}Se_{0.91}$ in Fig 5.7 was excited by a 3 KeV e-beam and measured with the 300 l/mm grating at NSLS. This spectrum comes from x-ray transitions to the 3d core levels at the Se site. The M_4 is for transition to the $3d_{3/2}$ core level, M_5 to $3d_{1/2}$. The theoretical spectra shown on the same figure are the Se p-like LPDOS taken from a calculation for pure ZnSe.[5.15]. The spectra are aligned to obtain the best match between the experimental and experimental features. The origin of the small peaks at 54.1 and 55.5 eV is not known, but they may be attributed with re-emission from core exciton states in the band gap. The overall agreement between theory and measurement is good except intensities at upper part of valence bands at 52.7 eV and 51.1 eV. Alloy sample and pure ZnSe have opposite trends in intensities at these two peaks. The peak at 51.1 eV is strong in measured $ZnS_{0.09}Se_{0.91}$ sample while weak in

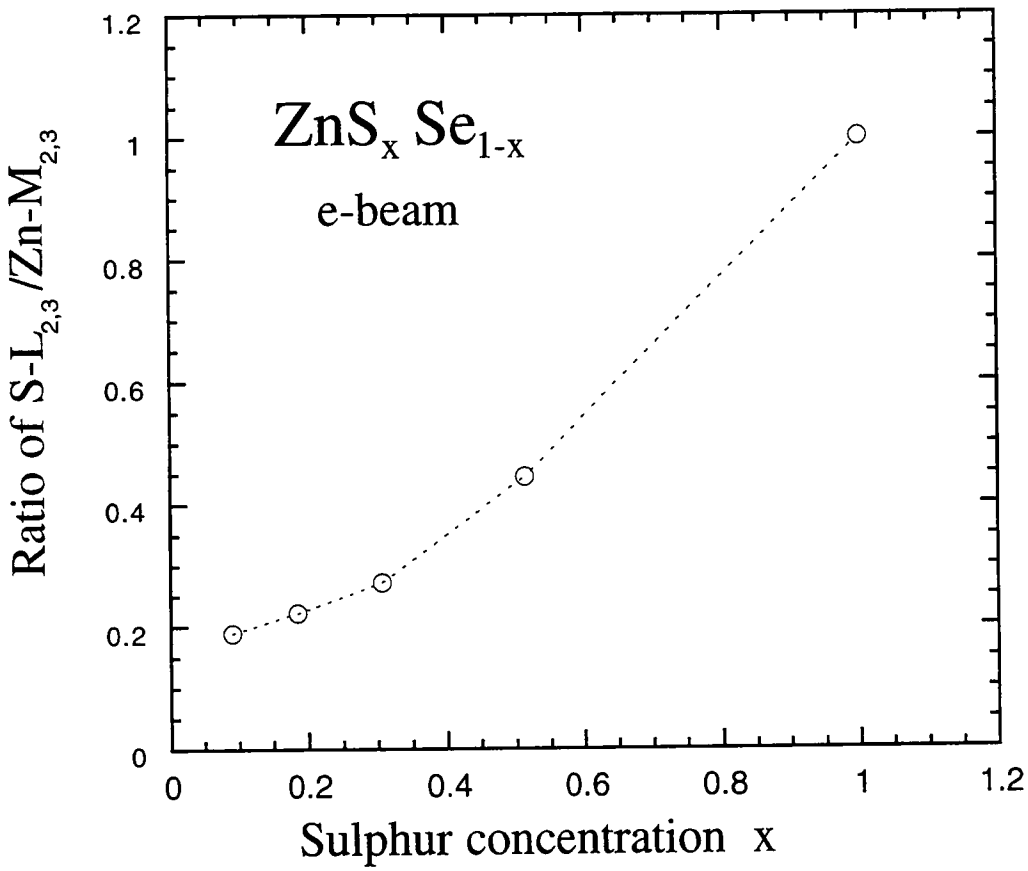

Fig 5.6 Relative intensity of S-$L_{2,3}$/Zn-$M_{2,3}$ in alloy ZnS_xSe_{1-x} from e-beam excitation.

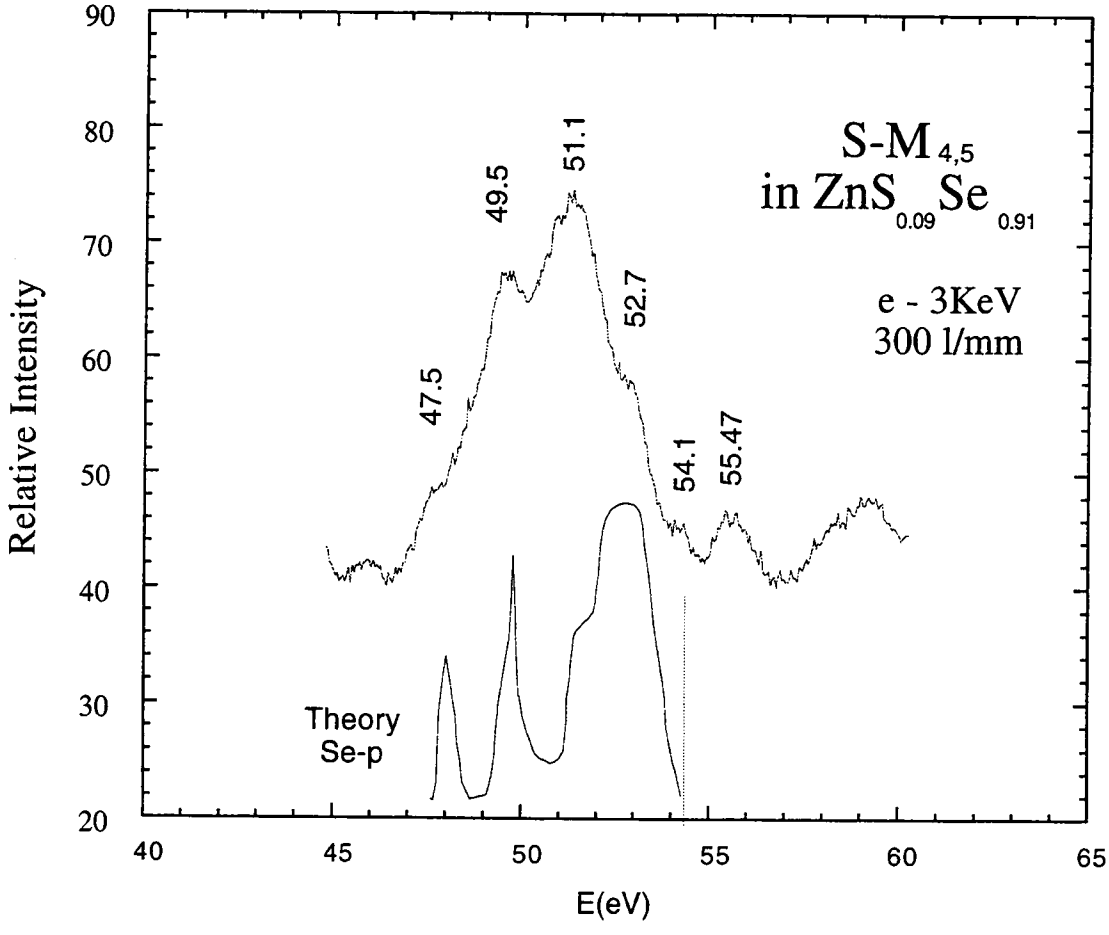

Fig 5.7 The Se $M_{4,5}$ spectrum of $ZnS_{0.09}Se_{0.91}$ by e-beam excitation.

pure ZnSe calculation. I believe that these deformed Se bands are due to the participation of sulfur in alloy, as expected from Fig 5.2.

It is hoped that in the future, using the enhanced intensities now available at the ALS, that these measurements can be repeated with near threshold excitation so that it will be possible to separate the S and Se spectra and low noise spectra of the region of the upper valence band.

Chapter VI.

Chemical bonding and d interactions in transition metal sulfides

The sulfur-$L_{2,3}$ spectra from MgS, MoS_2, WS_2, NiS, FeS, GaS and SnS have been measured with soft x ray spectroscopy using both e beam and photon excitation to study the participation of d electrons in the electronic properties of Transition Metal Sulfides (TMS). The study is made possible by the fact that the metal d-electrons contribute to S spectrum as we have previously seen in CdS and ZnS. MgS provides comparison with a compound in which the metal atom contains two s, but no d electrons. MoS_2 and WS_2 are technologically important compounds involving the early transition metals for which substantial experimental and theoretical studies are available. FeS and NiS are late transition metal compounds that have been widely studied.. The ZnS and CdS samples discussed in a previous chapter are representative of compounds with just filled d-shells, and GaS and ZnS are compounds which border the transition region at higher atomic numbers.

The only important contribution to the spectrum of MgS is the S 3s orbital, which is present in very similar form in the spectra of all compounds presented here. MoS_2 and WS_2 are interpreted primarily using molecular orbital theory. The use of photon excitation near threshold permits us both to separate the L_2 and L_3 spectra as was done with CdS and ZnS, and to study resonance effects that assist in the identification of the orbitals contributing to the observed spectra. Strong correlation effects are seen in the NiS and FeS spectra which produce widely separated peaks associated with $3d^8$ and $3d^7$ states. For excitation near threshold, strong resonance effects are seen in both

compounds. As we have seen, the filled d-bands of CdS and ZnS are non-bonding states which lie in a sub-band gap between a lower valence band derived from the S 3s orbital and the UVB. The failure of theory to properly place these states in the band gap provide evidence that the rather subtle interactions of these d-states with other valence electrons are not yet completely understood. Finally, for GaS and SnS, the d bands do not contribute significantly to the spectra, though a very weak feature is observed in GaS that may be associated with overlap transitions from Ga d-states.

A. Introduction

Sulfur is abundant on the earth and easy to combine with transition metal elements to form XS, XS_2, X_2S_3 and other complex materials with a variety of lattice structures. These materials provide us rich resources and have many interesting electric and magnetic properties. For example, in the 3d series, FeS acts as a normal narrow gap semiconductor; its neighbor, CoS is a ferromagnetic material; NiS is an insulator with a metal-nonmetal phase transition at 260K°; Copper pyrite (CuS) is metallic with a metal-superconductor transition at low temperature; and ZnS is a wide gap semiconductor. These properties are quite different even though these compounds belong to the same 3d TMS series

These materials are interesting not only for their wide range of properties, but also for their applications [6.1-6.2]. CdS, MoS_2, WS_2 are among the best known solar cell semiconductors because these sulfide materials have proper energy gaps to convert visible light to electrical energy with reasonable converting efficiency [6.1]. Their electronic properties are still incompletely explored. Some sulfur compounds and metal-sulfur complexes play key roles in biological materials. Many of the structures used in

quantum well structures and studies of quantum confinement utilize TMS elements. Despite these features, relatively little attention has been given to the electronic properties of these materials until very recently.

These varying properties of transition metal compounds are conditioned by the number of electrons, n_d ($1< n_d <10$), in the open d shell and their correlations in solids. Previous studies of TMS show properties which may be best described with independent particle, ie. band structure, models, and others that may be best described with strong correlation models such as the crystal field multiplet model, or Mott-Hubbard model (see chapter II). TMSs provide a good system to study these many body correlation in solids.

Both theoretical and experimental studies of d electrons in transition metal compounds have been reported [6.3-6.11], but the picture is still not very clear now. Here are some of the issues: The locations of d bands in CdS and ZnS are much deeper in the sub-band gap than predicted by theory indicating that the s-d and p-d interactions in these materials are not fully understood [6.10] Chemical bonding in NiS has been a subject of long controversy. The well known Mott-Hubbard model, with strong d-d interactions, successfully accounts for chemical bonding in early transitional metal compounds involving Ti, V and others, and predicts that NiO has d-d type bonding, while the photon emission experiments on NiO indicate a charge transfer type band gap. [6.12-6.16] Previous studies of Cu, Ag, Ga and In compounds[6.9] have shown various d interactions and chemical bonding in TMS.[6.9]

In qualitative terms, we can say that the deep lying S 3s state, whose spectral peak is found with essentially the same energy position and intensity for all compounds, does not contribute significantly to the bonding. The bonding states are derived from the S 3p (partially filled) and S 4s (empty) and TMns (filled), TM(n-1)d (partially filled) and TM

np (empty) states. In chemical language, the bonding is associated with the frontier orbitals derived from these states, and the contribution of the d-orbitalas is conditioned primarily by its location within the valence band with respect to these orbitals. The bonding can be described in terms of d-d, d-p, s-p and s-d interactions[6.13].

Previous studies are reported for NiS [6.2, 6.12-6.21], MoS_2 [6.22-6.34], WS_2 [6.33,6.35-36], FeS [6.2, 6.20-27, 6.37-6.41], GaS [6.42-6.45] and SnS [6.46-6.50]

B. Results and Discussion.

The samples studied were mostly commercial powdered samples with the following characteristics: MgS (99%, 1 micron, cubic); MoS_2(99%, 1 micron, Hex.); WS_2(99.8%, 1 micron, Hex.); FeS(99.9%, 100 mesh, Hex.); NiS(99.995%, 100 mesh, Hex.);and SnS(99.5%, 8 mesh, Orthorhombic). The powders were pressed into pills by a few tons of pressure before loading. The GaS (Hex.) was a 6mm sample with a shiny surface. Since these materials have been measured over a substantial period of time, results from the NSLS, CAMD, and the ALS are all presented here, along with spectra excited by both energetic electrons and photons. Spectra obtained from each of the materials are presented first along with descriptions of their principal features. The results are then further discussed as a whole.

MgS

The S $L_{2,3}$ spectrum of MgS is presented in Figure 6.1. The spectrum was taken at the NSLS with the experimental apparatus described in Chapter II. The spectrum presented here was excited with a 3 KeV e-beam at a beam current < 0.4 mA, and recorded with the 1200 l/mm grating of the SXE spectrometer. The pressure during data

acquisition was approximately 7 x 10^{-9} torr. Also plotted in Fig. 6.1 is an sulfur K-spectrum [6.52] and a calculated total density of states (TDOS) [6.51,6.53] taken from the literature.

The primary feature of the S L spectrum in this compound is the large peak located at 148.5 eV. This peak is associated with the lower valence band, which can be understood as a broadened atomic 3s state. The spectrum is further broadened by the splitting of the S 2p core levels, and by core hole and valence hole lifetimes. The intensity of the spectrum in the region of the upper valence band is very low and in this spectrum is not separable from the noise. In contrast, the S K spectrum shown in the figure, which provides a measure of the p-like density of states at the sulfur site, coincides accurately with the upper valence band, consistent with the fact that the UVB is derived from the S 3p states.

In semiconductors with mixed ionic/covalent bonding like those formed from the third row of the periodic table, the intensity of the L spectra in the region of the upper valence band provides a measure of the covalent bonding, being strongest in covalently bonded Si, much weaker in the P-$L_{2,3}$ spectrum of AlP and almost zero in highly ionic MgS.

MoS_2.

Figure 6.2 shows the S-$L_{2,3}$ spectrum of MoS_2 excited with 172eV photons at the ALS light source. Very similar spectra have been measured by us at CAMD with higher energy photon excitation, and by others with excitation by energetic electrons. This spectrum is a convolution of the L_2 and L_3 edges. As in CdS and ZnS, it is possible to obtain a pure L_3 spectrum by exciting between the L_2 and L_3 threshold. The spectrum Fig

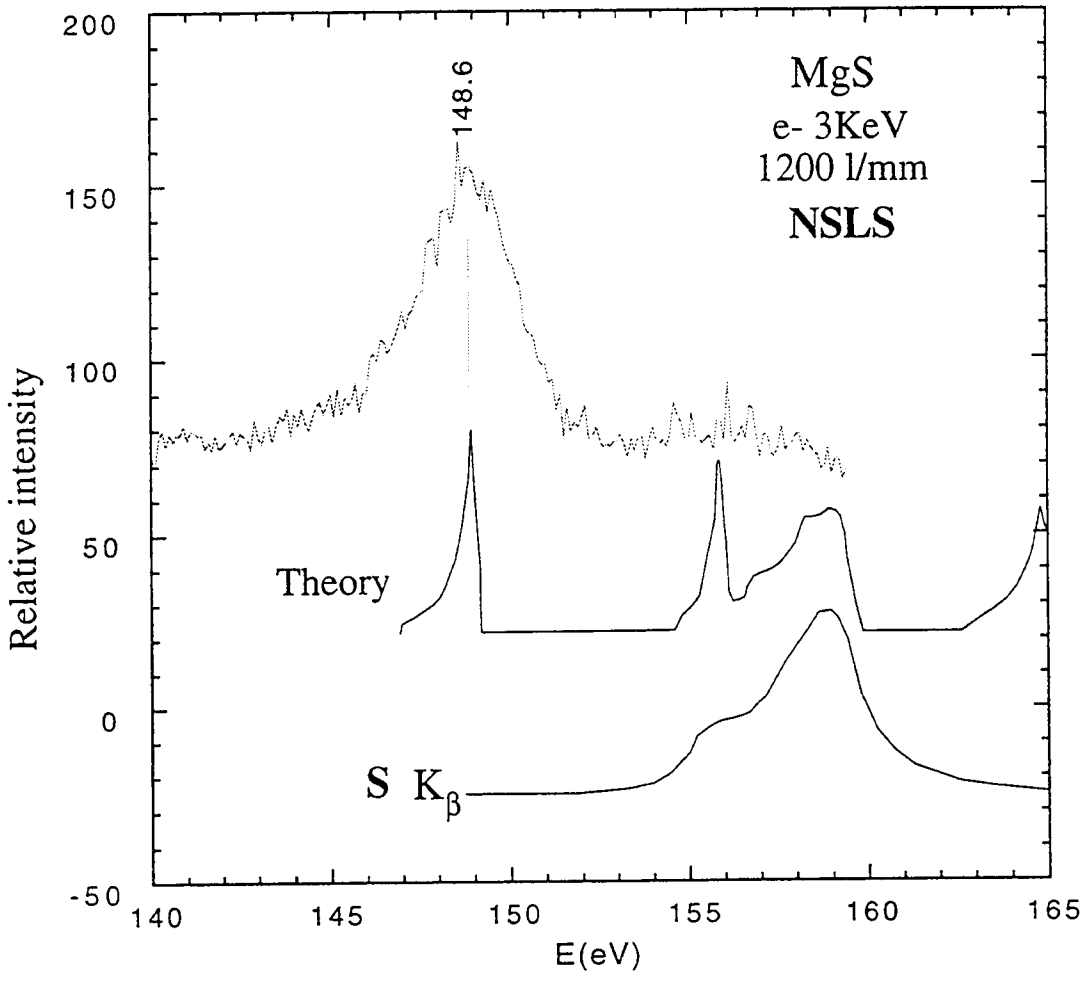

6.1 The S $L_{2,3}$ spectrum from MgS using e-beam.

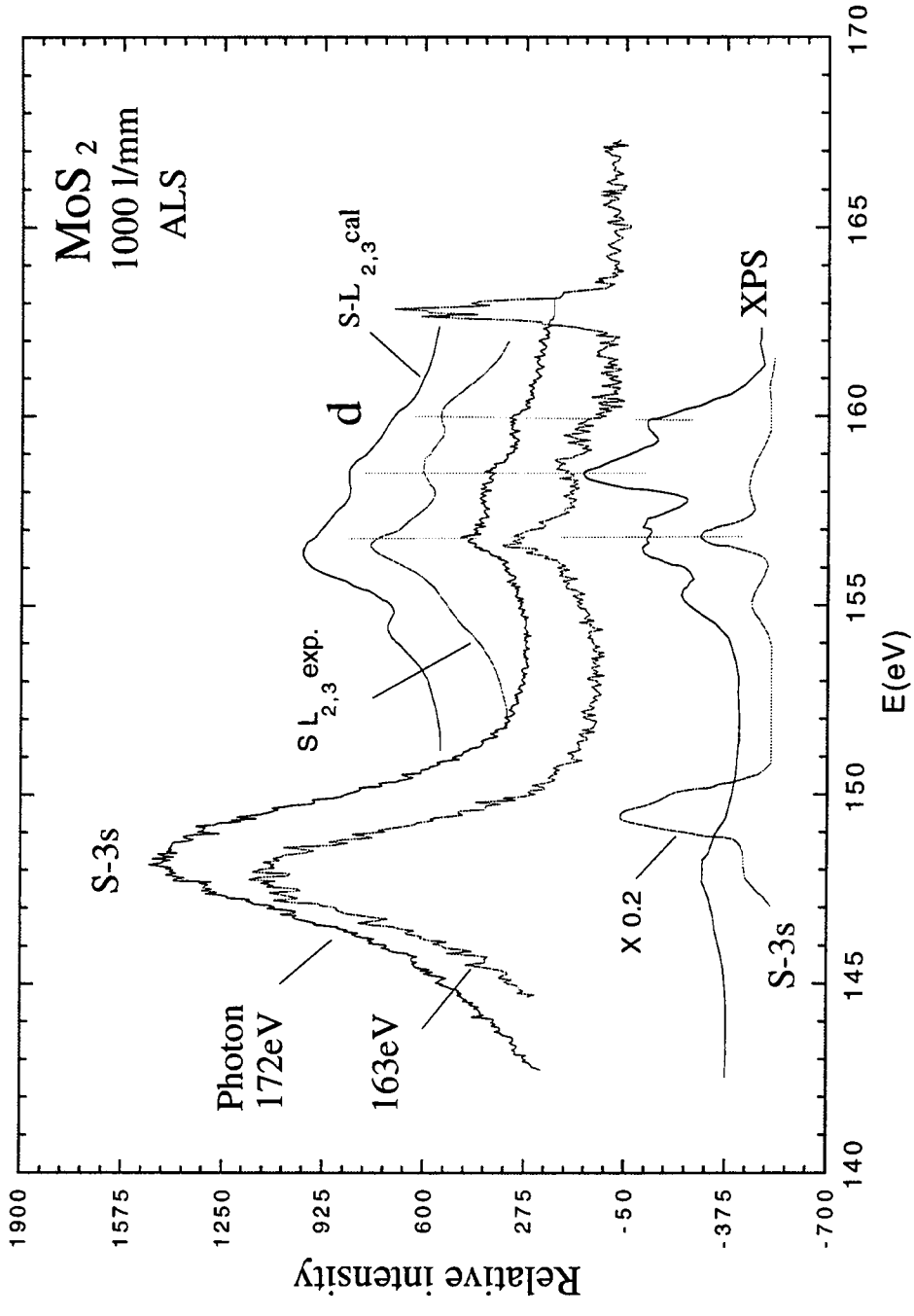

Fig 6.2 The S-$L_{2,3}$ emission spectra of MoS_2.

marked L_3 was obtained in this way with excitation by 163.2 eV photons. Other near threshold spectra are described in subsequent paragraphs. We have plotted on the same figure an e-beam excited S-$L_{2,3}$ spectrum taken by Aita[6.30] an XPS spectrum [6.22], and a calculated fit to the sulfur L spectrum [6.30].

In Figure 6.3, we plot the absorption spectrum of MoS_2 at the sulfur L edge obtained by measuring the ratio of the integrated photon flux in the S L SXF spectrum to the incident photon flux as a function of photon energy. The incident energy was stepped at 0.2 eV intervals and the total SXF yield recorded. This SXF yield provides a measure of the absorption due to excitation of the S 2p core levels. So long as normal two step excitation/deexcitation processes govern the fluorescence yield so that the radiative and non-radiative processes maintain a constant ratio, this absorption curve should be essentially the same as that obtained by measuring the photoyield. This "pre-edge" spectrum is, in fact, very similar to the photoyield curves of Didsiulis et al.[6.22] In both cases there is a small, structured absorption region between 162.5 and 166.5 eV below the main threshold at about 167 eV. We argue below that this small absorption feature is associated with localized absorption resonances derived from an empty Mo4d and S3p orbitals (2e' and 2e" in molecular orbital theory). The main absorption above 167 then corresponds to excitation into delocalized conduction band states derived from S3p and Mo5s and Mo5p atomic orbitals.

In Figure 6.4, we display SXF spectra for excitation near threshold. These spectra are normalized to incident flux so that the total area in the spectra are proportional to the amplitude of the absorption curve of Figure 6.3. The narrow high energy peak is the elastic peak, whose energy directly indicates the energy of the incident photons on the energy scale of the SXE spectrometer. This elastic peak has two absorption maxima, one

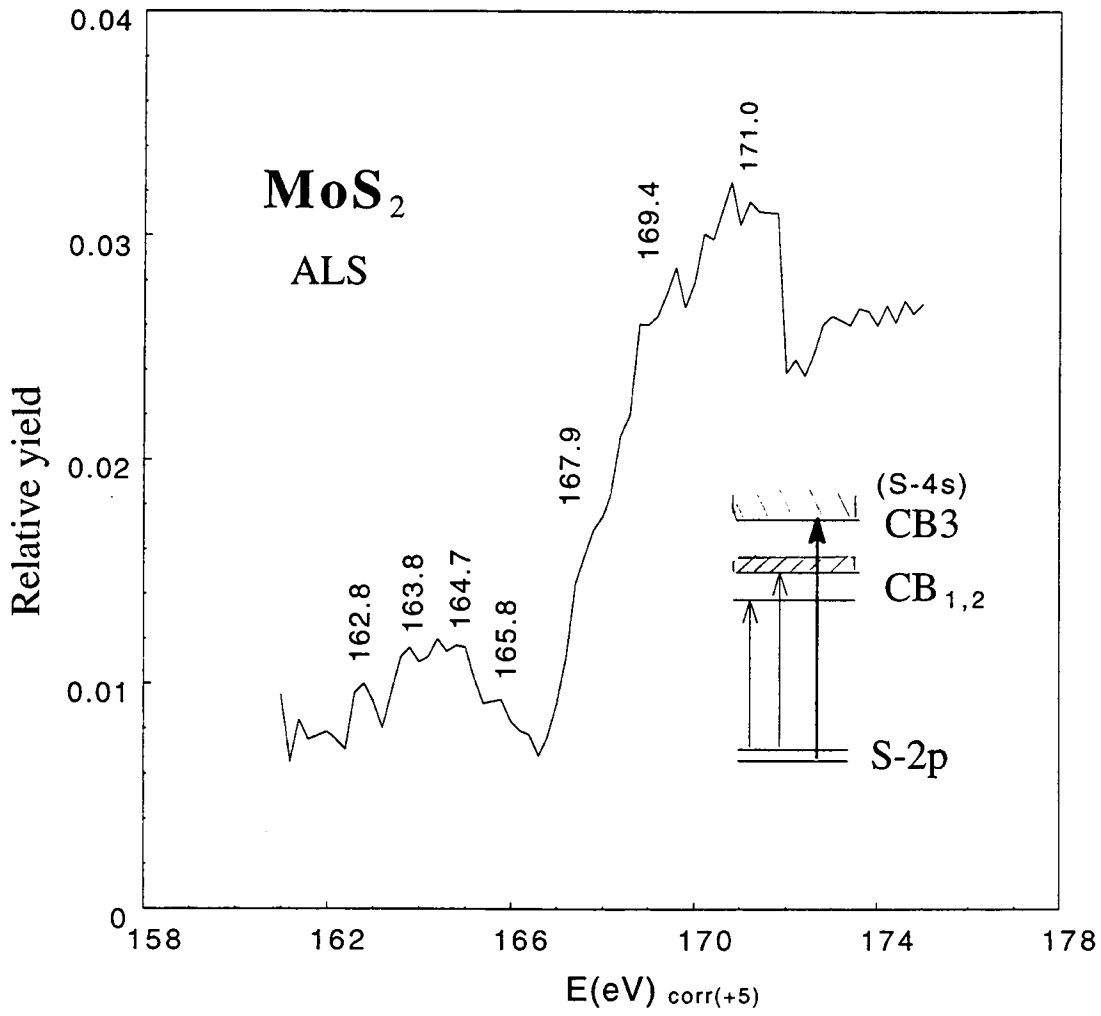

Fig 6.3 The absorption of MoS_2

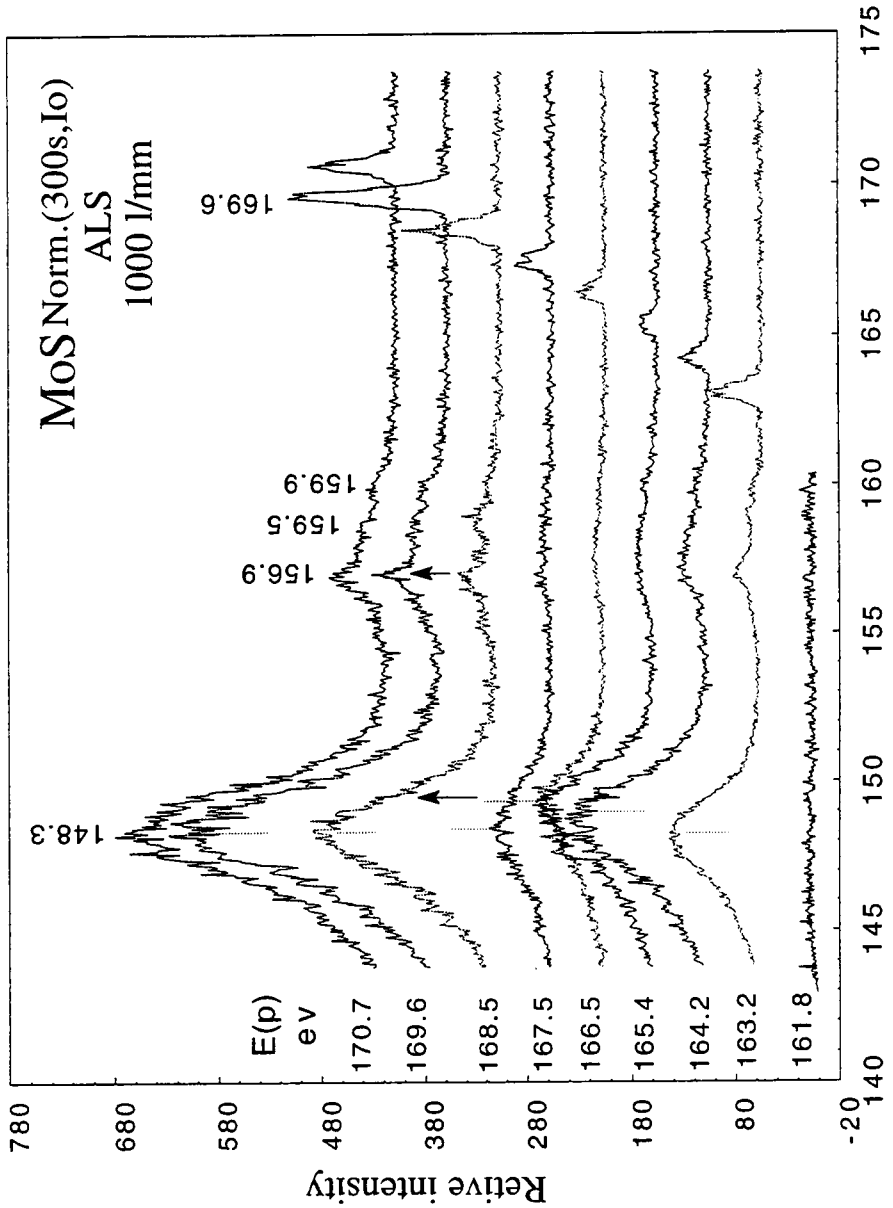

Fig 6.4 The threshold effect of MoS_2.

at the position of the 163.2 eV very near the onset of absorption, and the second at 167 eV, just at the onset of the second absorption threshold.

The SXF spectra extend from about 145 to 161 eV. Their overall spectral intensities show two resonances, the first in the region of the "pre edge" absorption peak and the second above 167 eV. The curve presented here at 163.2 eV is that used to define the L_3 spectrum of Figure 6.2. Careful study of the curves in the threshold region indicate that there is a very strong resonant enhancement of the spectra in a very narrow region just at threshold. In the absorption spectrum, this is the small peak at 162.8 eV for the L_3 threshold and the peak at 163.8 eV for the L_2 spectrum. This assignment is confirmed by the emission spectra by fitting the S3s peak with two peaks having the shape of the L_3 spectrum and separated by 1.15 eV. The L_2 and L_3 intensities determined in this way are plotted in Figure 6.5a for an excitation energy of 165 eV where the contribution of both spectra are nearly equal. In Figure 6.5b, the L_3 and L_2 are plotted as a function of excitation energy. Clearly, there are at least two resonances in this region that turn on first for the L_3 and then for the L_2 spectra.. At 166.5 eV, just below the major absorption threshold, both spectra have fallen to nearly zero. At the second threshold, the L_3 and L_2 spectra turn on again in order and eventually approach the 2/1 ratio expected for excitation in regions where sharp absorption resonances are not present.

While the SXF spectra indicate the presence of at least two resonance features in the "pre-edge" region, the absorption curve of Figure 6.3 provides more detailed information. Below 161 eV, the structure in this curve is associated with scattered exciting light reaching the SXE detector. The structural features above this energy are true absorption features that are reproducible. This curve has at least six peaks visible between 161 and 167 eV. A sharp absorption peak less than 1 eV wide, and centered at

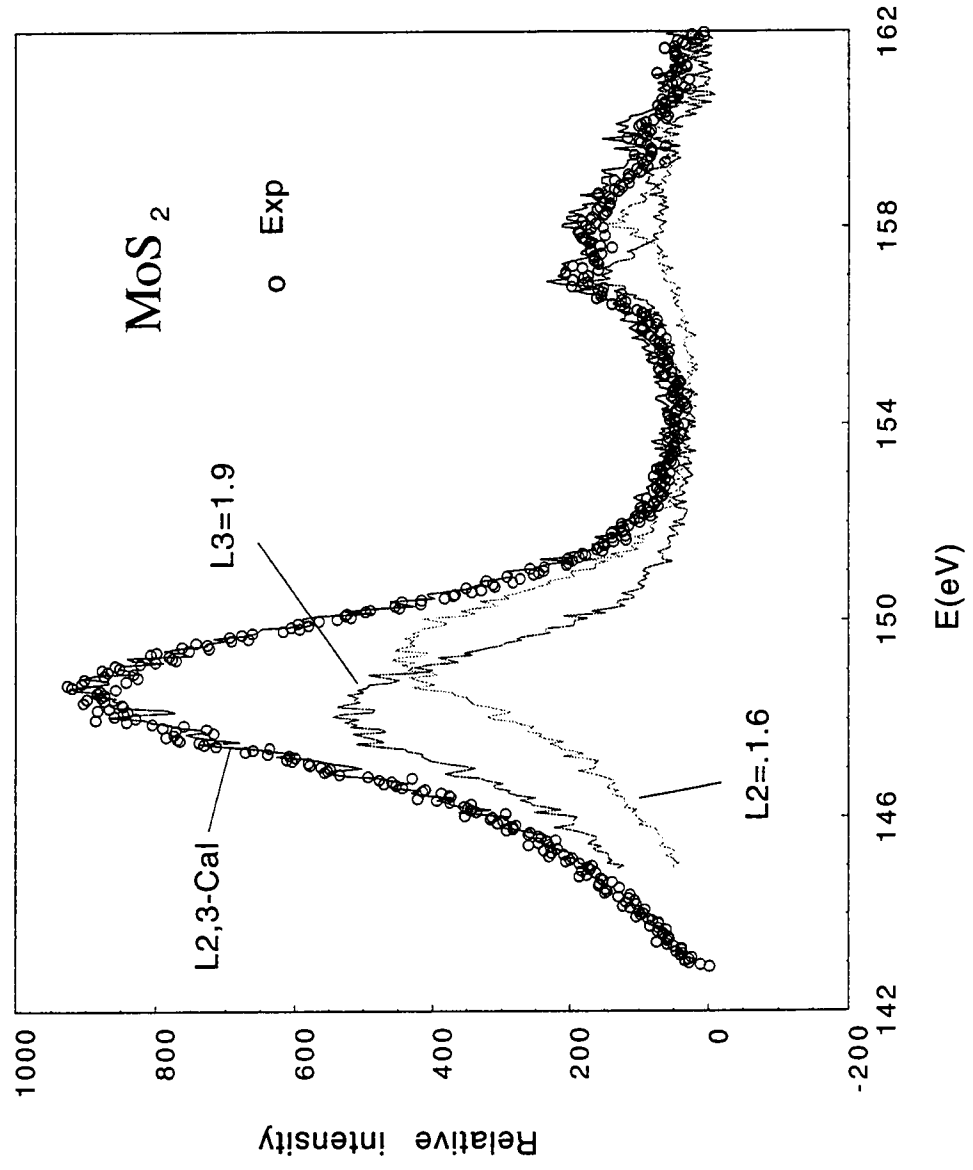

(a). The deconvolution of L_2, L_3 spectra of 165eV photon excited spectra.

Fig 6.5 The branching ratio of S L_2 and L_3 spectra of MoS_2.

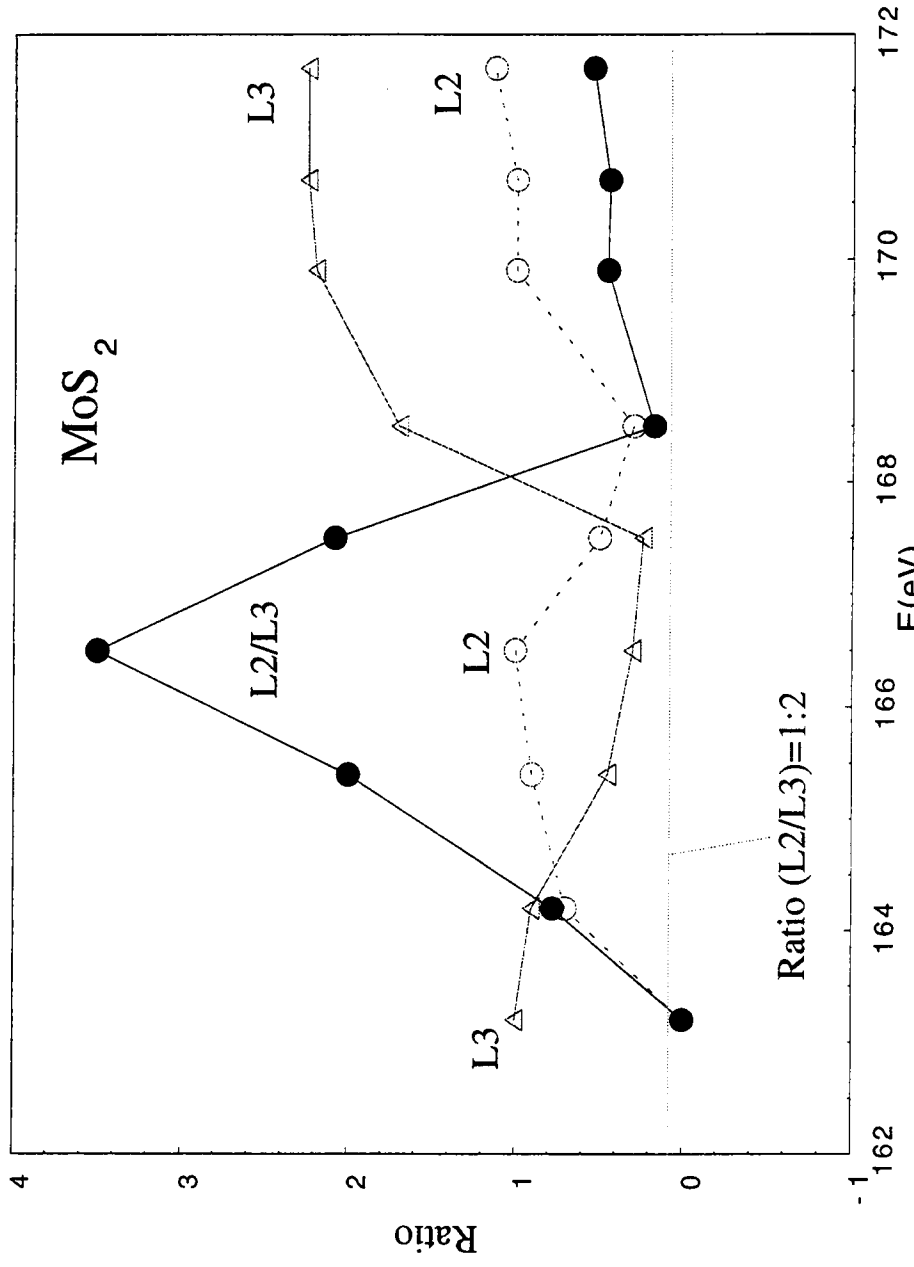

(b). Branching ratio of L_2/L_3 of MoS_2 at threshold.

Fig 6.5 (continued)

163 is associated solely with the L_3 spectrum. At higher energies, contributions from both spectra are present. The presence of six peaks indicates that there are three absorption maxima for each of two core levels giving a total of six peaks in the absorption spectra. The first absorption peak is very sharp and separated from the second and third, which appear to be broader and overlapping. A similar conclusion was reached by Didsiuilis et al in their analysis of photoabsorption data obtained from photoyield measurements in the pre-edge region. Inverse photoemission measurements which provide a measure of empty state density have been interpreted in terms of two resonances with a separation of about 1.2 eV located in the region just above the Fermi edge.[6.33]

Efforts have been made to fit MoS_2 spectra using both band structure and molecular orbital models. Simunek and Wiech used pseudopotential calculations, in which various parameters were adjusted to obtain the results shown in Figure 6.2. To aid in the interpretation of the spectra, their calculated densities of states were then projected onto s,p,d Gaussian orbitals of Mo and s and p orbitals of S. These projected orbitals were then used to calculate the transition matrix elements used to fit the spectra. Their fit to the $L_{2,3}$ spectrum and the sulfur s PDOS from which it is derived, is shown in Figure 6.2. It should be noted that this density of states is not associated with the S3s state, but represents the contributions of other orbitals, predominantly Mo4d orbitals, that sum to produce electronic density with s-like symmetry at the S site.

Most other authors have used molecular orbital calculations to obtain insight into the observed spectra. Essentially the same model has used to interpret data at both the Mo4p and the S2p absorption edges. The general scheme is shown in Figure 6.6 and

shows the MOs derived from interactions of the Mo 4d, 5s, and 5p orbitals and the S 3p orbital.[6.22] The MO diagram is based on an MoS_6 trigonal prism,

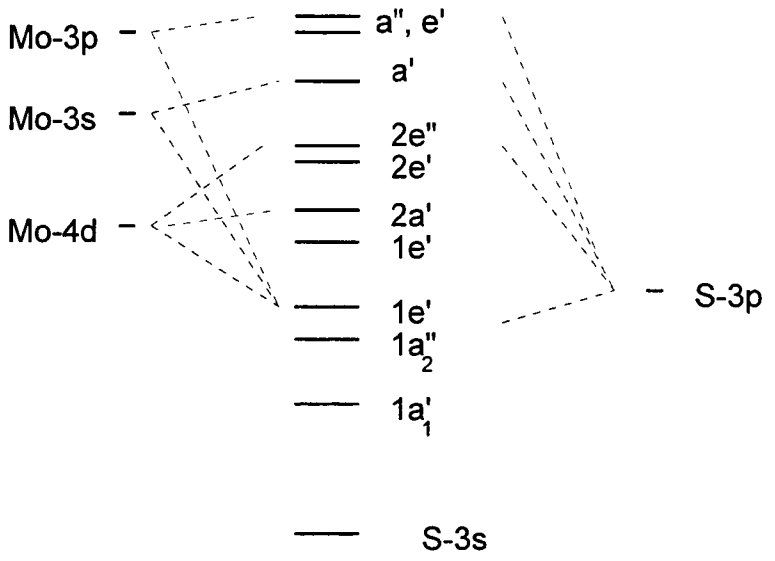

Fig. 6.6 MO orbitals of MoS_2.

which represents one-half of the MoS_2 unit cell. Symmetry considerations for the D_{3h} point group show that the Mo 4d orbitals can mix into MO's having a_1', e', and e" symmetries, while the Mo 5s orbital must mix into a_1' and the Mo 5p level will mix with a_1" and e" MOs. Of particular interest in this model are the 2e' and 2e" MOs which are derived from empty Mo4d orbitals and have been identified with the resonant absorption features detected found in the "pre-edge" region. While suggestive, these MO calculations are not adequate to account for our results, which indicate the presence of at least three absorption peaks in the "pre-edge" region.

The threshold spectra of MoS_2 do not provide convincing evidence that the one-step inelastic scattering processes like those present in the Zn $M_{2,3}$ spectra of ZnS contribute to the sulfur L spectra of MoS_2. The resonance effects we see are all consistent with resonances in the absorption process only, in that the intensities of S3s peak and the upper valence band (UVB) region of the emission spectra rise and fall together. We see some evidence in the spectra that the relative magnitudes of peaks in the UVB change with intensity, especially near the strong elastic resonance visible in the 169.6 eV excitation energy spectrum. Such changes would be evidence for the contribution of inelastic scattering processes similar to those seen in the upper region of the Si spectrum. The noise in the spectra and the complications of absorption resonances in L_3 and L_2 spectra make it impossible to definitely confirm such changes of relative peak heights and shapes from the present data.

WS_2

In this section, we present emission and absorption spectra for the sulfur L_2 and L_3 edges. The results are found to be very similar to those observed in the very similar MoS_2 compounds. Both materials are layered compounds with essentially identical hexagonal, in-plane geometries, but have somewhat different stacking sequences. Most of the comments made above for MoS_2 are equally applicable to WS_2.

Figure 6.7 shows the S-$L_{2,3}$ spectrum of WS_2 with 184eV photon excitation at ALS. The S-$L_{2,3}$ spectra of MoS_2 under the same experimental condition are included for a comparison. WS_2 was found very easy to excite and its S-$L_{2,3}$ x-ray intensity is higher than that of MoS_2. For convenience, these two spectra were normalized to the same

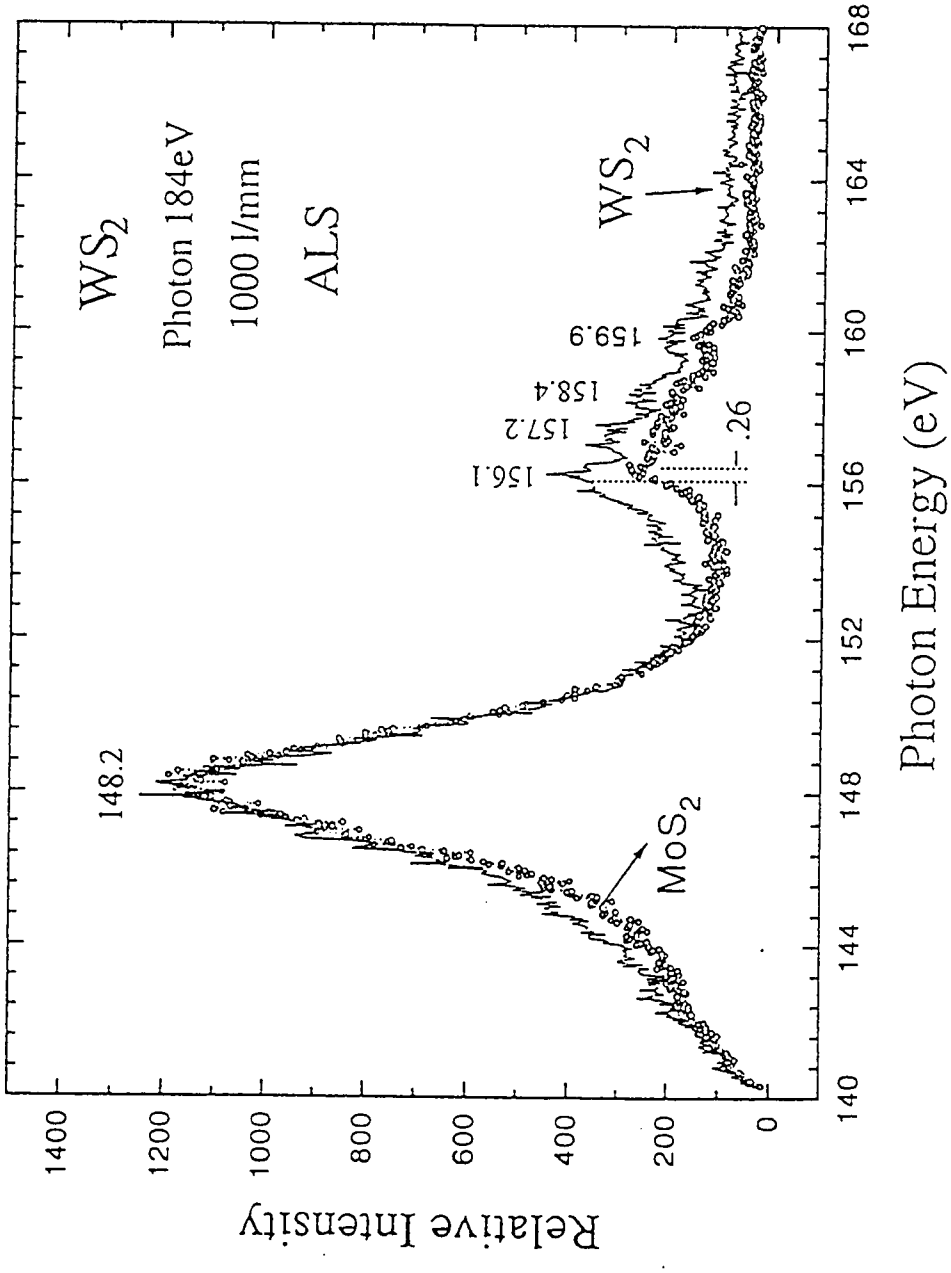

Fig 6.7 The S-$L_{2,3}$ spectrum of WS_2 with 184eV photon excitation at ALS.

height at the S3s lower valence band peak. The two spectra are very similar in shape. The sulfur 3s band in WS_2 has the same location with MoS_2 but has a little larger width at the low energy edge of the peak. The upper valence band is clearly separated into four peaks at 156.1 eV, 157.2 eV, 158.4 eV and 159.9 eV and a hint of a fifth at 162 eV. Relative to the 3s band, the upper valence band in WS_2 is stronger than that in MoS_2; the lowest peak of the upper valence band in WS_2 is shifted down by 0.26 eV as compared to that in MoS_2.

The absorption spectra of WS_2 is presented in Figure 6.8. Like MoS_2, it has a "pre-edge" feature between about 161 eV and 166 eV followed by a strong increase in absorption above about 166 eV. The pre-edge feature is not as completely separated from the main threshold as in the Mo compound. Four peaks, plus a shoulder are resolved in the pre-edge region. Electron energy loss spectra (ELS) [6.33] indicate the presence of two localized states separated by about 1.4 eV in the same region just above the Fermi level. XPS spectra of WS_2 [6.35] show similar features in the region of the upper valence band.

In Figure 6.9, we present threshold spectra obtained at the ALS for WS_2. At the lowest energies, only the L_3 spectrum is present. Figure 6.10 compares the L_3 spectrum obtained with 163.2 eV excitation with the $L_{2,3}$ spectrum obtained with 171 eV excitation. At slightly higher energies, the L_2 excitation dominates the spectra just above its threshold. As with MoS_2, the S3s peak was analyzed for the relative contribution of L_3 and L_2 levels. One of these fits is shown in Figure 6.11a. The relative spectral amplitudes determined in this way are plotted as a function of energy in Figure 6.11b.

To our knowledge, band structure calculations for WS_2 with projected densities of states suitable for comparison with x-ray spectra are not available in the literature. The

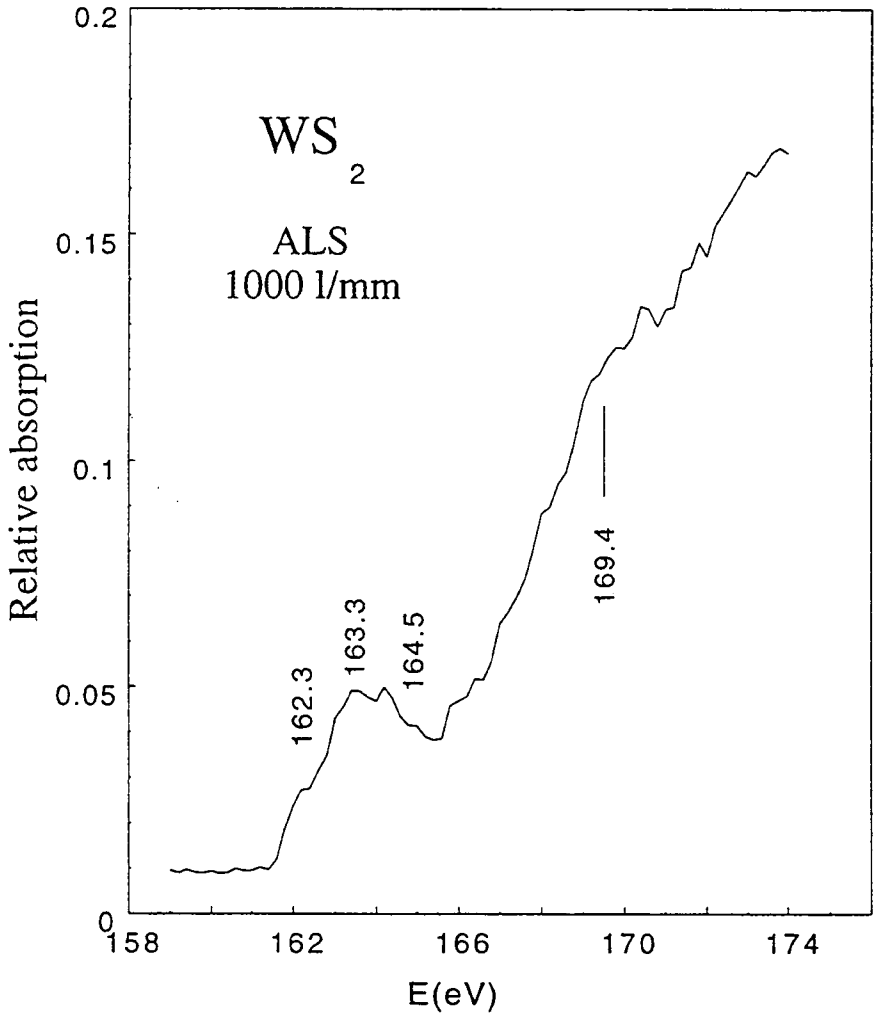

Fig 6.8 The absorption of WS_2.

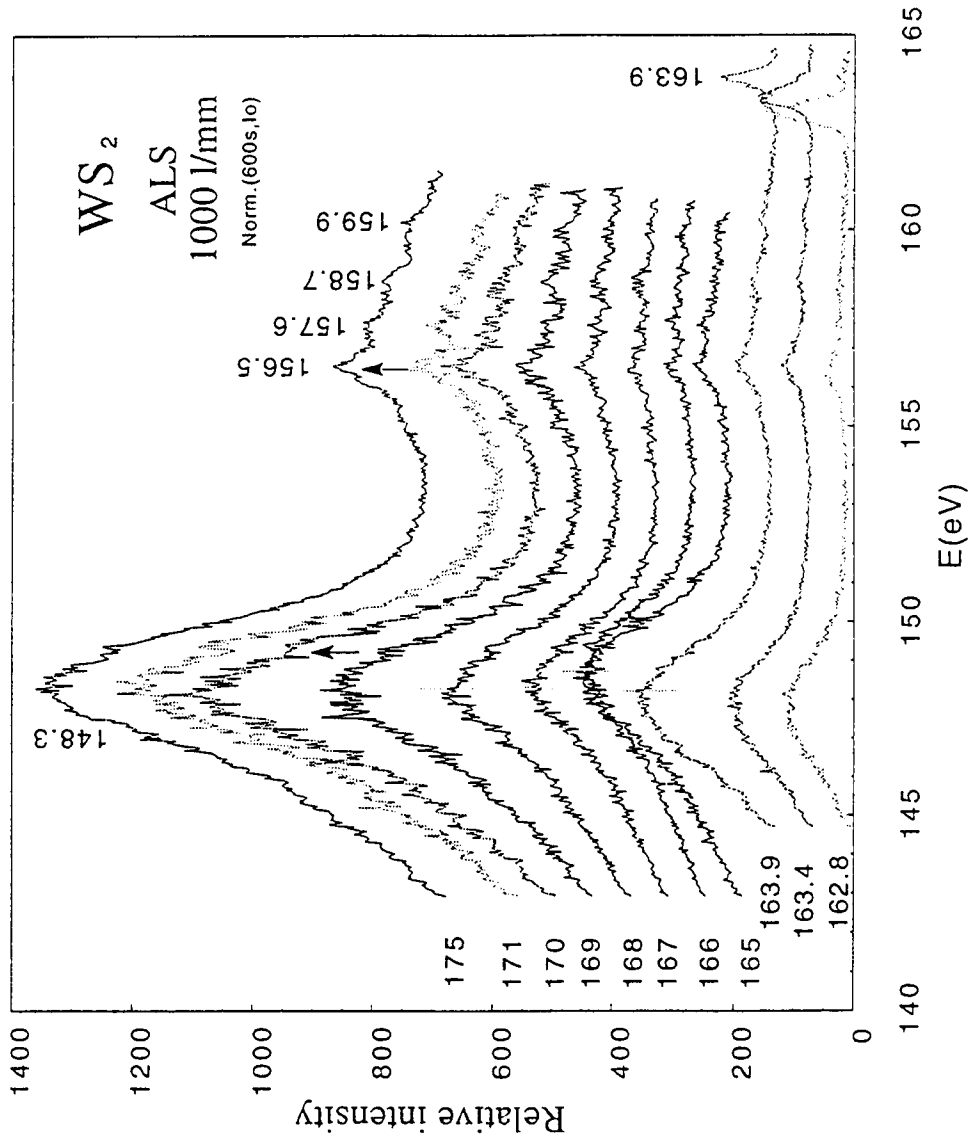

Fig 6.9 The threshold effect of WS_2.

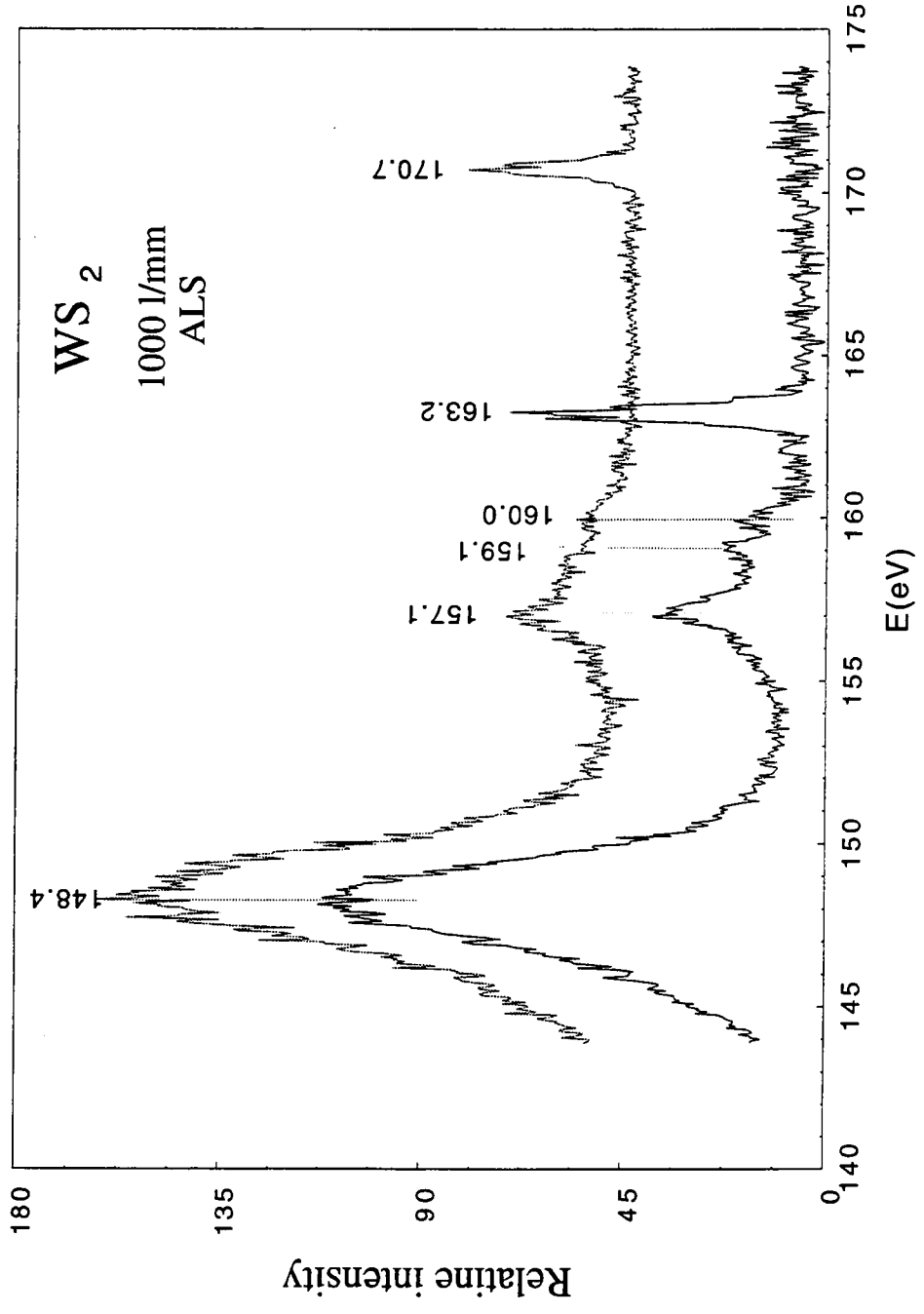

Fig 6.10 A comparison of L_3 and $L_{2,3}$ spectra of WS_2.

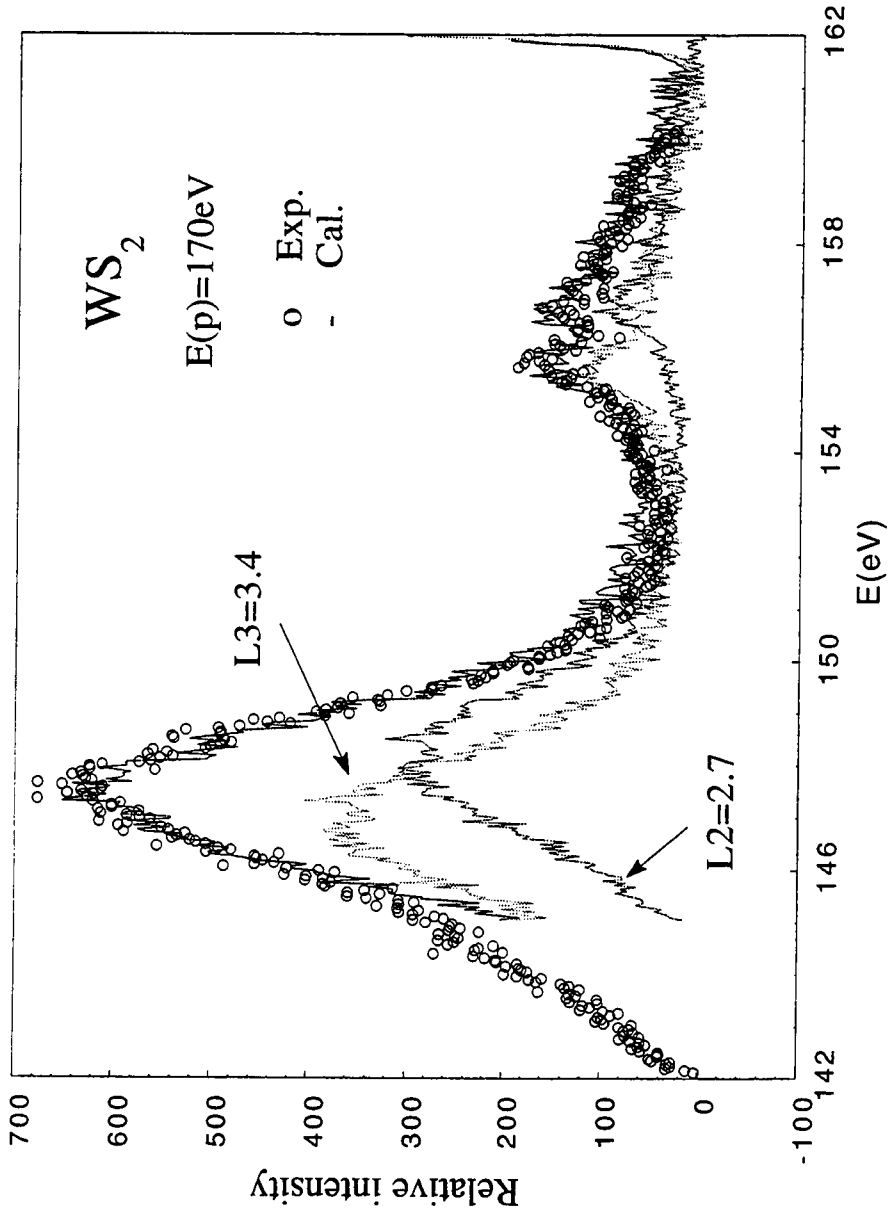

(a). The deconvolution of L_2, L_3 spectra of 170eV photon excited spectra.

Fig 6.11 The branch ratio of S L_2 and L_3 spectra of WS_2.

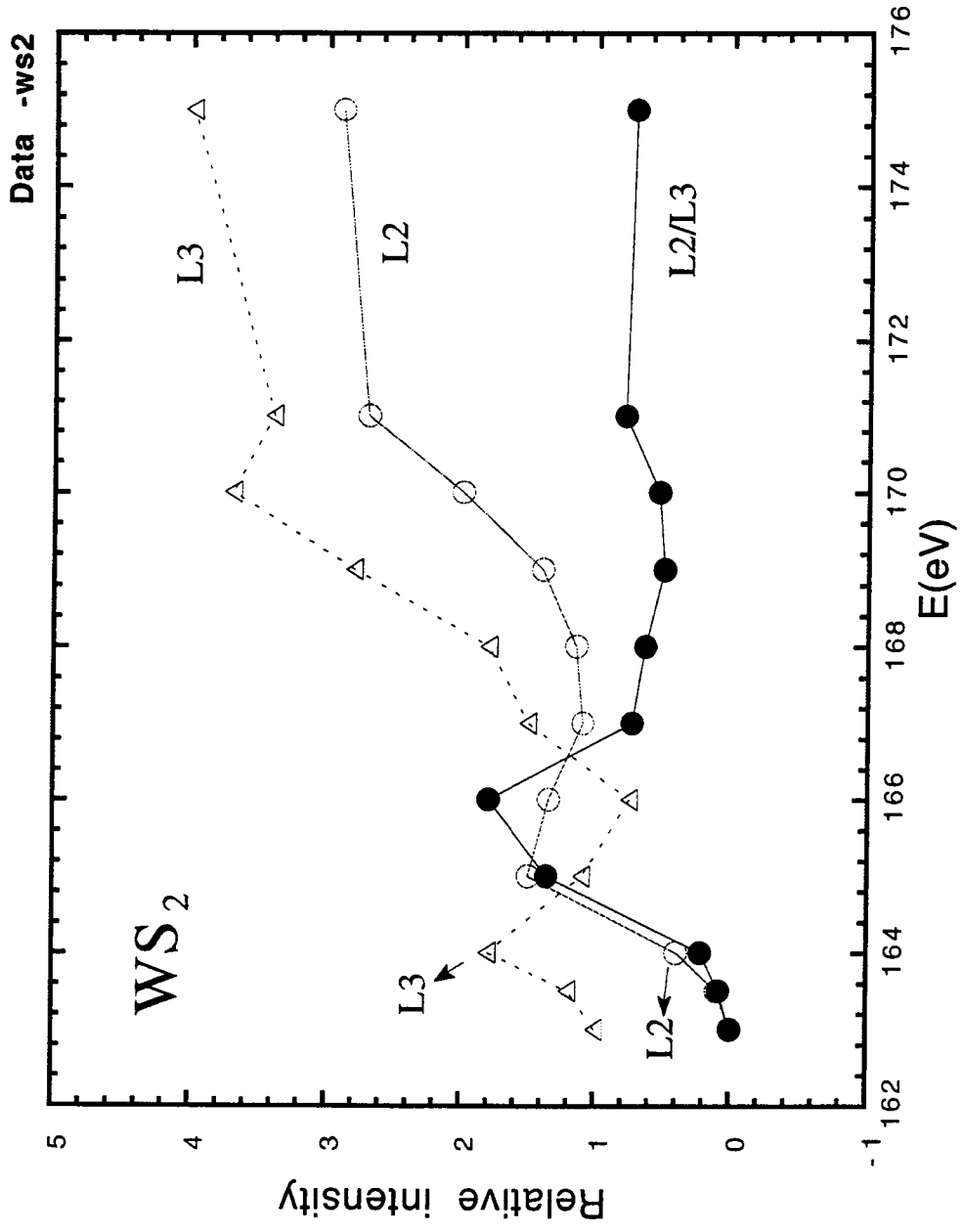

(b). Branching ratio of L_2/L_3 of WS_2 at threshold.

Fig 6.11 (continued)

same molecular orbital theory used in for MoS_2 is also applicable to WS_2, but at best can provide a qualitative interpretation of spectral data.

NiS and FeS

Of all of the spectra discussed in this dissertation, these are theoretically the most complex. The essential problem is that strong d-d Coulomb interactions, which are not properly accounted for in band structure calculations, play an essential role in the interpretation of the data. Fortunately, the essential features of the explanation of the NiS spectra have been given in a paper by Zaanen, Sawetzky, and Allen, who treat the TM4d electrons as an impurity atom in a host band structure derived from the S3p and TM4s and TM4p electrons.[6.14] The d-d interactions and the atomic term splittings are then accounted for, as well as the interactions between discrete and continuum states. No such explicit calculations are available for FeS, but the qualitative characteristics of the spectra are very similar to those found for NiS, modified by some very interesting additional structure.

Fig 6.12 shows the sulfur $L_{2,3}$ spectrum of NiS taken at the ALS with 184eV photon excitation. Also plotted on the figure are an XPS-spectra taken with photon energy of 1253eV and an inverse photoemission spectrum taken with 1486eV electrons., BIS-spectrum [Allan, Zaanan, Sawatzky - 6.14] of [6.16]

The theoretical curve is taken from the calculation for NiS cited above [6.14]. The solid line in the calculation corresponds to a photoemission spectrum where there is a hole left in the d-state after emission. The dashed spectrum is calculated for inverse photoemission which adds an electron to an empty state above the Fermi level. The labels on the peaks indicate the origin of the structural features. The lowest peak, as

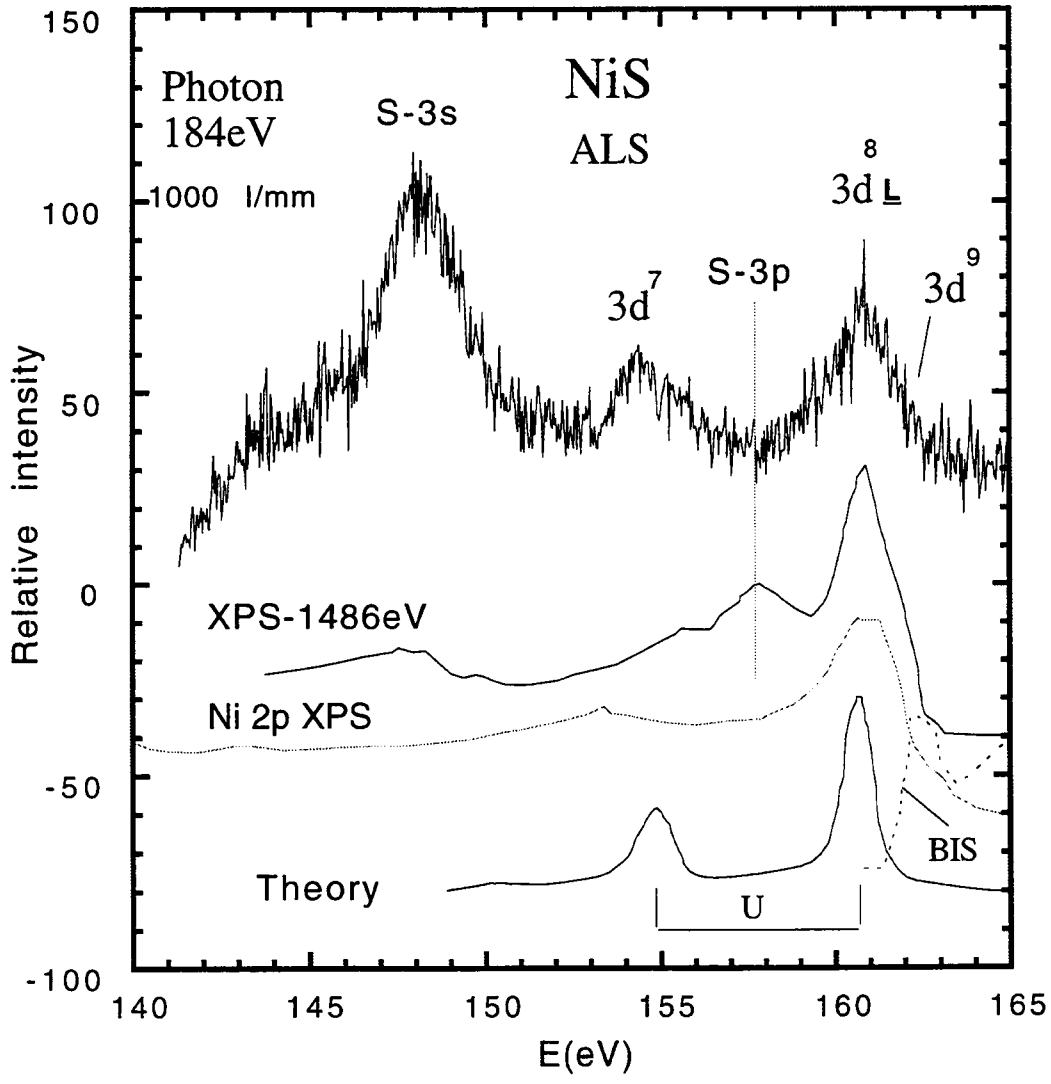

Fig 6.12 The S-$L_{2,3}$ spectra of NiS.

usual is the S3s peak. The peak centered at 153 eV is the $3d^7$ d-band and the higher peak, extending to the Fermi edge is the $3d^8\underline{L}$ charge transfer peak, where $\underline{L}$ represents a hole on the S3p valence band. An electron above the Fermi level fills a $3d^9$ state.

We note that the two d-related bands are broad, and that the $3d^7$ band is asymmetric, with an indication of a shoulder on its high energy edge. The broadening and asymmetry are indications of crystal field splittings that are not accounted for in the theory of Zaanan et al. As we shall see below, the sub-structure of these two major peaks is much more prominent in NiS.

In Figure 6.13a, we plot sulfur L spectra of NiS excited near threshold. These spectra were taken at CAMD with poorer resolution of the exciting light than at the ALS. The major feature to be noted is the S3s peak turns on before the d-band related peaks; the d-bands only appear with higher energy excitation This point is demonstrated explicitly in Figure 6.13b, which plots the relative magnitude of the S3s, and d1 and d2 peaks as a function of excitation energy. Also plotted in 6.13b is an absorption curve for the S2p threshold.[6.21] FeS discussed below shows similar behavior.

In Figure 6.14, we plot the photon excited sulfur L spectrum of FeS. In this spectrum, the S3s spectrum is artificially narrowed on its low energy edge by the cutoff of the spectrometers detector. The remaining two peaks are the analogues of the similarly located peaks in the NiS spectra and are labeled as $3d^5$ and $3d^6\underline{L}$ because Ni has eight d electrons in the neutral atom, while Fe has only six. The major qualitative difference between the NiS and FeS spectra is that FeS has clearly resolved peaks in both d bands. A three peak structure is clearly resolved in the lower energy d-band. In the higher d-band, the, a central peak and two shoulders are barely resolved.

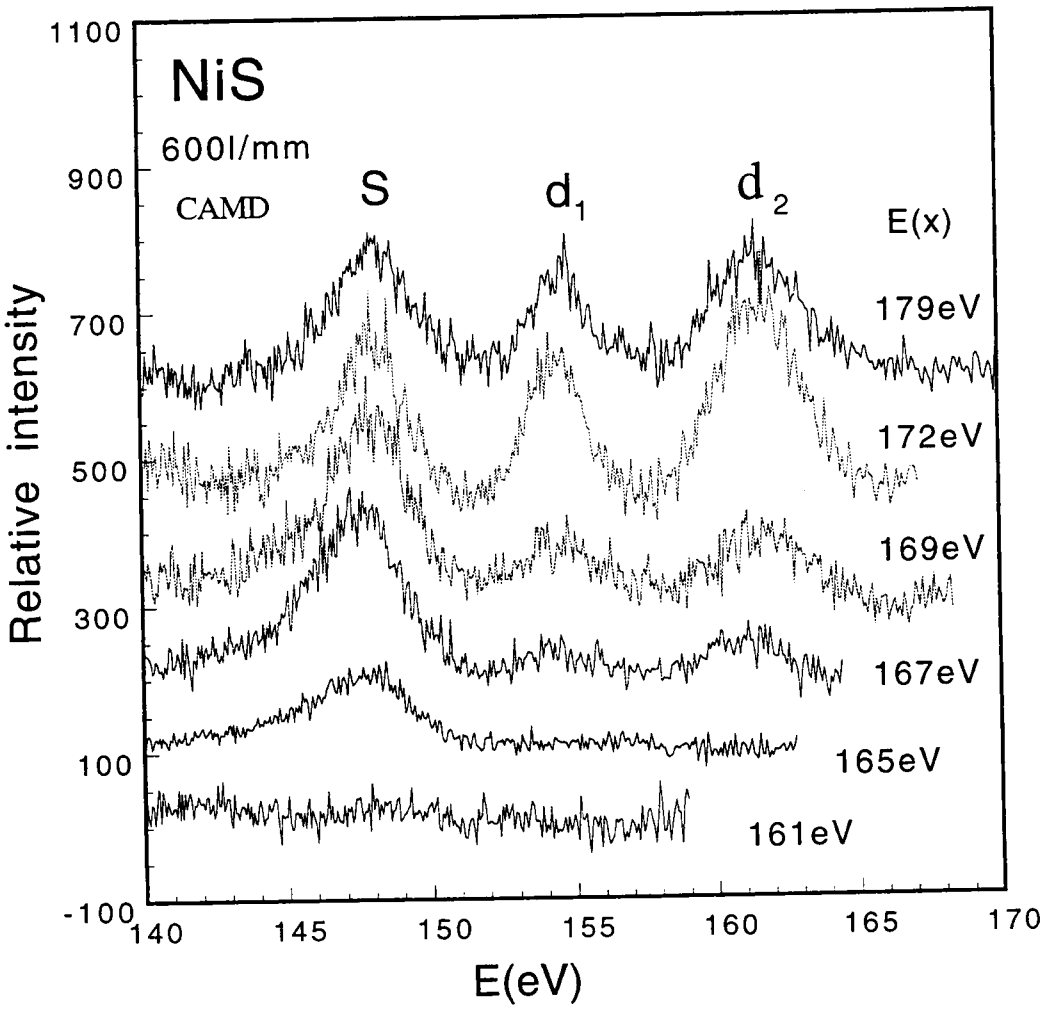

(a). S $L_{2,3}$ spectra of NiS with photon excitations.

Fig 6.13 The threshold effect of NiS measured at CAMD.

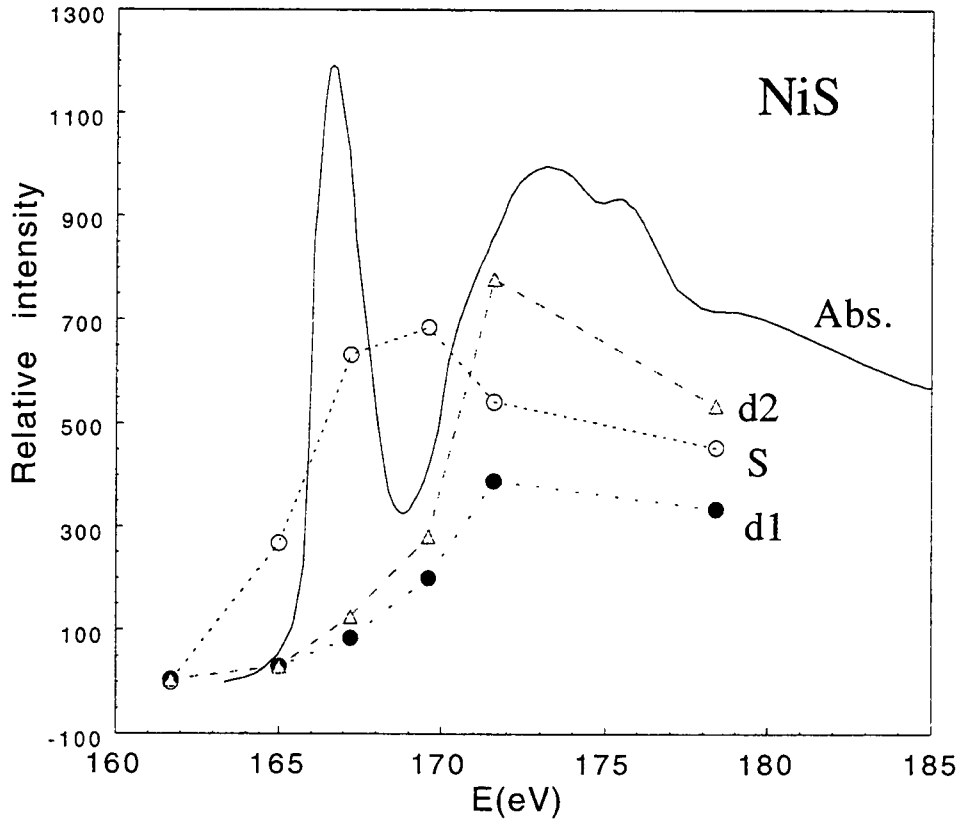

(b). Excitations of each bands

Fig 6.13 (continued)

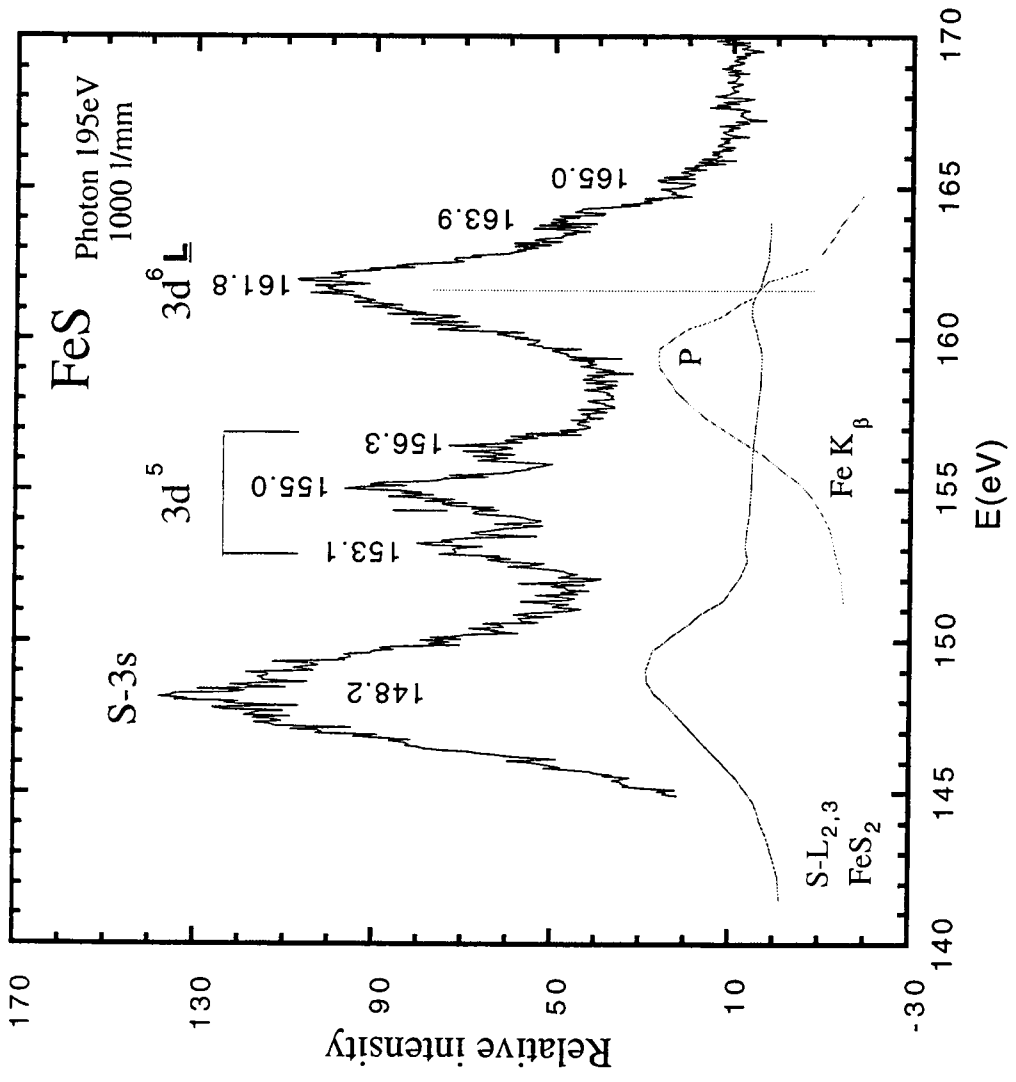

Fig. 6.14 The S $L_{2,3}$ spectra of FeS.

In Figure 6.15a, we plot the sulfur L spectra of FeS excited near threshold. These spectra have many interesting features. As with NiS, the S3s peak appears at lower excitation energy than the d-bands. In these spectra, it is very clear that structural features of the d-bands do not turn on an off uniformly as the excitation energy is varied. All of the peaks within the d bands remain fixed in energy position, but their relative magnitudes are strongly modulated as the excitation energies are increased. In Figure 6.15b, the relative peak intensities are plotted as a function of energy along with an absorption curve taken from the literature.[6.20] We note that the behavior shown here is dramatically different from MoS_2 and WS_2, where all spectral features appear to turn off and on in unison depending only on the rate of core hole creation. The first absorption peak in absorption curve is a exciton state of d band. At least one more resonance at 172eV in NiS, and three more resonances,at 169eV, 175eV and 181eV in FeS, are presented in these pictures. These are derived from resonant absorption and emission between 2p core levels and subbands in conduction bands with s/d characters.

Further comments on the NiS and FeS spectra are included in the discussion section below. However, ideas that might provide a suitable theoretical explanation for the threshold spectra of NiS and FeS are presently under discussion, so that our conclusions will be tentative pending further experimental and theoretical studies.

GaS and SnS

The sulfur $L_{2,3}$ spectra of GaS were measured using 3 KeV e-beam excitation and the ALS SXE spectrometer The spectrum is presented in the Fig 6.16 along with a theoretical calculation from the literature [6.43], an experimental S-Kβ spectrum and an XPS spectrum dominated by the Ga3d states [6.42]. The main feature at 148eV is the

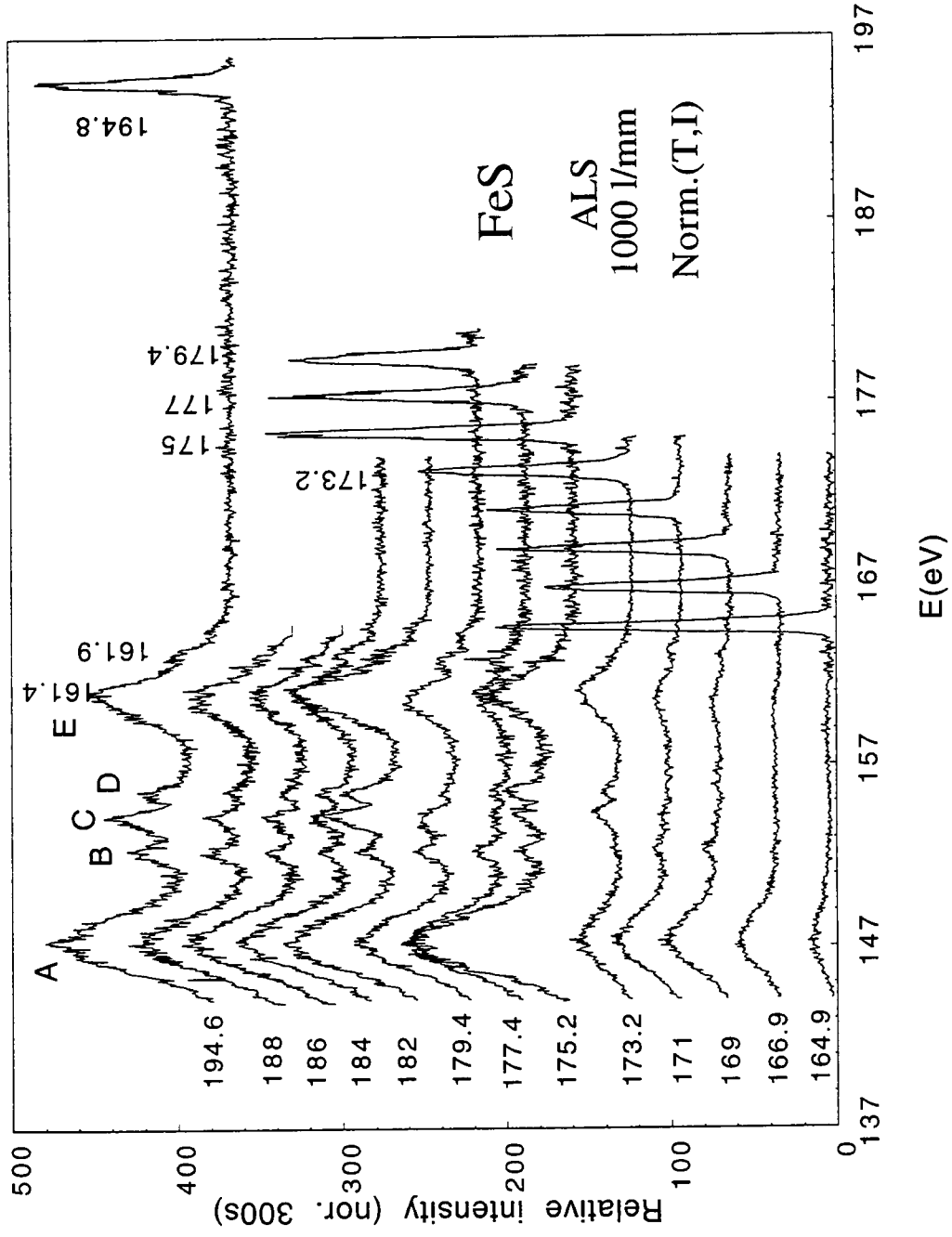

(a). S $L_{2,3}$ spectra of FeS with photon excitations.

Fig 6.15 The threshold effect of FeS measured at ALS.

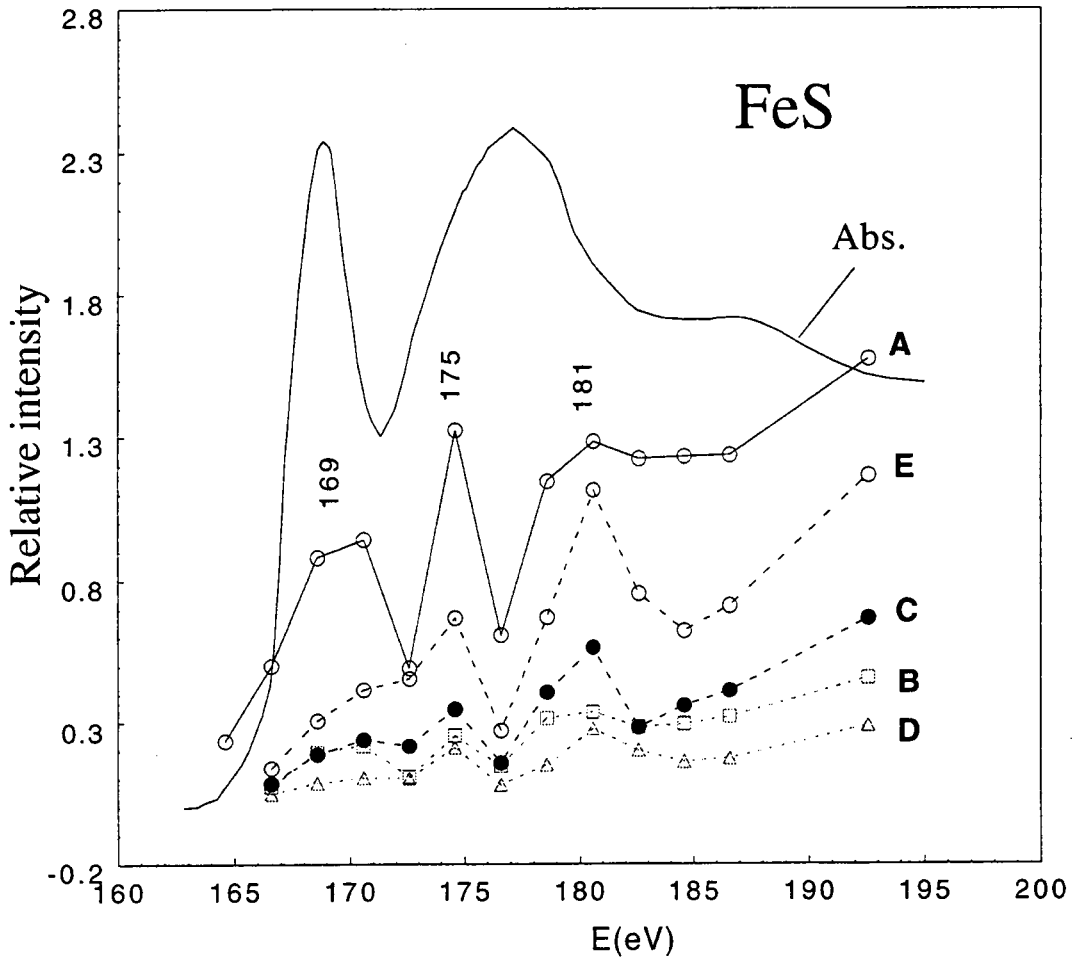

(b). Excitations of each bands

Fig 6.15 (continued)

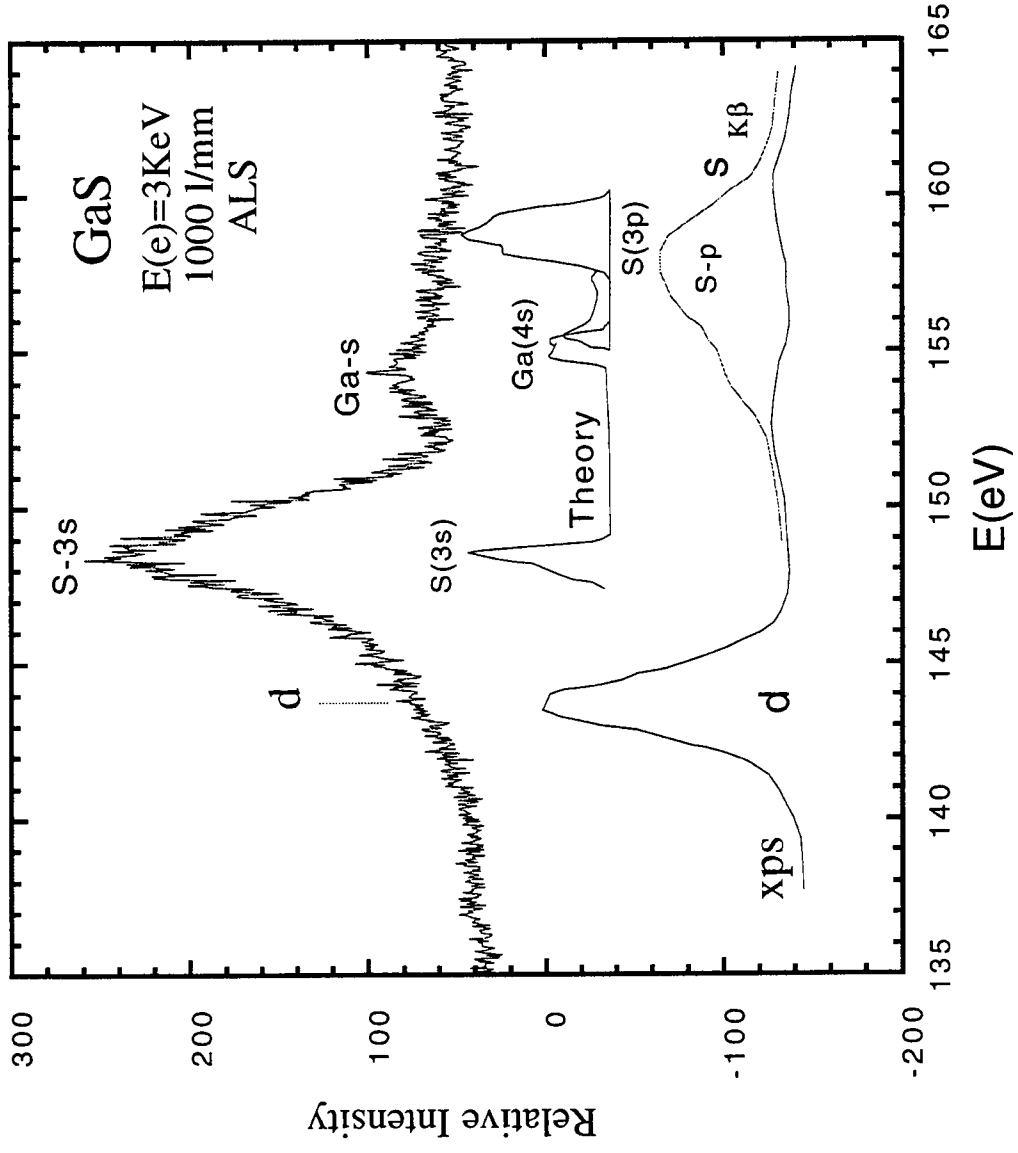

Fig. 6.16 The S $L_{2,3}$ spectra of GaS.

usual sulfur 3s orbital. The upper valence band is derived primarily from the S3p orbitals as indicated by the intensity of the S K spectrum in this region. The feature at 154 eV, which extends to the top of valence band at about 160 eV provides evidence for weak covalent bonding in this system. A very weak should is found at about 5 eV below the S3s band at the energy position of the d states, which may result from weak crossover transitions from the Ga d states to the S 2p core levels..

The sulfur $L_{2,3}$ spectrum of α-SnS is shown in Fig 6.17. It was measured using 3 KeV e beam excitation at the ALS. For comparison, a total density of state calculation from the literature [6. 47] is plotted on the same figure.. The main feature at 148.4 eV is the usual sulfur 3s orbital. The peak at 153.7 eV, about 5 eV higher, is at the position of the Sn 5-s orbital. The long tail of upper valence band extends to the upper edge of valence band at about 160 eV. No evidence of emission from Sn d states are observed in these spectra.

C. Discussion.

Figure 6.18 plots the sulfur L spectra for all of the materials discussed in this chapter together with ZnS and CdS spectra from Chapter IV [6.10]. The d bands are marked on each spectra. These spectra contain many interesting features. The S3s state is very similar in every spectra, and contributes little to the bonding. In all of the TMS spectra, the TM d-states interact strongly with the S 3p states in the region of the UVB. Most of the spectra, with the exception of NiS and FeS, can be accounted for qualitatively with one-electron theory, so that band structure calculations can provide a fairly adequate description of the observed emission spectra. In NiS and FeS, d-d interactions have the dramatic effect of generating two d-bands, whose energy state differ depending on

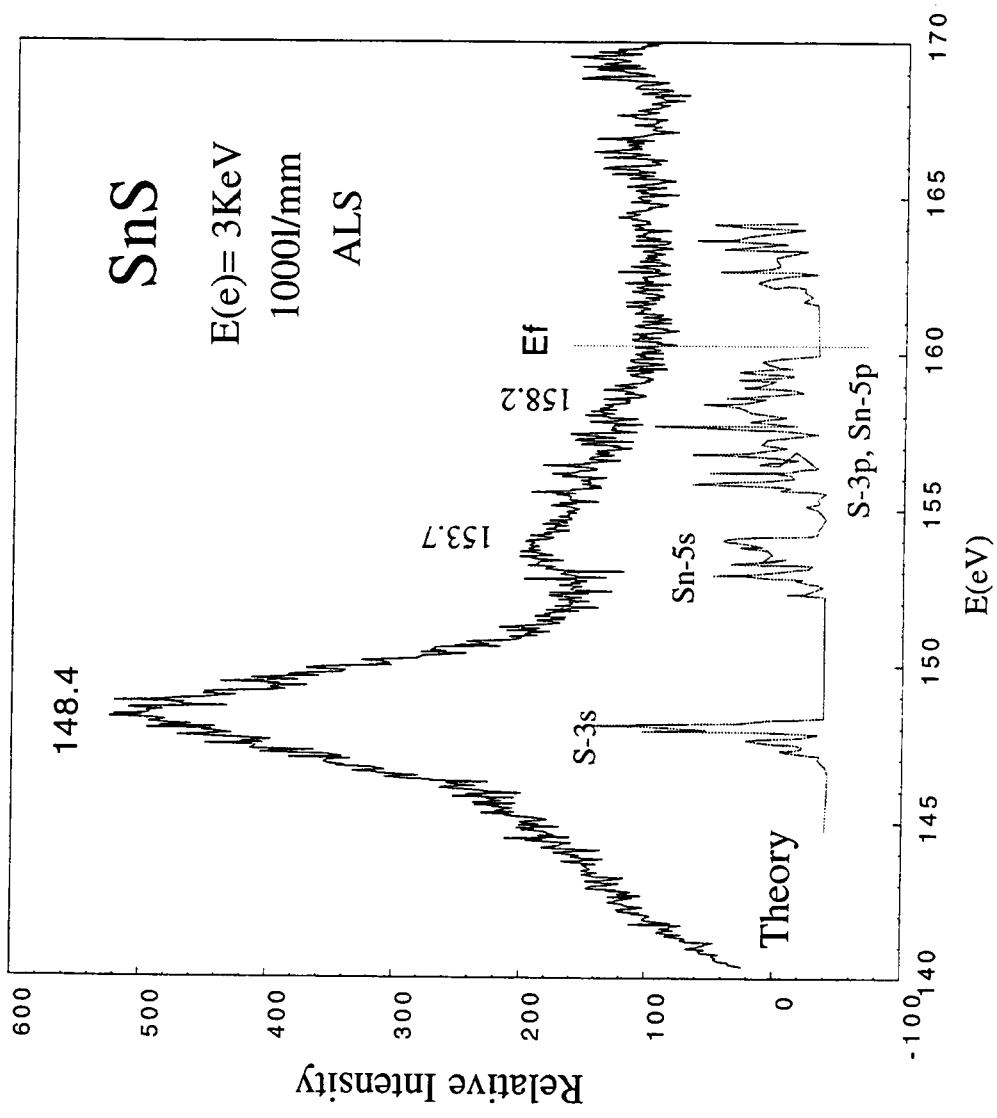

Fig. 6.17 The S $L_{2,3}$ spectra of SnS.

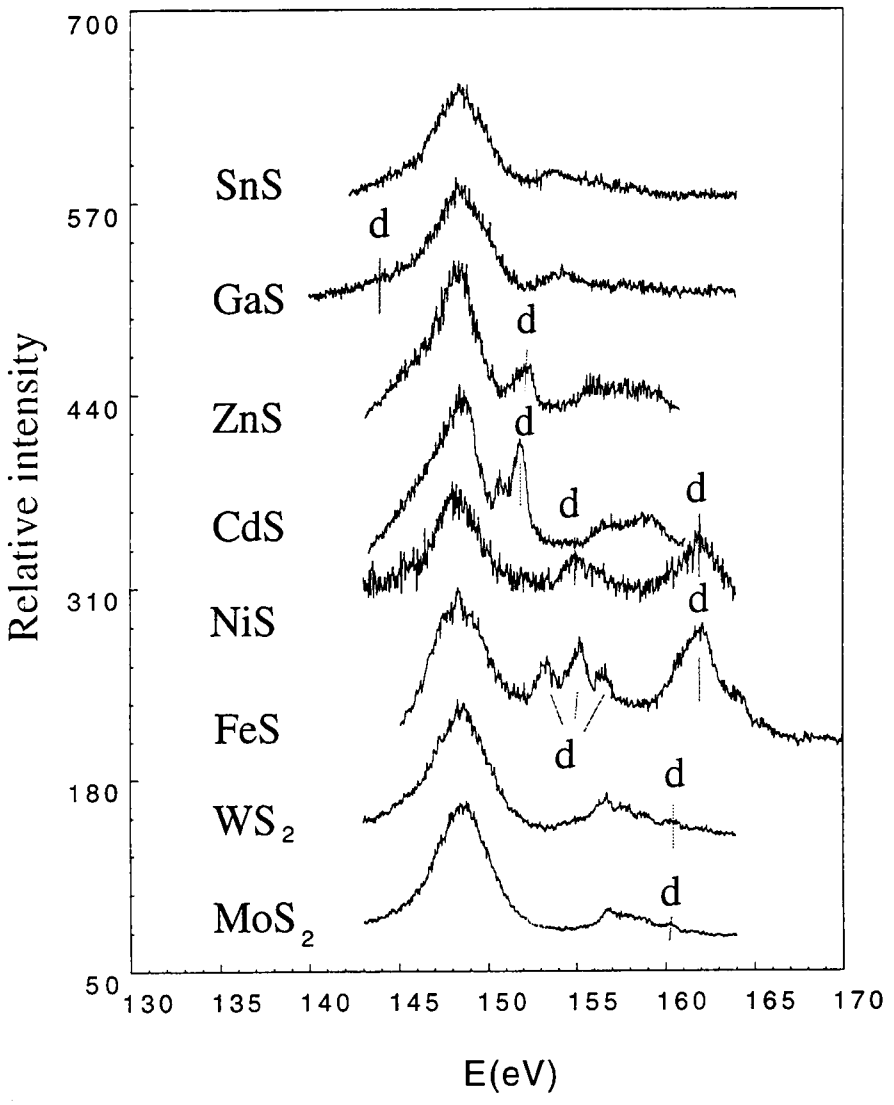

Fig 6.18 The d bands of S-$L_{2,3}$ spectra in TMS.

whether the valence hole in the final state is located in a localized d-orbital, or in a distributed UVB state.

The d-d interactions displayed so strongly In the FeS spectra seem to provide the best explanation for the displacement of d-bands in CdS and ZnS from the position high in the subband gap calculated by band theory to several eV lower energy. The energy shift then represents the difference in energy between d^{10} neutral states and d^{9} final state of the SX emission process. It also seems probable atomic term splittings may account for the doubling observed in the d-bands of these materials.

These observations suggest that an adequate description of the SX spectra of the TMSs will have to be developed along the lines of the treatment of NiS by Zaanan et al., in which the d-electrons are treated as part of an impurity atom in a s/p host lattice.

In the absorption spectra, for most of these compounds, there is a strong evidence for localized states just above threshold which produce resonant absorption effects in the spectra. These states can most appropriately be thought of as localized excitonic states derived from the d^{n+1} states of the TM d-bands. Again, an atomiclike treatment of the d-electrons seems to provide the best possibility for accurately treating localization and correlation effects.

The results reported here have demonstrated a rich variety of electronic state and bonding behavior in these sulfur compounds, and indicate that further studies are needed to develop a coherent picture of the S compounds. In particular, it would be desirable to measure spectra of the TMs to complement the S spectra presented here. It would also be desirable to have measurements of the S K spectra to provide information on the p-like density of states. These spectra, located at about 2.47 KeV are beyond the range of our current instrumentation, but can be undertaken through collaborations with others.

Finally, it would be useful to study additional materials, particularly compounds involving the early transition metals, and sulfides with different crystal structures and different valencies. For example, it would be useful to study FeS_2 as well as FeS. There are also many opportunities for useful studies on alloys with the improved capabilities of the ALS facility. Many of these studies are planned for the near future at the ALS and CAMD.

References

References

[1.1] Derek J. Fabian, Soft X-ray Band Spectra and the electronic structure of metals and materials. 1968.

[1.2] B. K. Agarwal, X - Ray Spectroscopy. p312 (1979).

[1.3] M. Campagna and Rose, Photoemission and Absorption Spectroscopy of solid and interfaces with synchrotron radiation. p1, 13 and p127 (1990).

[1.4] M. Cardona and L. Ley, Photoemission in Solids (II). P11 (1978).

[1.5] G. D. Mahan, Phys. Rev. **163**, 612(1974). Also, G. D. Mahan, Many-particle Physics. (1981).

[1.6] P. Unger, J. Igarashi and P. Fulde, Phys. Rev. B **50**,10485 (1994).

[1.7] T. A. Callcott, D. L. Ederer and E. T. Arakawa, in Science with soft x-rays, SPIE, 447, 61(1984); Also, T. A. Callcott et al, Nucl. Instr. Meth. **A319** 128 (1992).

[1.8] J. Nordgren and N. Wassdahl. Acta Physica Polonia A. **82** 2 251 (1992).

[1.9] A. Muller and B. Kebs, Sulfur, Its significance for Chemistry, for Geo, Bio- and Cosmisphere and Technology. p277 (1984)

[1.10] T. Taguchi, Y. Yamada, Y. Endoh, Y. Nozue, J. T. Mullins, T. Ohno, Y. Masumoto, S. Tasumoto, S. Takeda. Superlattices and Microstructures. **10**, 207 (1991).

[1.11] N. Nerron, Science. **29** 1429 (1993). Also, V. L. Coloin, and A.P. Allevisators, Phys. Rev. Letters. **66** 21 2786 (1991).

[2.1] José Luís Martins, N. Troullier and S. -H. Wei, Phys. Rev. B **43**, 2213 (1991).

[2.2] C. S. Wang and B. M. Klein, Phys. Rev. B **24**, 3393 (1981).

[2.3] Xu Zeng and Meichun Huang, Journal of Luminescence, **40** & **41**, 913 (1988)

[2.4] Sylvester N. Ekpenuma and Charles W. Myles, J. Phys. Chem. Solids. **51**, 93 (1990).

[2.5] L. Ley, R. A. Pollak, F. R. McFeely, S. P. Kowalczyk and D. A. Shirley, Phys. Rev.B **9**, 600 (1974).

[2.6] Edit by M. Campagnam R. Rosei, J. C. Fuggle, Photonemission and absorption spectroscopy of solids and interfaces with synchrotron radiation. p130 (1990).

[2.7] B. K. Agarwal, X-ray Spectroscopy.(1979).

[2.8] J. Tulkki and T. Åberg, J. Phys. B: Atom. Molec. Phys. **13** 3341 (1980); T. Åberg, K. Reinikainen and O. Keski-Ranhkonen, Physical Review A. **23** 153 (1981); J. Tulkki, Physical Review A. **27,** 3375 (1983). Also, see McGraw-Hill Encyclopedia of Physics. Edited by Sybil P. Parker, p1171, (1993)

[2.9] K. E. Miyano, D. L. Ederer, T. A. Callcott, W. L. O'Brien, J. J. Jia, L. Zhou, Q. Y. Dong, and Y. Ma, Phys. Rev. B **48**, 1918 (1993).

[2.10] J. A. Carlicle, Eric L. Shirley, E. A. Hudson, L. J. Terminello, T. A. Callcott, J. J. Jia, D. L.Ederer, R. C. C. Perera and F. J. Himpsel, Phys. Rev. Lett. **74**, 1234 (1995).

[2.11] Y. Ma, Phys. Rev. **49** 5799 (1994). Also, Y. Ma, N. Wassdahl, P. Skytt, J. Guo, J. Nordgren, P. D. Johnson, J-E. Rubensson, T. Boske, W. Eerhardt and S. D. Kevan, Phys. Rev. Letters. **69** 2598 (1992).

[2.12] to be submitted.

[2.13] J. J. Jia, J. A. Carlicle, Eric L. Shirley, T. A. Callcott, to be submitted.

[2.14] D. L. Ederer, T. A. Callcott, J. J. Jia, L. Zhou. to be submitted

[2.15] Frank de Groot, thesis, 'X-ray absorption of transition metal oxides'. 1991.

[2.16] L.S. Butler and J. F. Harrrod, Inorganic Chemistry, chapter 24 (1989)

[2.17] J. Zaanen, G.A. Sawatzky, Journal of Solid State Chemistry **88**, 8 (1990). Also see J. Zaanen, G.A. Sawatzky and J.W. Allen, Journal of Magnetism and Magnetic Materials **54-57**, 607 (1986).

[2.18] J. Zaanen, and G.A. Sawatzky, Can. J. Phys. **65**, 1262 (1987).

[2.19] Michihide Kitamura, Chikara Sugiura, and Shinji Muramatsu, Solid State Comm. **67**, 313 (1988).

[2.20] G. L. Zhao, J. Callaway, and M. Hayashibara, Phys. Rev. B **48**, 15781 (1993).

[2.21] D. J. Stukel, R. N. Euwema, T. C. Collins, F. Herman and R. L. Kortum, Physical Review, **179** 740 (1969).

[2.22] Peter s, Peter Krüger and Johannes Pollmann, Phys. Rev. B **47**, 6971 (1993).

[2.23] A-I. Ali and P. M. Lee, Physica Scripta, **38**, 441 (1988).

[2.24] Sylvester N. Ekpenuma and Charles W. Myles, J. Phys. Chem. Solids, **51** 93 (1990). Also, see Akiko Kobayashi, Otto F. Sankey, Stephen M. Volz and John D. Dow, Phys. Rev. B, **28** 935 (1983).

[2.25] N. Troullier and José Luís Martins, Phys. Rev. B **43**, 1993 (1991). Also, see K. J. Chang, Sverre Froyen and Marvin L, Cohen, Phys. Rev. B **28**, 4736 (1983).

[2.26] G. D. Mahan, p25 in 'Photonemission and Absorption Spectroscopy of Solids and interfaces with Synchrotron Radiation' edited by M. Campagna and R. Rose, 1990.

[3.1] T. A. Callcott, W. L. O'Brien, J. J. Jia, Q. Y. Dong, D. L. Ederer, R. N. Watts, and D. R. Muller, Nucl. Instr. Meth. A**319** 128 (1992). Also, T. A.. Callcott, D. L. Ederer and E. T. Arakawa, in Science with Soft X-Rays, SPIE, **447**, 61

(1984); T. A. Callcott, C. H. Zhang, K. -L. Tsang, E. T. Arakawa, D. L. Ederer and J. Kerner, Nucl. Instrum. Methods Phys. Res. B **40/41**, 398 (1989); T. A. Callcott, K. L. Tsang, C. H. Zhang, D. L. Ederer and E. T. Arakawa, Rev. Sci. Instrum. **57** 2680 (1986).

[3.2] A. Asfaw and D. L. Ederer, L. Zhou, L. Lin, K. Osborn, T. A. Callcott, K. E. Miyano and E. Morikawa, Rev. Sci. Instrum. **66** 1627 (1995).

[3.3] T. A. Callcott, C. H. Zhang, D. L. Ederer, D. R. Muller, J. E. Rubensson and E. T. Arakawa, Nucl. Instr. Meth A**291**, 13 (1990).

[3.4] See ALS First Phase Scientific Program 1993/1994, LBL PUB-706, pp 11-16 (1992).

[3.5] T. A. Callcott, K. -L. Tsang, C. H. Zhang, D. L. Ederer, E. T. Arakawa, Nucl. Instrum. Meth. A **266**, 578 (1988).

[3.6] J. W. McCamy and Douglas H. Lowndes, unpublished (1993).

[3.7] J. J. Jia, dissertation 'bonding in transition-metal silicides studied via soft x-ray emission spectroscopy' 1991.

[3.8] C. H. Zhang, dissertation 'Soft x-ray emission spectroscopy and its application in dilute in Mg and LiAl alloys' 1987.

[4.1] T. Taguchi, Y. Yamaha, Y. Endoh, Y. Nozue, J. T. Mullins, T. Ohno,Y. Masumoto and S. Takeda, Superlattices and Microstructures, **10**, 207 (1991).

[4.2] H. M. Yates, J. O. Williams and D. J. Cole-Hamilton, Appl. Phys. Lett. **59**, 2835 (1991).

[4.3] A. Müller and B. Kebs, Studies in Inorganic Chemistry, **5**, 277 (1984).

[4.4] N. G. Stoffel, Phys. Rev. **B** 28, 3306 (1983).

[4.5] N. Troullier and José Luís Martins, Phys. Rev. B **43**, 1993 (1991).

[4.6] J. E. Jaffe, R. Pandey and M. J. Seel, Phys. Rev. B **47**, 6299 (1993).

[4.7] J. S. Lin, A. Qteish, M. C. Payne, and V. Heine. Phys. Rev. B **47**, 4174 (1993).

[4.8] James E. Bernard and Alex Zunger, Phys. Rev. B **36**,3199 (1987).

[4.9] Sylvester N. Ekpenuma and Charles W. Myles, J. Phys. Chem. Solids. **51**,93 (1990).

[4.10] S. I. Kurganskiĭ, O. V. Farberovich and É. P. Domashevskaya, Sov. Phys. Semicond. **14** , 775 and 837 (1980).

[4.11] José Luís Martins, N. Troullier and S. -H. Wei, Phys. Rev. B **43**, 2213 (1991).

[4.12] Paul Bendt and Alex Zunger, Phys. Rev. B **26**, 3114 (1982).

[4.13] Peter Schröer, Peter Krüger, and Johannes Pollmann, Phys. Rev. B **47**, 6971 (1993)

[4.14] C. S. Wang and B. M. Klein, Phys. Rev. B **24**, 3393 (1981).

[4.15] Xu Zeng and Meichun Huang, Journal of Luminescence, **40** & **41**, 913 (1988)

[4.16] K. J. Chang, Sverre Froyen and Marvin L. Cohen, Phys. Rev. B **28** , 4736 (1983).

[4.17] Akiko Kobayashi, Otto F. Sankey, Stephen M. Volz and John D. Dow, Phys. Rev. B **28**, 935 (1983).

[4.18] R. N. Euwema, T. C. Collins, D. G. Shankland and J. S. DeWitt, Phys. Rev. **162**, 710 (1967). Also, T. K. Bergstresser and M. L. Cohen, Phys. Rev. **164**, 1069 (1967)

[4.19] A-I. Ali Dahr and P. M. Lee, Physica Scripta **38**, 441 (1988).

[4.20] H. Aourag, B. Khelifa, L. Hamerlaine and H. Belarbi, Physics Letters A. **145**, 455 (1990).

[4.21] Michael Rohlfing, Peter Krüger, and , Johannes Pollmann, Phy. Rev. Letters. **5**, 3489 (1995).

[4.22] Chikara Sugiura, Yasuomi Hayasi, Hiroyosi Konuma, Shigeru Sato and Makoto Watanabe, J. Phys. Soc. Japan. **29**, 1645 (1970).

[4.23] Chikara Sugiura, Yasuomi Hayasi, Hiroyosi Konuma and Setsuo Kiyono, J. Phys. Soc. Japan **31**, 1784 (1971).

[4.24] K. O. Magnusson, S. A. Flodström, P. Mártensson, J. M. Nicholls, U. O. Karlsson, R. Engelhardt and E. E. Koch, Solid State Commun. **55**, 643 (1985).

[4.25] L. Ley, R. A. Pollak, F. R. McFeely, S. P. Kowalczyk and D. A. Shirley, Phys. Rev.B **9**, 600 (1974).

[4.26] C. J. Vesely, and D. W. Langer, Phys. Rev. B **4** , 451 (1971).

[4.27] C. J. Vesely, R. L. Hengehold and D. W. Langer, Phys. Rev. B **5**, 2296 (1972).

[4.28] R. L. Hengenhold and F. L. Pedrotti, Phys. Rev. B **6** , 2262 (1972).

[4.29] A. V. Ivanov, L. D. Timakova and V. N. Kupriyanov. Opt & Spectrosc, **31**, 171 (1971). Also A. V. Ivanov, L. D. Timakova and V. N. Kupriyanov, Bulletin of the Academy of Sciences of USSR. Physical series., **36**, 251 and 255 (1972).

[4.30] G. Deroubaix and P. Marcus, Surface and Interface Analysis. **18**, 39 (1992)

[4.31] W. L. O'Brien, J. Jia, Q. Y. Dong, T. A. Callcott, K. E. Miyano, D. L. Ederer, D. R. Muller, and C. C. Kao, Phys. Rev. Lett. **70**, 238 (1993).

[4.32] J. E. Rubensson, D. Muller, R. Shuker, D. L. Ederer, C. H. Zhang, J. Jia, and T. A.Callcott, Phys. Rev. Lett. **64**, 1047 (1990)(4.32). Also D. L. Ederer, Bulletin of The American Physical Society. **38**, 1-880 march meeting (1993)

[4.33] Y. Ma, N. Wassdahl, P. Skytt, J. Guo, J. Nordgen, P. D. Johnson, J. E. Rubensson, T. Boske, W. Eberhardt and S. Kevan. Phys. Rev. Lett. **69**, 2598 (1992); Also Y. Ma, Phys. Rev. B **49**, 5799 (1994).

[4.34] K. E. Miyano, D. L. Ederer, T. A. Callcott, W. L. O'Brien, J. J. Jia, L. Zhou, Q. Y. Dong, and Y. Ma, Phys. Rev. B **48**, 1918 (1993).

[4.35] T.A. Callcott, D. L. Ederer and E. T. Arakawa, in Science with Soft X-Rays, SPIE, **447**, 61 (1984); Also T.A. Callcott, C.H. Zhang, K. -L. Tsang, E. T. Arakawa, D. L. Ederer and J. Kerner, Nucl. Instrum. Methods Phys. Res. B **40/41**, 398 (1989).

[4.36] T. A. Callcott, C. H. Zhang, D.L. Ederer, D. R. Muller, J. E. Rubensson and E. T. Arakawa, Nucl. Instr. Meth A**291**, 13 (1990); Also T. A. Callcott, W. L. O'Brien, J. J. Jia, Q. Y. Dong, D. L. Ederer, R. N. Watts, and D. R. Muller, Nucl. Instr. Meth. A **319** 128 (1992).

[4.37] T.A. Callcott, K. L. Tsang, C. H. Zhang, D. L. Ederer and E.T. Arakawa, Rev. Sci. Instrum. **57** 2680 (1986). Also T.A. Callcott, K. -L. Tsang, C.H. Zhang, D. L. Ederer, E. T. Arakawa, Nucl. Instrum. Meth. A **266**, 578 (1988).

[4.38] A. Asfaw and D. L. Ederer, L. Zhou, L. Lin, K. Osborn, T. A. Callcott, K. E. Miyano and E. Morikawa, Rev. Sci. Instrum. **66** 1627 (1995).

[4.39] See ALS First Phase Scientific Program 1993/1994, LBL PUB-706, pp 11-16 (1992).

[4.40] J. W. McCamy and Douglas H. Lowndes, unpublished (1993).(4.41). Also, J. C. Fuggle and J. E. Inglesfield, Topics in Applied Physics. Vol. **69**, 347 (1992).

[4.42] Enrico Clementi and Carla Roetti, Atomic Data and Nuclear Data Tables. **14**, 177 - 478 (1974).

[4.43] O. Madelung, M.Schulz and Weiss, Landbolt-Börnstein: Numerical Data and Functional Relationships in Science and Technology, **III/22a.** Semiconductors: Intrinsic properties of group IV elements and III-IV, II-VI compounds, Springer-Uerlag, Berlin-Heidelberg, (1987). p170 and p199.

[4.44] N. Wassdahl, J.-E. Rubensson, G. Bray, P. Glans, P. Bleckert, R. Nyholm, S. Cramm, N. Mårtensson and J. Nordgren, Phys. Rev. Lett. **64**, 2807 (1990).

[4.45] P. Livins and S. E. Schnatterly, Phys. Rev. B **37**, 6731 (1988).

[5.1] Q-Y. Dong, W. L. O'Brien, J. J. Jia, T. A. Callcott, Phys.Rev. B **46**, 15116 (1992).

[5.2] Sylvester N. Ekpenuma and Charles W. Myles, J. Phys. Chem. Solids. **51**, 93 (1990).

[5.3] Robert L. Gunshor, and Arto V. Nurmikko. MRS BULLETIN July Vol. XX, No 7, 15(1995). Tittle: II-VI blue-green laser diodes: A frontier of Materials Research.

[5.4] T. Taguchi, Y. Yamada, Y. Endoh, Y. Nozue, J. T. Mullins, T. Ohno,Y. Masumoto, and S. Takeda. Superlattices and Microstructures. **10**, 207 (1991)

[5.5] L. Quiroga, F. J. Rodríguez, A. Camacho and C. Tejedor, Phys. Rev. B **42**, 11198 (1990).

[5.6] A. Schneider, K. P. Geyzers, J. Söllner and M. Heuken, J. Appl. Phys **74** 7181 (1993).

[5.7] LB, New Series, III/14b2. structure Data of elements and intermetallic phases, 244 and 469 (1986).

[5.8] H. M. Yates, J. O. Williams, D. J. Cole-Hamilton. Appl. Phys. Lett. **59**, 2835 (1991).

[5.9] P.R. Newbury, K. Shahzad, J. Petruzzello, D. A. Cammack. J. Appl. Phys. **66**, 4950 (1989).

[5.10] Jun Zhou, Hideo Goto, Nobuhiko Sawaki and Isamu Akasaki, Jan. Journal of Applied Physics, **27**, 229 (1988).

[5.11] R. Mach, P. Flögel, L. G. Suslina, A. G. Areshkin, J. Maege and G. Voigt. Phys. Stat. Sol. (b). **109**, 607 (1982).

[5.12] K. E. Kirschfeld, N. Nelkowski and T. S. Wagner, Physical Review Letters, **29**, 66 (1972).

[5.13] J. W. McCamy and Douglas H. Lowndes, to be submitted (1993).

[5.14] Y. Cai and M. F. Thorpe, Phys. Rev. B **46**, 15879, 15872 (1992).

[5.15] James E. Bernard and Alex Zunger, Phys. Rev. B **36**, 3199 (1987).

[5.16] Xu Zeng and Meichun Huang, Journal of Luminescence, **40** & **41,** 913 (1988).

[5.17] K. L. Tsang, J. E. Rowe, T. A. Callcott, R. A. Logan, Phys. Rev. B **38**, 13277 (1988).

[5.18] W. L. O'Brien, J. Jia, Q-Y, Dong, T. A. Callcott, K. E. Miyano, D. L. Ederer, D. L. Mueller, C-C Kao, Phy. Rev. Letters. **70**, 238 (1993)],

[5.19] W.L. O'Brien, J. Jia, Q-Y, Dong, T. A. Callcott, D. L. Mueller, D.L. Ederer, D. Shinn and S. C. Woronick, Phys. Rev. B **44**, 13277 (1991).

[6.1] A. Muller and B. Kebs, Studies in Inorganic Chemistry, **5** 277-309 and **3**-37 (1984).

[6.2] G. L. Zhao, J. Callaway and M. Hayashibara, Phys. Rew. B **48**, 15781 (1993).

[6.3] S.-H. Wei and Alex Zunger, Phys. Rev. B **37**, 8958 (1988).

[6.4] J. Zaanen and G. A. Sawatzky, Journal of Solid State Chemistry **88**, 8 (1990).

[6.5] P. Unger, J. Igarashi and P. Fulde, Phys. Rev. B. **50**, 10485 (1994).

[6.6] Michihide Kitamura, Shinji Muramatsu and Chikara Sugiura, Phys. Rew. B**33**, 5294 (1986).

[6.7] J. Zaanen, G. A. Sawatzky, J. Fink, W. Speier and J. C. Fuggle, Phys. Rew. B **32**, 4905 (1985).

[6.8] B.T. Thole and G. van der Laan, Phys. Rev. B **38**, 3158 (1988).

[6.9] E. P. Domashevskaya, V. A. Ternkhov, L. N. Marshakova, Ya. A. Ugai, V. I. Nefedov and N P. Sergushin, Journal of Electron Spectroscopy and Related Phenomena, **9** 261 (1976).

[6.10] L.Zhou, T.A. Callcott, Q. Y. Dong, J. J. Jia, K. Miyano, D. L. Ederere, J. W. McCamy, Douglas H. Lowndes and R. C. C. Perare to be published in Phys. Rev. B.

[6.11] Michael Rohlfing, Peter Krüger, and , Johannes Pollmann, Phy. Rev. Letters. **75**, 3489 (1995).

[6.12] A. E. Bocquet, T. Mizokawa, T. Saiton, H. Namatame and Fujimori, Phys. Rev. B **46** 3771 (1992).

[6.13] A. Fujimori, M. Matoba, S. Anzai, K. Terakura, M. Taniguchi, S. Ogawa, and S. Suga, Journal of Magnetism and Magnetic Materials, **70** 67 (1987).

[6.14] J. Zaanen, G. A. Sawatzky, and J. W. Allen, Journal of Magnetism and Magnetic Materials, **54-57,** 607 (1986). Also Phys. Rev. Lett. **55**, 418 (1985).

[6.15] J. Zaanen and G. A. Sawatzky, Can. J. Phys. **65**, 1262 (1987).

[6.16] S. Hüfner, T. Riesterer and F. Hulliger, Solid State Commun. **54** 689 (1985).

[6.17] J. M. Tyler and J. L. Fry, Phys. Rev. B **1** 4604 (1970)

[6.18] L. F. Mattheiss, Phys. Rev. B **10** 995 (1974).

[6.19] R. V. Kasowski, Phys. Rev. B **8**, 1378 (1973).

[6.20] Chikara Sugiura, Yohichi, and Isao Suzuki, Phycal Rev, **10** 338 (1974).

[6.21] Michihide Kitamura, Chikara Sugiura and Shinji Muramatsu, Solid State Commn. **67**, 313 (1988).

[6.22] Stephen. V. Didziulis, Jsffrey. R. Lince, David, K. Shuh, Tahomas. D. Durbin, and Jory A.Yarmoff, Journal of Electron Spectroscopy and Related Phenomena, **60** 175 (1992).

[6.23] K. Fives, I. T. McGovern, R. McGrath, R. Cimino, G. Hughes, A. McKinley, G. Thornton, J. Phys.: Condens. Matter **4**, 5639(1992).

[6.24] Jeffrey R. Lince, Stephen V. Didziulis and Jory A. Yarmoff, Phys. Rev. B **43**, 4641 (1991).

[6.25] R. Coehoorn, C. Haas, J. Dijkstra, C. J. F. Flipse, R. A. De Groot and A. Wold, Phys. Rev. B **35,** 6195 (1987). and R. Coehoorn, C. Haas and R. A. de Groot. Phys.Rev. B **35,** 6203 (1987).

[6.26] R. Mamy, A. Boufelja and B. Carricaburu, Phys. Stat. Sol. (B). **141,** 467 (1987).

[6.27] I. Abbati, L. Braicovich, C. Carbone, J. Nogami, I. Lindau and U. Del Pennino, Journal of Electron Spectroscopy and Related Phenomena, **40,** 353 (1986).

[6.28] M. Kasral, M. E. Fleet, T. K. Sham, G. M. Bancroft, K. H. Tan and J. R. Brown, Solid State Commun., **68,** 507 (1988).

[6.29] B. Sonntag, and F. C. Brown, Phys. Rev. B **10,** 2300 (1974).

[6.30] A. Šimünek and G. Wiech, Phys. Rev. B **30,** 923 (1984).

[6.31] W. Müller, G. Wiech and A. Šimunek, Physics. Letters. **98** A 66 (1983).

[6.32] L. F. Mattheiss, Phys. Rev. B **8** 3719 (1973).

[6.33] R.A.Bromley, R. B. Murray, and A. D. Yoffe, J. Phys. c: Solid State Phys. **5** 759

(1972).

[6.34] M. Sancrott, L.Braocovich, C. Chemelli and G. Trezzi, Solid. State Commun. **66**, 593 (1988).

[6.35] Toshimichi Ito, Motohiro Iwami and Akio Hiraki, Journal of the Physical Society of Japan, **50,** 106 (1981).

[6.36] W. Jaegermann, F. S. Ohnchi and B.A. Parkinson, Surf. Sci. **201**, 211 (1988).

[6.37] Edited by Chapman Hall, Chemical bonding and spectroscopy in Mineral Chemistry, 263 (1985).

[6.38] C. Sugiura and Muramatsu, Phys. Stat. Sol. B **K157** (1985).

[6.39] H. L. Park and W. B. Whitf, Phys. stat. sol.(b). **144**, k69 (1987). Also, E. Puppin, M. Finazzi and F. Ciccacci, Solid State Commun. **82**, 489 (1982).

[6.40] J. A. Tossell, The Journal of Chemical Physics. **66**, 5712 (1977).

[6.41] B.G. Tagiev, F. Sh. Aidaev, G. M. Niftev and T. M. Abbaova, Solid State Communications, **71**, 701 (1989).

[6.42] G. Dräger, W. Czolbe, E. Schulz, A. Simunek, J. Drahokoupil, Yu. N. Kucherenko and V. V. Nemoshkalenko, Phys. Stat. Sol.(b) **131**, 193 (1985).

[6.43] G. Scamarcio, A. Cingolani, M. Lugarà and F. Lèvy, Phys. Rev. B **40**, 1783 (1989).

[6.44] Y. Depeursinge, IL Nuovo Cimento, **64 B**, 111 (1981)

[6.45] F. Antonangeli, M. Piacentini, A. Balzarotti, V. Grasso, R. Girlanda and E. Doni, IL Nuovo Cimento, **51 B** 181 (1979).

[6.46] Martin Parenteau and Cosmo Carlone, Phys. Rev. B **41,** 5227 (1990).

[6.47] A. R. H. F. Ettema,R. A. de Groot, C. Haas, and T. S. Turner, Phys. Rev. B **46**, 7363, (1992).

[6.48] Youichi Ohno, Phys. Rev. B **49,** 7851 (1994).

[6.49] Youichi Ohno, Journal of The Physical Society of Japan, **59** 3740 (1990).

[6.50] H. Cohen, M. Folman, T. Maniv, R. Brener, E. Lifshits and Z. Esterlit, Phys. Rev. B**46**, 4446 (1992).

[6.51] V. S. Stepanyuk, A. A. Grigorenko, A. A. Katsnel'son, A. Sas, O. V. Farberovich and V. V. Mikhailin, Sov. Phys. Solid State **32** (6), 1028 (1990).

[6.52] Chikara Sugiura, Michihide Kitamura, Shinji Muramatsu, Shizuko Shoji and Shinjiro Kojiha, Japanese Journal of Applied Physics, **28** 1525 (1989). Nobuhiko Yamashita,

[6.53] V. S. Stepanyuk, A. Szász, O. V. Farberovich, A. A. Grigorenko, A. V. Kozlov, and V. V. Mikhailin, Phys. Stat. sol.(b) **155**, 215 (1989).

[6.54] T.A. Callcott, (35). T.A. Callcott, D. L. Ederer and E. T. Arakawa, in Science with Soft x-rays, SPIE, 447, 61 (1984); Also T. A. Callcott, C. H. Zhang, K. -L. Tsang, E. T. Arakawa, D. R. Muller, Nucl. Instr. Meth. A **319** 128 (1992). T.A. Callcott, K. L. Tsang, C. H. Zhang, D. L. Ederer and E.T. Arakawa, Rev. Sci. Instrum. **57**, 2680 (1986). Also T.A. Callcott, K. -L. Tsang, C.H. Zhang, D. L. Ederer, E. T. Arakawa, Nucl. Instrum. Meth. A **266**, 578 (1988).

[6.55] A. Asfaw, D. L. Ederer, L. Zhou, L. Lin, K. Osborn, T.A. Callcott, K. E. Miyano and E. Morikawa, Rev. Sci. Instrum. **66** 1627 (1995).

[6.56] See ALS First Phase Scientific Program 1993/1994, LBL PUB-**706**, pp 11-16 (1992).

Vitae

Ling Zhou is a native of China. She graduated in physics from Peking University, after a six year program leading to a degree equivalent to a MS degree in the United States. After graduation, as a research scientist at the Institute of Atomic Energy, Academia Sinica, Beijing, China, she specialized in studies of nuclear structure, interaction and applications using nuclear γ spectroscopies. She come to University of Tennessee in 1987 as a visiting scientist working with nuclear physicists at the university and Oak Ridge National Laboratory. In 1990, she entered the graduate program in solid state physics at the University of Tennessee. She earned the MS degree in 1992 and the Ph.D. degree in December, 1995. Her dissertation research was in the field of soft x-ray spectroscopy, and was carried out at the National Synchrotron Light Source at Brookhaven National Laboratory, the CAMD light source at Louisiana State University, and the Advanced Light Source at Lawrence Berkeley National Laboratory. Dr. Zhou is a member of the American Physical Society and Chinese Physical Society.